University of Southampton

Faculty of Science & Mathematics

School of Ocean and Earth Sciences

Doctor of Philosophy

Naoisé O'Reilly

Combining Altimetry and Hydrography with Inverse Methods

September 2007

Graduate School of the

National Oceanography Centre, Southampton

This PhD dissertation by

Naoisé O'Reilly

has been produced under the supervision of the following persons

Supervisor/s

Peter Challenor

Chair of Advisory Panel

Ian Robinson

Member/s of Advisory Panel
Peter Challenor, Ian Robinson, Stuart Cunningham

"Water covers about 70% of the earth's surface. It makes up around 65% of our bodies and a fair proportion of Guinness Stout."

Inscription Guinness Hopstore Dublin.

Abstract:

We describe a generalization of the Bernoulli inverse method, which produces an estimate of Sea Surface Height (SSH) across the region of interest rather than simply at station positions. Real-time 'float' observations and satellite altimetry measurements are used to map a 'sea surface elevation' to study the large-scale ocean circulation in the North Atlantic. The inverse has been applied to simulated Argo floats and satellite altimetry tracks in the Ocean Circulation and climate model (OCCAM). The Bernoulli inverse method predicts the SSH by finding geostrophic streamlines along which the Bernoulli function is conserved. These streamlines are defined where modified potential temperature and salinity are conserved. This predicted SSH is combined with that measured by the satellite altimetry. The revised method uses linear regression to give a surface solution for the region rather than solving the function at fixed positions, hence increasing the resolution of the problem by combining the altimetry measurements for the region. We will present results of a comparison study where real-time Argo and satellite altimetry have been used in combination with OCCAM using the same method to see how robust the solutions are for the North Atlantic.

Contents

Table of Figures

Table of Tables:

Appendix B

DECLARATION OF AUTHORSHIP

I, ……., [please print name]
declare that the thesis entitled [enter title]
……
……
……
and the work presented in the thesis are both my own, and have been generated by me as the result of my own original research. I confirm that:

- this work was done wholly or mainly while in candidature for a research degree at this University;
- where any part of this thesis has previously been submitted for a degree or any other qualification at this University or any other institution, this has been clearly stated;
- where I have consulted the published work of others, this is always clearly attributed;
- where I have quoted from the work of others, the source is always given. With the exception of such quotations, this thesis is entirely my own work;
- I have acknowledged all main sources of help;
- where the thesis is based on work done by myself jointly with others, I have made clear exactly what was done by others and what I have contributed myself;
- none of this work has been published before submission, **or** [delete as appropriate] parts of this work have been published as: [please list references]

Signed: ……..
Date:…….

Acknowledgements:

My first thanks have to go to the JRD and satellite team, particularly David Crowell and Steve Hall for getting me started in the field of research. I would like to thank Peter Challenor for taking my on as a student and giving me such an interesting project to work on. He has been an excellent supervisor, always enthusiastic and positive. He always makes everything seem possible. I feel that Steven Alderson should have been an honorary supervisor for all the help he has given me.

So many people in the JRD, especially the satellite team have helped me from the beginning. I would like to thank Helen Snaith for answering all my stupid questions and Christine Gommenginger for answering the ones that were too stupid to safely ask Helen. I would like to thank Andrew Shaw for his help with matlab and Gadget.

I would like to give a big thank you to Val Byfield, Lisa Redbourne-Marsh and Paolo Cipollini, for adopting me as an office mate in the last few months of my project.

I would like to thank Collette Robertson, Val Byfield, Richenda Houseago-Stokes, Paolo Cipollini and Ian Robinson for giving me the extra work outside of my PhD which allowed me to survive the last year. It has also given me a lot of extra experience and knowledge that I really value.

Of course I have to thank all of my friends who I have drunk coffee with, spent nights in the pub with and who have generally tried to help keep me sane during the time I have spent in Southampton, especially those who are English and who have had to learn to put up with my complaining about England. To mention a few ….Chris Rowan, Stuart Painter, Steph Henson, Sandy Thomalla, Anna Hickman , Donna Shillington , Doug McNeall, Amanda Gunston, Sinhue Torres, Janet Sumner, Jo Hopkins and Alex Mustard. I am sure that I have forgotten someone! Not forgetting my friends at home Martin French, Paul Clune and Naimh Nestor.

Going back in time I would like to thank two teachers who saw I had the potential to in fact finish school never mind go any further, Sally Shields and Jim Golden. I would like to say that NUI, Galway were extremely supportive during my undergraduate degree. The person who helped me most to get through my time in Galway was Agnes O Farrell.

Lastly but most importantly I would like to thank Naish and Olga for putting up with me through all of my academic struggles.

Chapter 1

Introduction:

Over the past decade, a vast amount of observational data about ocean circulation has been made available to researchers by programmes such as WOCE (World Ocean Climate Experiment) and emerging programs such as ARGO (Woods Hole Oceanographic Institution, 1999), not to mention the vast quantities of satellite altimetry data acquired by the Topex mission (1992-2006), ERS1 (1991-1995), ERS2 (1995-2005), ENVISAT (launched 2002), and the Jason mission launched in 2002.

An emerging area in oceanography, stimulated by recent improvements in computational and modelling capabilities, is using this data to constrain ocean circulation models, a process referred to as data assimilation. This is a way of producing a best estimate of a system we wish to understand from a mixture of sometimes conflicting observational data sets and our understanding of the physics of the ocean. Data assimilation brings together the measurements, the known errors in these measurements and the governing equations of the system. This is beneficial for a variety of applications such as the forecasting of climate systems, designing observing systems, filling in data-poor regions and estimating unobserved parameters.

Forward Modelling

Generally in assimilation methods we take the observational data and incorporate it into a numerical model of the system. An example of this process is show in Figure 1 below. The poorly guessed model forecast (dashed line), can be improved by assimilating noisy measurements into a mathematical model to provide an improved estimate of the trajectory of the system (solid line).

Figure 1 : A schematic of how data assimilation methods are used. From: Making the most of earth observations with data assimilation, 2nd Envisat Summer School (http://envisat.esa.int/envschool/programme.html).

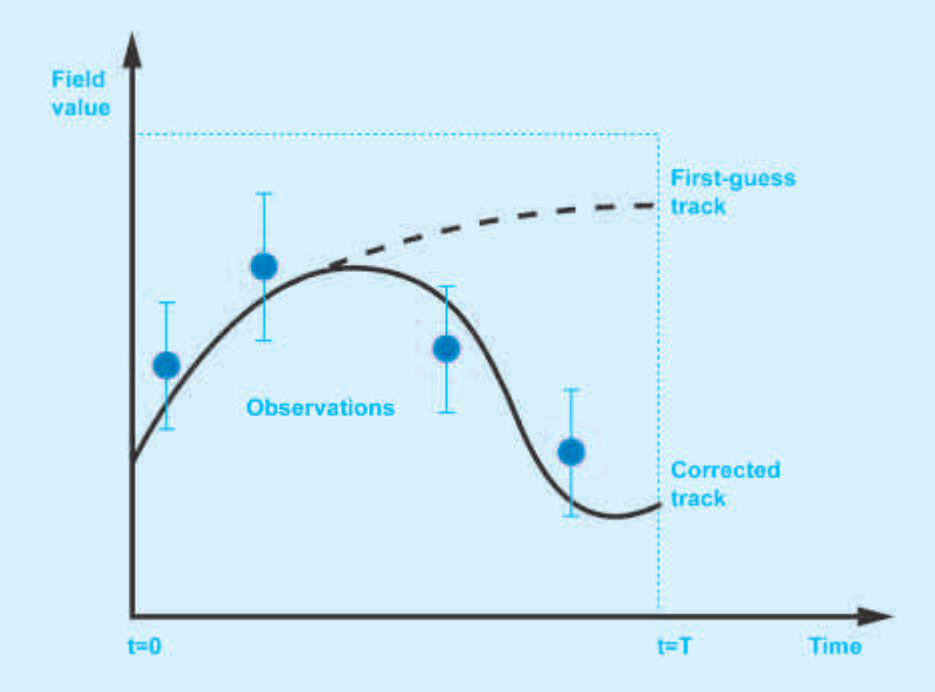

An example of this approach is in seasonal forecasting, in particular the El Niño Southern Oscillation (ENSO), which since 1997-98 has dominated media

attention because of its linkage to many severe climatic consequences around the globe. ENSO is a disruption of the coupled ocean-atmosphere system in the tropical Pacific, where westerly blowing trade winds relax and allow warmer western Pacific water to move eastwards toward South America. This change in the system has ripple effects on climatic conditions in many regions globally, including increased rainfall across the southern tier of the US and in Peru, which have caused destructive flooding, and drought in the West Pacific, sometimes associated with devastating brush fires in Australia, more details at (http://www.pmel.noaa.gov/tao/elnino/el-nino-story.html).

El Niño can be seen in measurements of the sea surface temperature (SST). SST data from the Tropical Atmosphere/Ocean Array (TAO), an array of approximately 70 moored buoys in the Tropical Pacific Ocean deployed by the National Oceanic and Atmospheric Administration (NOAA) have aided in tuning ENSO models well enough that the climate prediction centre (http://www.cpc.ncep.noaa.gov/products/analysis_monitoring/enso_advisory/index.html) can now predict the ENSO conditions for the next 3-6 months at a time. For example, presently the conditions are still within the ENSO-neutral range, (McPhaden, 1993).

Inverse Modelling

This is an example of a forward problem – the data is used to "tune" a pre-existing model, forcing it to fit a set of external observations. However, a problem with this approach is that the data cannot then be used to assess

the validity of the initial conditions used to set up the model. So where the system being studied is poorly understood, it is often a better approach to use inverse methods. An inverse study starts with the observational data and uses this to infer information about the underlying system, making no prior assumptions about initial conditions or parameters. Because many aspects of ocean circulation are still poorly understood, inverse methods are potentially a very useful method to improve our understanding of it dynamically using a combination of observations and theory.

Of all the inverse methods that can be used to approach this problem , the Bernoulli inverse is unique because in comparison to other inverse methods, such as the box inverse, it does have a unique solution (Fukumori, 2001; Stammer, 2004) (see Chapter 4). The original Bernoulli inverse (Killworth, 1986) was obtained using density and potential vorticity, the latter of which is difficult to measure. However, the Bernoulli function can also be obtained from modified potential temperature (Saunders, 1995; Cunningham, 2000), which can be extracted from standard temperature-salinity profiles. This project aims to further develop this more practical application of the Bernoulli inverse. We have chosen to focus on mapping a 'Sea Surface Elevation' (SSH) for a region of the North Atlantic (30-6° N, 5-60° N), using a combination of measurements from the ARGO float network and satellite altimetry. Creating an accurate map of SSH in this region would allow large-scale circulation to be reconstructed, and also monitor changes related to the North Atlantic Oscillation (NAO). The NAO has a considerable effect on

climatic variability across a large area, from the eastern coast of the United States to Siberia and from the Arctic to the subtropical Atlantic, especially during the winter period, and appears to be controlling much of the recent warming trend observed in the Northern hemisphere (see McCartney (1996), Hurrell et al. (2001) and Chapter 2). Though we understand some of the consequences of the NAO we have not yet managed to be able predict it in the same manner as the ENSO.

Monitoring such changes requires datasets collected over a period of decades or more, which are only now becoming available. This project utilised two data sources: satellite altimetry from Topex/Jason and temperature-salinity profiles obtained by the ARGO float network.

Satellite Altimetry

Satellite altimetry can measure variations in SSH across large areas. Unfortunately despite all the advances in satellite altimetry, we are still unable to separate changes in SSH due to the mean flow field from small-scale changes in the geoid. Figure 2 shows how the SSH as measured from an altimeter is calculated in relation to the reference ellipsoid. This is a theoretical reference point used to determine the height of the satellite in orbit over the globe. Deviations in SSH from this surface of equipotential gravity arise from forces at the sea surface, for example pressure gradient forces, wind and buoyancy forces or atmospheric pressure. However, Figure

2 also shows that local variations in e.g. seafloor topography can cause the geoid to deviate from the reference ellipsoid. The SSH change caused by these variations can be up to two orders of magnitude larger than those due to changes in the mean flow field of the ocean. Therefore to investigate these smaller amplitude signals it is essential to remove the geoid signal from the altimetry (Wunsch and Gaposchkin, 1980; Chelton, 2001).

Figure 2: schematic summary of the sea surface height referenced to the geoid.

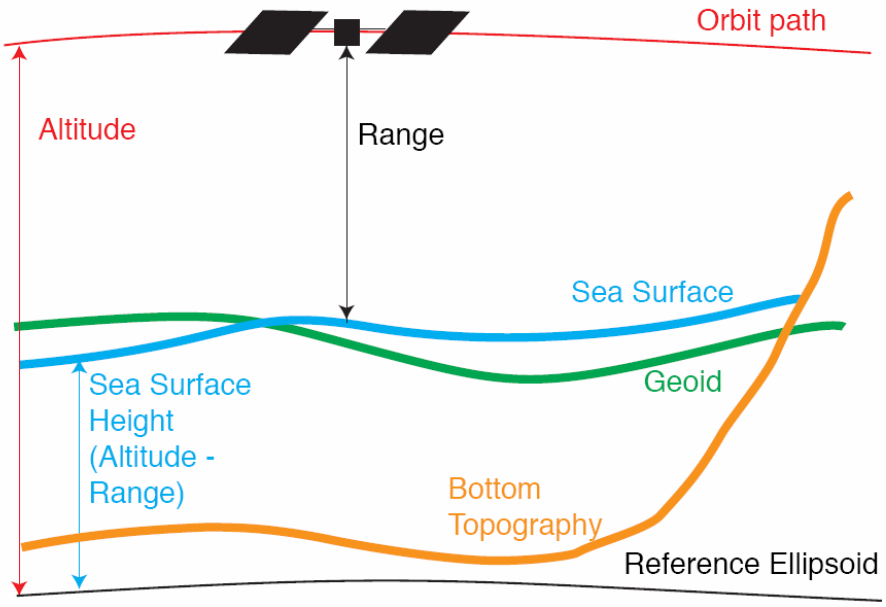

In the past, remote sensors have either been content to examine "changes" in the dynamic height field, or they have combined the altimetry field with another set of real time observations. The difference between the observations and the satellite altimetry at the same times can then be used as an estimate of the geoid, and this signal can then be removed from the

subsequent satellite measurements to give an estimate of absolute geostrophic velocity value. The only previous work done in this area using the Bernoulli inverse and satellite altimetry adopted this method to combine along track CTD data with ERS-1 altimetry (Tokmakian, 1994, see also Chapter 4). The altimetry data was used as an *a priori* solution for the inverse.

ARGO

Until recently we have lacked a long term observing system to collect temperature and salinity profiles at depth in the North Atlantic and the global ocean in general. This has changed with the deployment of the ARGO float network. It is hoped that ARGO will be the next step in obtaining global ocean observations, by autonomously collecting temperature and salinity profiles and mid-depth velocity measurements on broad spatial scales (see Chapter 3 for more details on the implementation and operation of the ARGO program).

A change in the sea surface height, h', may be written as:

Equation 1

$$h' = \frac{1}{g}\int_{Z_{ref}}^{0} (\rho')^{-1} dp + \frac{1}{\rho g} P'(z_{ref}),$$

where ρ' is the change in water density (a function of temperature T, salinity S and pressure P), P' is change in pressure, Z_{ref} is the depth of a reference level and g is gravity, and ` denotes the change from Z_{ref} (Argo, 1999). The first term on the right can be calculated directly from ARGO float profile data. This term represents the changes in the water column due to changes in the water properties (for example, hot water is less dense than cold water) and therefore represents dynamic flow. The second term refers to changes in the reference pressure, or deviations of the geoid from the reference ellipsoid. This can be obtained from the measured velocity of the floats as they drift at a referenced depth. It can also be calculated if h' is measured by satellite altimetry.

Why do we want to add altimetry to the problem and why can altimetry not be used on its own?

It was shown by (Guinehut, 2002) from model simulations that an array such as ARGO could retrieve most of the variance of the large scale circulation of the North Atlantic, about 65-70% at 1000m. But ARGO will only give us a very sparse dataset (although the design configuration of an approximately one float per 3°, at the time of the work described in this thesis only 40% of the program was complete, a very sparse coverage, which gave us data from approximately 100 floats in the study area). Using a simple Bernoulli solution of just the ARGO data, we would only obtain the sea surface height difference between the locations of the floats (e.g., Alderson and Killworth,

2005). Satellite altimetry observations provide data over a much larger spatial scale than the floats alone. Guinehut (2002) also comment that they feel combining the floats with satellite altimetry should reduce aliases due to mesoscale variability and hence better constrain the solution.

Rather than using the altimetry to simply constrain the problem as done by (Tokmakian, 1994), we will use the Bernoulli solution of the ARGO temperature and salinity profiles to obtain the absolute dynamic height values at the float locations. We will then combine these with the altimetry measurements for the region, but rather than simply having a series of dynamic height values only at certain ARGO float locations, as in the solution of Cunningham (2000), we have opted to solve for a surface solution (see Chapter 5). This means that we may combine all the ARGO data and Jason measurements for the North Atlantic to create a surface picture of the changes in absolute velocity for the whole region. We will be able to obtain 10-day snap shots using these two data sets. So for the first time the altimetry will be incorporated directly into the solution, and we will also have obtained absolute measurements for the whole study area by using the ARGO and Jason satellite altimetry to their full potential. It also represents an important breakthrough in using ARGO data as it was originally intended, to provide real-time monitoring of oceanographic changes.

How we approached the problem:

This project was divided into three principal stages. First we developed the methodology. New procedures were developed to combine ARGO data with satellite altimetry, and to overcome problems such as the distribution of ARGO data on a highly irregular, non-stationary grid due to the continuous, non-uniform, drifting motion of the floats. This drift is also constantly changing the position of the ARGO floats relative to the Jason satellite tracks.

In the second stage these procedures were validated using data extracted from the OCCAM model. A predictor-corrector routine was modified to simulate the behaviour of ARGO floats in OCCAM, and used to obtain simulated data for a Bernoulli inverse. Because we could extract the sea surface height directly from OCCAM at simulated float positions as well as obtaining simulated profiles of the potential temperature and salinity, we could directly compare the model SSH and the SSH obtained from the Bernoulli solution. We used simulated model data to run both float only solutions and solutions containing simulated Jason and float data. This was first done for a point only method, where we obtain values for the SSH only at the points at which measurements were made, and then using the surface fitting method. Simple polynomial functions were initially used, but in order to consider what difference a more complex basis function would make to the solution we also fitted a GAM (generalized additive model) to the "point"

solution. We then compared this solution to the one obtained from our Bernoulli surface solution.

In the final stage of the project we have applied the method to real ARGO and Jason observations.

Each stage of method development described above required us to produce a large amount of new programming code. The majority of coding has been done using python. This is a very efficient computer language, so using it should make sure that our method is computationally efficient enough to run over a large basin such as the North Atlantic region.

Structure of thesis:

Chapter 2 discuss the large-scale oceanography of the North Atlantic, and provides a background for interpreting the features observed in our solutions.

Chapter 3 outlines the data used in the project, giving details of the OCCAM model, Jason altimetry data and the operation of the ARGO floats. We also discuss how these data were combined to reach the end result of a Sea Surface Elevation for the North Atlantic.

Chapter 4 discusses inverse methods, particularly the Bernoulli inverse used in this project, and how these methods have been used in the past to obtain a point solution for the Sea Surface Height at set locations. There is also some discussion of the conserved variable used in this study, modified potential temperature. We present the results from the simulation of the floats in the OCCAM model and the point solution obtained for the model data.

Chapter 5 describes the background for surface fitting and linear regression used to obtain the surface solution, and presents the results of surface fitting of simulated data from the OCCAM model before obtaining a solution from real ARGO and Jason data.

Chapter 6 describes the fitting of a generalized additive model, GAM to the Bernoulli "point" solution from Chapter 4 and compared with the surface solution obtained in Chapter 5.

We conclude in Chapter 7 with a discussion of both the positive outcomes of this research and problems that have been encountered applying the method to real time data. Future applications of the method we have developed are also discussed.

Chapter 2

This chapter gives a brief overview of the large-scale oceanographic features of the North Atlantic, which are likely to influence the topography of any surface solution obtained from ARGO and Jason data. This project does not attempt to specifically address any of the major scientific problems in this complex field. Rather, it is concerned with developing a general method which can be used to tackle these problems in the future. Our discussion is therefore limited to general features which we would expect to obtain in any surface solution of SSH in the North Atlantic region, and the processes which control them.

Circulation of the Atlantic:

Circulation in the North Atlantic is driven by a combination of two different processes. There is the vertical circulation, also referred to as the meridional or thermohaline circulation, which is driven by temperature and salinity gradients. There is also the horizontal or wind driven circulation. The balance between these forces, and the Coriolis forces resulting from the Earth's rotation, control the path of geostrophic currents, for example the North Atlantic current.

The wind-driven surface circulation can be clearly observed in drifting buoy experiments such as those conducted by Krauss (1986) (Figure 5). In

contrast, the vertical overturning circulation is much less fully described, because it is difficult to make direct measurements, but its large-scale features are well-represented by the popular concept of the 'Great Ocean Conveyor Belt' (Broecker and Peng, 1987; Broecker, 1991) (Figure 3).

Figure 3: Diagram of the ocean conveyor belt taken from Broecker (1991).

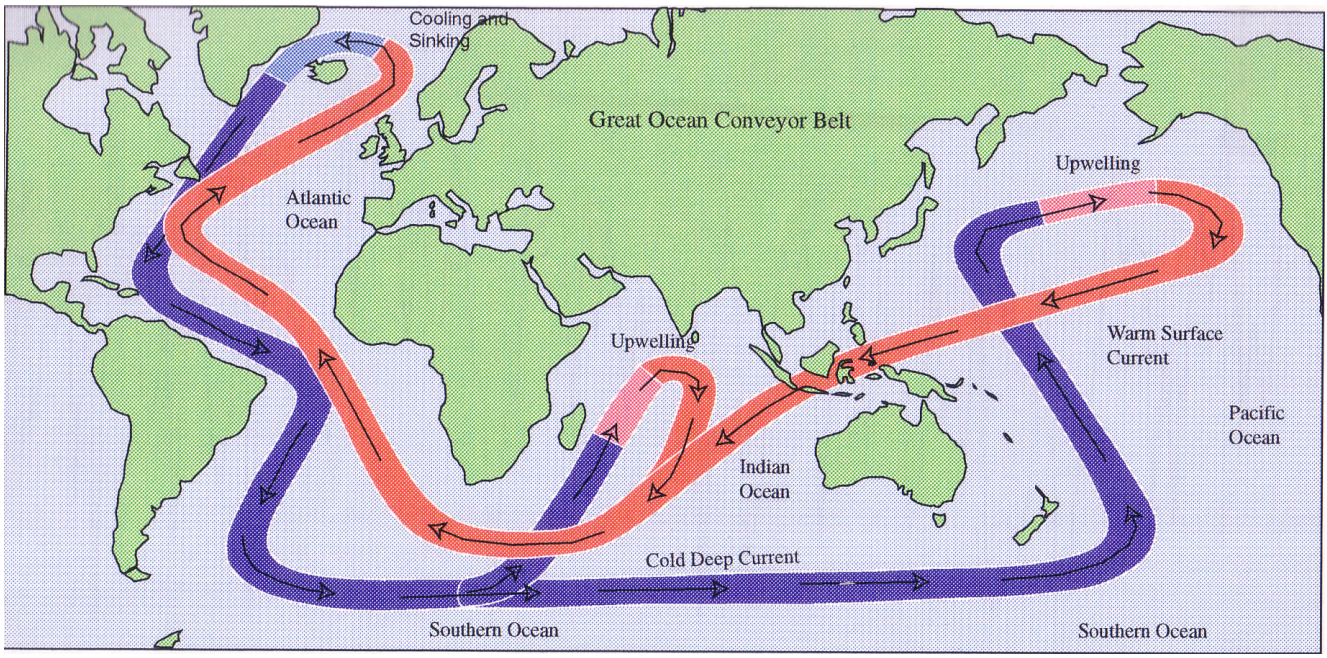

Figure 3 shows the importance of the linkages between the different components of the Earth's Climate System which result from this global circulation. The lower limb of the conveyor is driven by cold water which downwells in the Norwegian Sea. Warm water from the Atlantic flows northward between Iceland and Scotland. In winter as the surface water cools it becomes denser. When it is denser than the water underlying it, the surface water sinks to its neutrally buoyant depth and then flows south into the Atlantic. This water mass is known as the North Atlantic Deep Water (NADW) and its route southwards is largely controlled by bathymetry (Figure

4). For example, it mainly moves into the southern North Atlantic through three gaps in the Greenland-Iceland-Scotland ridge.

Figure 4: Bathymetry map of the North Atlantic region. X's represent simulated float positions in the OCCAM model (see Chapters 3 and 4 for more details).

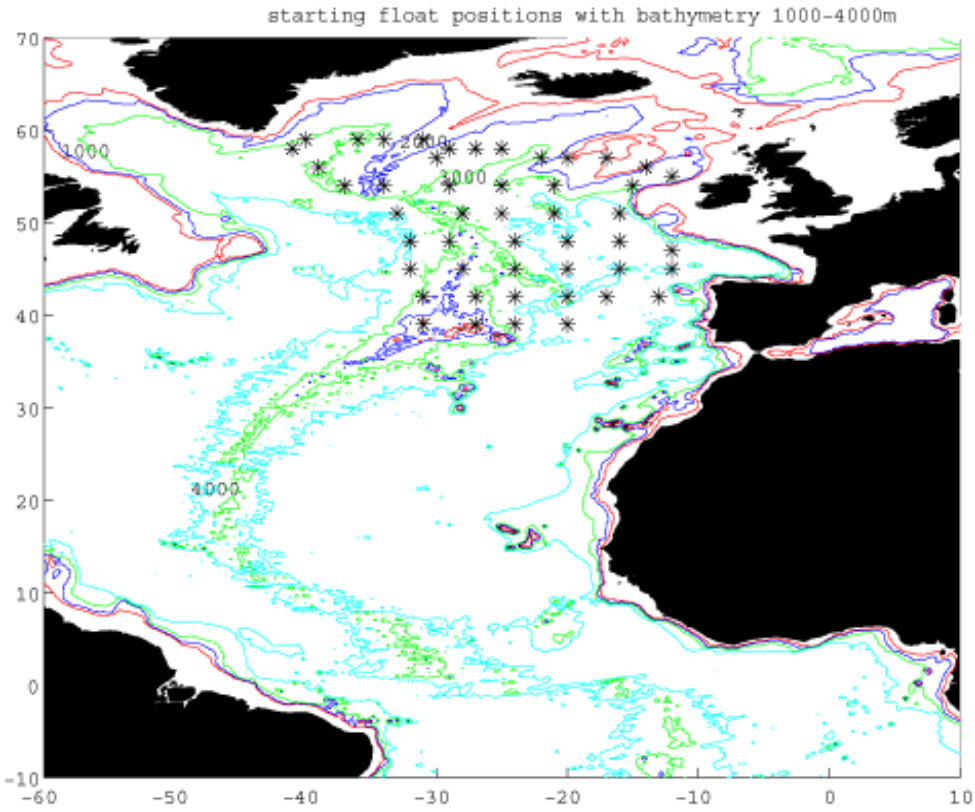

The lower limb of the conveyor eventually joins the rapidly moving Antarctic Circumpolar Current.

A consequence of NADW formation is an intensification of the wind-driven western boundary current in the North Atlantic (The Gulf Stream), which moves water northward from the tropics to replace the downwelling water in the Norwegian Sea. The northward flux of a warm Gulf Stream, and the southward flux of cooler thermocline and cold North Atlantic Deep Water, is

referred to as the meridional overturning circulation (MOC), and redistributes heat from the equator, where there is large solar heating, to higher latitudes. This heat is released to the atmosphere over the northern Atlantic and is responsible for Europe's surprisingly mild winters.

The overall effect of the geostrophy and the flow associated with the MOC on SSH values in the North Atlantic is to create a positive slope from the North West to the South East, along which the surface flow (the Gulf Stream) moves into the northern North Atlantic. However, many details of this general picture, particularly the smaller-scale spatial and temporal variability of the deep MOC, are still poorly known. In March 2004, a new project started as part of the RAPID climate change program. Nineteen moorings were deployed across the Atlantic at 26.5°N to monitor the deep meridonal overturning circulation (Srokosz, 2004). Three additional moorings were deployed on the western boundary along 26.5°N (by Prof. Bill Johns, University of Miami) to resolve transport in the Deep Western Boundary Current and Dr Molly Baringer (NOAA/AOML) leads the monitoring of the northward branch of the MOC using submarine telephone cables in the Florida Straits. The entire monitoring array system created by the three projects will be recovered and redeployed annually until 2008. From this program it is hoped that we will have a much better picture of the deep vertical circulation.

We now move on to discuss the horizontal, wind driven circulation. The wind

driven currents in the South Atlantic are dominated by the sub-tropical gyre (Figure 5) and the Gulf Stream. In the Northern Atlantic, from the Newfoundland Rise the Gulf Stream continues as the North Atlantic Current (NAC). The classical picture of the NAC and its different branches is due to Dietrich et al. (1975). The NAC is associated with a strong thermohaline front, which separates western North Atlantic Central Water from the Labrador Current (La, Figure 5) and slope water.

Figure 5: Schematic picture of the North Atlantic circulation, derived from drift experiments by Krauss (1986). Gu = Gulf Stream; Na = North Atlantic Current (NAC); La = Labrador Current; Ir = Irminger Current; Ng= Norwegian Current; Og/Wg = East/West Greenland Current. Horizontal shading marks the extent of the sub-tropical gyre; the vertical shading represents an area of eastward drift associated with the NAC. Numbers represent estimated flow in Sv.

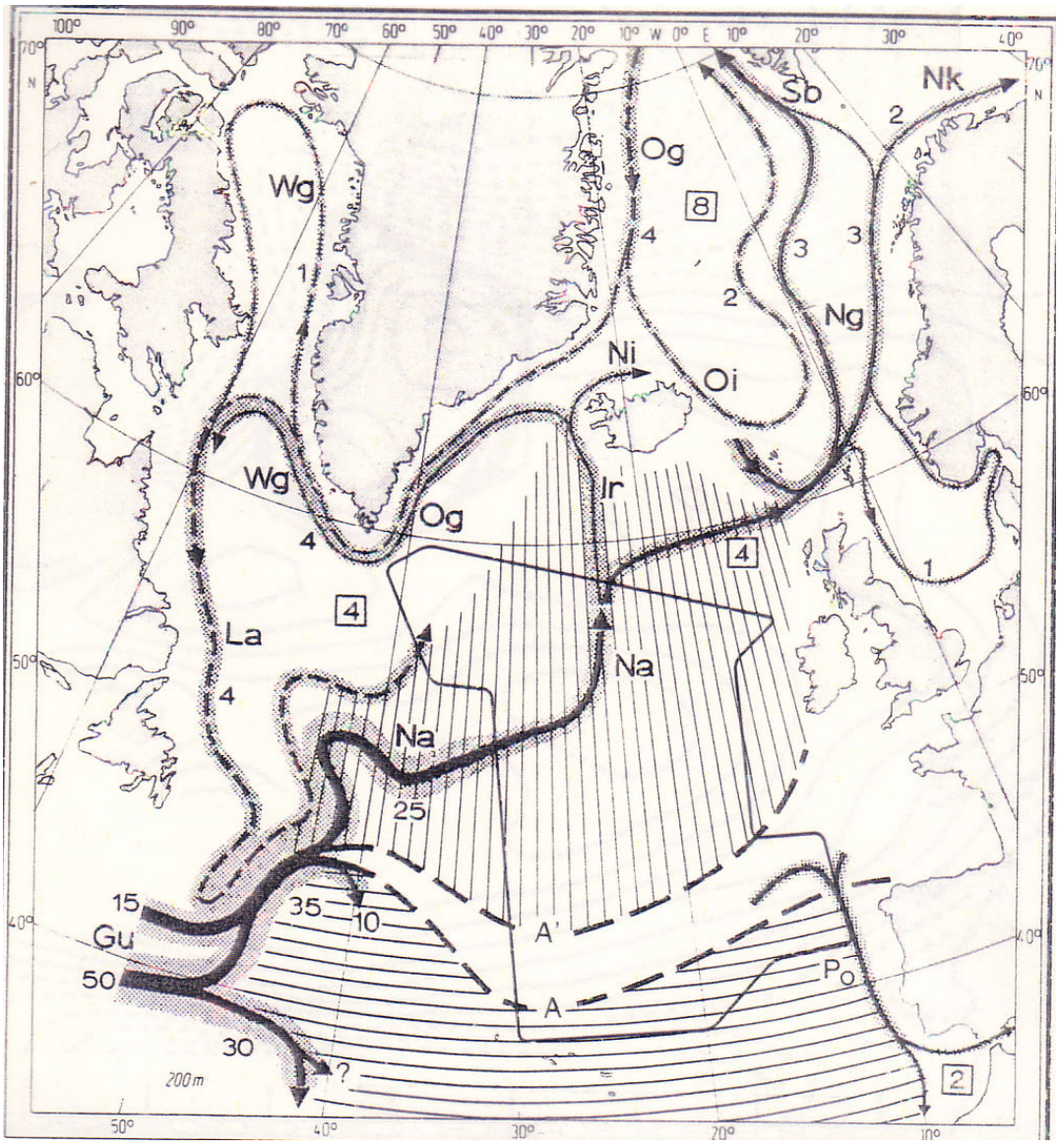

The drifting buoy experiments of Krauss (1986) indicate that the rapid flow of the NAC is superposed on a broader region of wind-driven, eastward drift (Figure 5). Between 51°N and 52°N, where the NAC crosses the Mid-Atlantic Ridge, loses its frontal character and branches into the Irminger and Norwegian currents (Ig and Ng, Figure 5).

Past this point, various interpretations of the structure of the recirculating gyre system in the Northern Atlantic have been proposed. Worthington *(1976)* proposed a closed, anticyclonic "northern gyre" in the Newfoundland Basin (Figure 6), with no contribution from the NAC. However, according to drift experiments the North Atlantic Current is not the rim of the subtropical gyre but an independent current, and the closed northern gyre is a misinterpretation of the intensive eddy field on the warm side of the NAC (Krauss, 1993).

Figure 6: Closed, anticyclonic 'northern gyre', as interpreted by Worthington (1976).

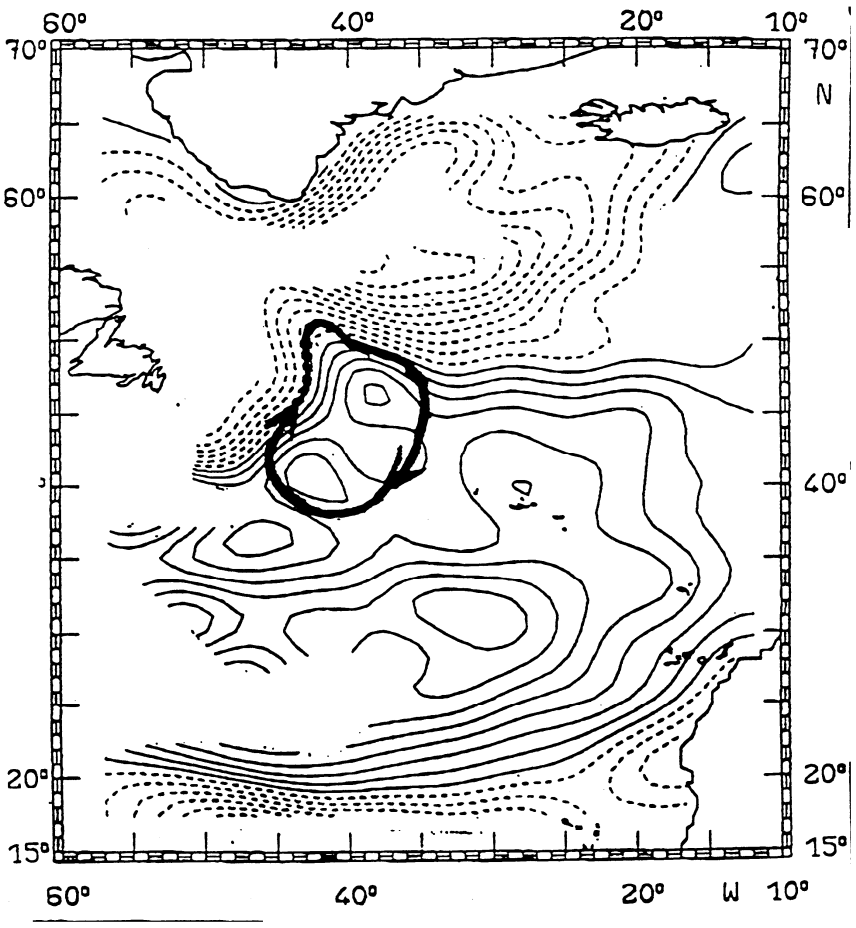

A more recent interpretation is shown in Figure 7. This clearly shows a two gyre system in the North Atlantic. In the west, the cyclonic sub-polar gyre is formed by the Irminger, East Greenland, West Greenland and Labrador currents. Where it divides at the Mid-Atlantic Ridge, two thirds of the NAC water is fed into this gyre (McCartney and Talley, 1984). The remaining third forms another cyclonic gyre system in the Norwegian-Greenland Sea to the east.

Figure 7: Simplified circulation of the upper layers of the North Atlantic. An adaption of Ellet (1993), from (Heywood et al., 1994).

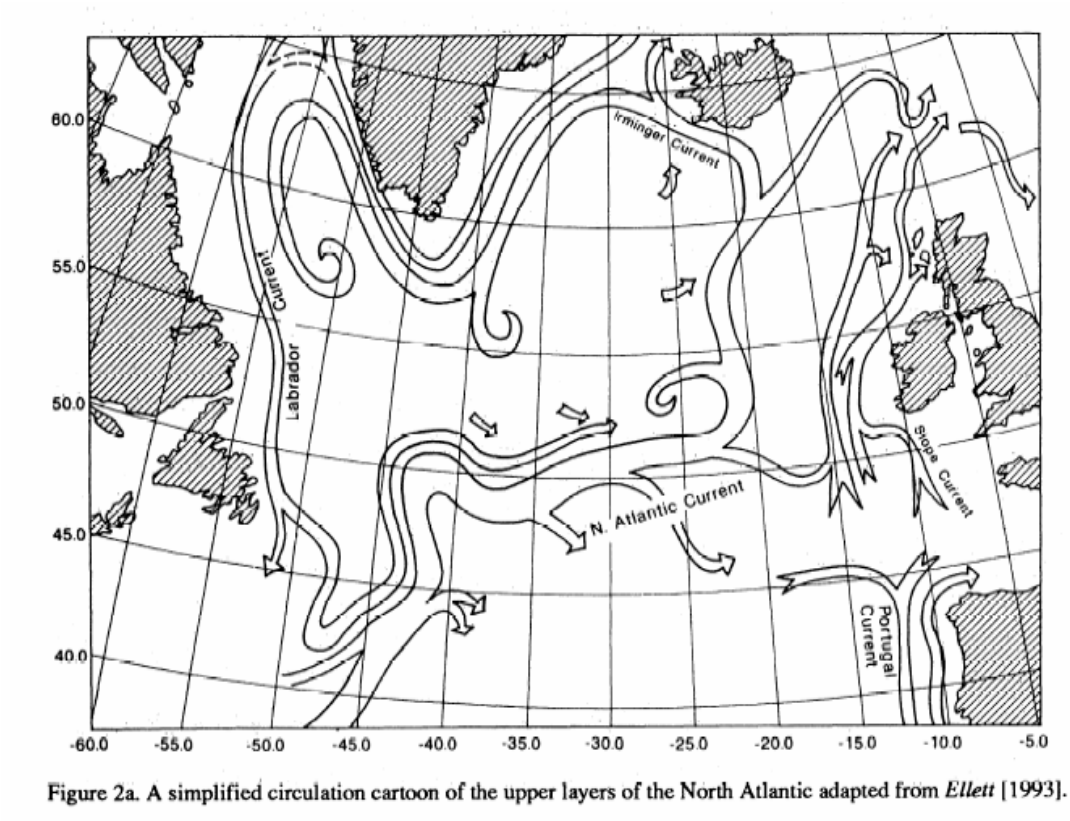

Figure 2a. A simplified circulation cartoon of the upper layers of the North Atlantic adapted from *Ellett* [1993].

Gyre circulation causes changes in SSH due to the action of the Coriolis force. In the northern hemisphere, water moving clockwise around an anticyclonic gyre system will be pushed into the centre of the gyre, causing an increase in SSH. Anticlockwise motion around a cyclonic gyre will move water outwards from the centre, causing a decrease in SSH. The circulation pattern in Figure 7 should produce an SSH low associated with the cyclonic sub-polar gyre. Also, the eastward movement of surface water shown in Figure 5 (the NAC and the broader wind-driven drift) will lead to higher SSH values in the western North Atlantic basin. We will see later (Chapters 4 and 5) that our point and surface solutions do a good job of obtaining this picture of the region.

The North Atlantic Oscillation (NAO)

The NAO is characterised by a variation in the north-south difference in surface air pressure in the Atlantic Ocean (Figure 8). The contrast between a low-pressure region centred near Iceland, and a high-pressure region in the subtropics near the Azores, drives the surface winds and wintertime storms from west to east across the North Atlantic. Over decadal timescales, there is an out of phase relationship between these two pressure systems. In a positive phase of the NAO, the pressure near Iceland is lower than normal, the pressure near the Azores tends to be higher than normal, and there is a larger pressure gradient between north and south (Figure 8a). In a negative phase of the NAO, the pressure near Iceland is higher, and the pressure near the Azores is lower, causing a smaller pressure gradient (Figure 8b).

Figure 8 shows the effects of the positive and negative phases of the NAO. Positive phases (Figure 8a) are associated with intensified meridional sea level pressure and sea surface temperature gradients, stronger than average westerlies at mid-latitudes and more northerly storm tracks toward Iceland. More temperate European winter conditions are seen and there is an increased production of Labrador Sea Water. Similarly, negative phases (Figure 8b) are associated with a southward shift of the Iceland low-pressure centre. There are weakened meridional sea level pressure and sea surface temperature gradients. The storm tracks are easterly across the Atlantic. A cooler subtropical gyre increases the production of Eighteen Degree Water and Nordic Sea Water, while decreasing the production of the Labrador Sea Water, *(McCartney and Curry, 2001)*.

Positive and negative phases of the NAO are defined by the NAO index, which is constructed from the differences in wintertime sea level pressure (SLP) between Portugal and Iceland, *(Hurrell, 1995)* (Figure 9). Portugal is chosen rather than the Azores due to the fact that there is a longer time series of data spanning 1864 to 1994. However, data from Portugal only represent the winter NAO index as they do not capture the summer meridional pressure gradient. To calculate the index, sea level pressure anomalies at each station are normalised by division of each seasonal pressure by the long-term mean standard deviation.

Figure 8: The (a) positive phase, and (b) negative phase, of the NAO, and their subsequent effects on the climate. From http://www.met.rdg.ac.uk/cag/NAO/

Positive phases (Figure 8a) are associated with intensified meridional sea level pressure and sea surface temperature gradients, stronger than average westerlies at mid-latitudes and more northerly storm tracks toward Iceland. More temperate European winter conditions are seen and there is an increased production of Labrador Sea Water. (Figure 8b), negative phases are associated with a southward shift of the Iceland low-pressure centre. There are weakened meridional sea level pressure and sea surface temperature gradients. The storm tracks are westerly across the Atlantic.

(a)

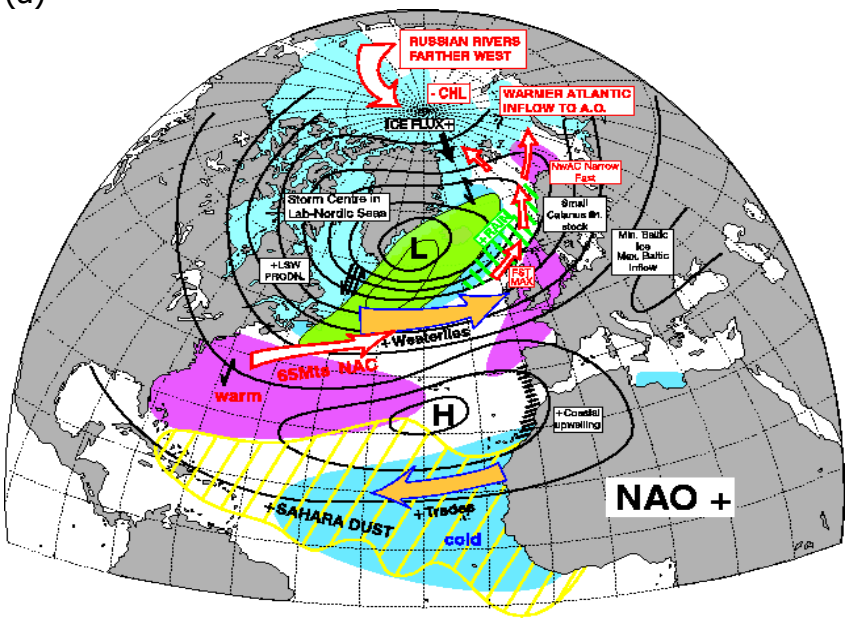

(b)

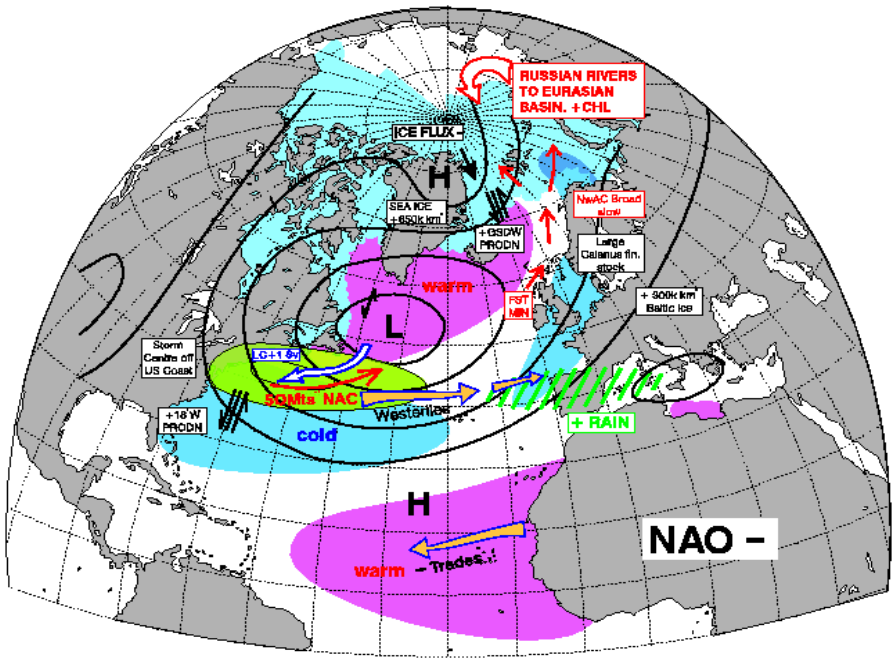

Figure 9: Variation in NAO index for past 150 years. From http://www.cgd.ucar.edu/~jhurrell/indices.html

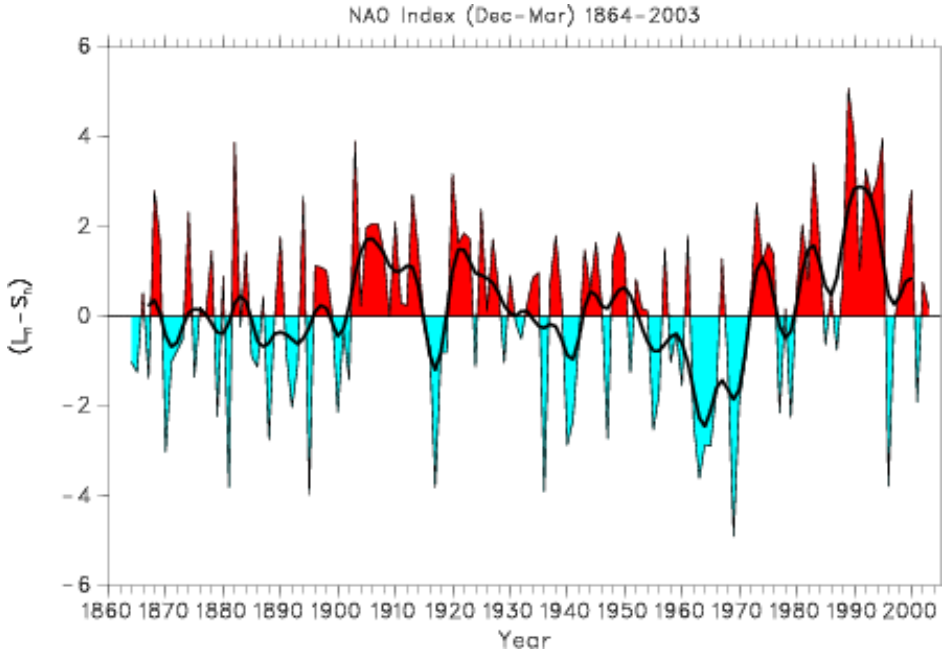

The NAO accounts for 30% of the extratropical hemispheric variability, (Hurrell, 1995), and strongly influences the weather and climate of Europe, Eurasia, northern Africa and eastern North America. The NAO is not believed to be just an atmospheric phenomenon, but is tied to the North Atlantic ocean as well. The NAO index exhibits interannual variability, which is characteristic of the atmosphere. However it persists in one phase or the other over decadal time periods, and the atmosphere is incapable of such organised behaviour on its own for timescales longer than a few weeks. This implies a strong oceanic influence.

In North America, Europe and North Africa, long-term changes in precipitation patterns and wintertime temperatures can be attributed to

changes in the phases of the NAO (McCartney, 1996; Hurrell, Kushnir et al., 2001). Figure 9 shows that in the 1940-50's, the NAO index was in a negative phase, causing colder winters in Europe and wetter conditions in southern Europe (Uppenbrink, 1999). Since the mid-1970's the NAO index has generally been high. During this time, winters in Europe have been relatively warm whereas those in the northwest Atlantic have been cold, and the Mediterranean has been particularly dry. Over the past decade, the NAO has remained in an extreme positive phase during the winters, and surface temperatures over the Northern Hemisphere are warmer now than at any other time over the past millennium.

Major oceanographic changes in the North Atlantic can also be linked to changes in the phases of the NAO index. Dickson et al. (2002), have shown, through analysis of long hydrographic records, that the system of overflow and entrainment that ventilates the deep Atlantic has steadily changed over the past four decades. From 1966 to 1992, the entire water column of the Labrador Sea has undergone radical change, getting much cooler (equivalent to a continuous heat loss of $8Wm^{-2}$ over a 26 year period) and fresher (equivalent to mixing in an extra 6m of fresh water at the sea surface) (Figure 10a). By lowering the density of the water column, the freshening has caused the steric height in the central Labrador Sea to be typically reduced by 8-10 cm, Dickson et al. (2002).

Dickson et al. (2002) believe that these long-term changes have led to sustained and widespread freshening of the deep ocean, and can be linked to the sustained evolution of the North Atlantic Oscillation (NAO) from its most extreme negative state recorded during winters of the 1960s to its most extreme positive state in the early 1990s. In particular, they propose that the freshening of the overflows into the deep Labrador Sea (Figure 10c) is due to the long-term freshening of the upper 1-1.5km of the Nordic sea. This is caused by effects of the amplifying NAO, including an increase in the direct export of sea ice from the Arctic Ocean, and an increase in the precipitation along the Norwegian Atlantic Current by approximately 15cm per winter.

We can see from the discussion above that changes in the phase of the NAO can potentially affect the SSH in the North Atlantic in two ways. Changes in the overlying atmospheric pressure gradient can potentially have a direct effect on the SSH. But oceanographic changes resulting from the wider effects of the NAO may also be detectable.

Figure 10: (a) Salinity changes in the central Labrador Sea since 1950, indicating a rapid and long-term freshening throughout the entire water column. (b) Paths of two main overflows of deep MOC water across the Greenland-Scotland ridge (dashed lines). (c) Time series of salinity measurements for overflow water, named and colour coded to match locations in (b). All figures from Dickson et al. (2002).

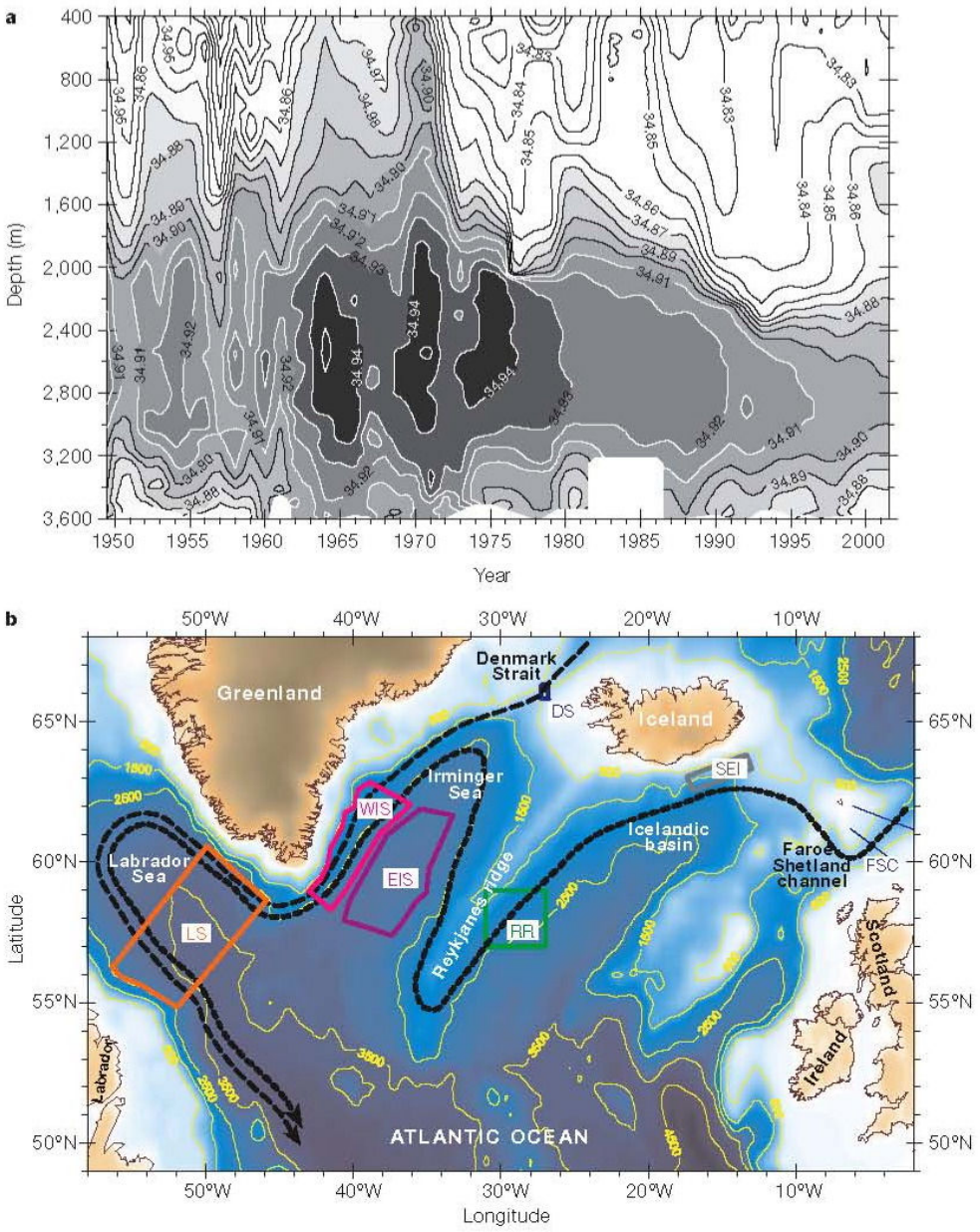

(c)

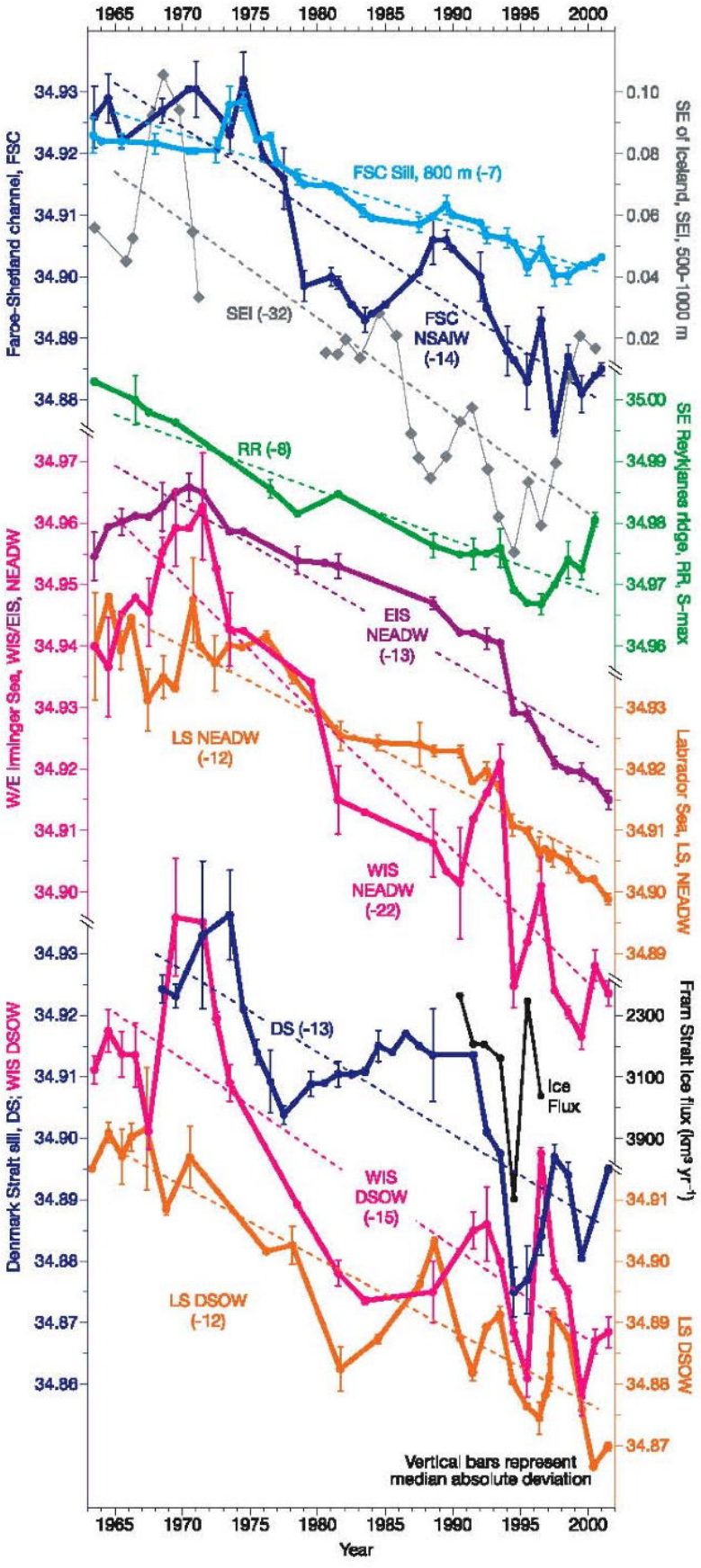
1965
1970
1975
1980
1985
1990
1995
2000
Faroe-Shetland channel, FSC
SE of Iceland, SEI, 500-1000 m
SE Reykjanes ridge, RR, S-max
W/E Irminger Sea, WIS/EIS, NEADW
Labrador Sea, LS, NEADW
Denmark Strait sill, DS; WIS DSOW
Fram Strait Ice flux (km³ yr⁻¹)
LS DSOW
FSC Sill, 600 m (-7)
SEI (-32)
FSC NSAIW (-14)
RR (-8)
EIS NEADW (-13)
LS NEADW (-12)
WIS NEADW (-22)
DS (-13)
Ice Flux
WIS DSOW (-15)
LS DSOW (-12)
Vertical bars represent median absolute deviation
Year

Chapter 3

Data types used in the method:

This chapter discusses the sources of the various data sets that have been used in this study: the Argo float array programme, the OCCAM (ocean circulation and climate model) model and the Jason satellite altimetry. We also discuss how Argo floats and satellite altimetry were simulated in OCCAM, so that our inversion methods could be tested.

ARGO data:

Argo is a global array of 3,000 free-drifting profiling floats. These floats are designed to measure the temperature and salinity of the upper 2000 m of the ocean. Argo deployments began in 2000 and by the end of 2005 the array was over 75% complete (Figure 11), and the number of floats is continually increasing.

When the network is complete, it will provide 3,000 temperature and salinity profiles and upper ocean velocities, distributed over the world oceans (approximately a 3° grid), every ten days. In comparison, the WOCE programme collected 20,000 temperature and salinity profiles over an eight year period between 1990 and 1998. For the first time this network allows for the continuous monitoring of the temperature, salinity and velocity

structure of the upper ocean. The data is made public within hours of collection.

Figure 11: Locations of the 1918 currently deployed ARGO floats, as of July 2005.

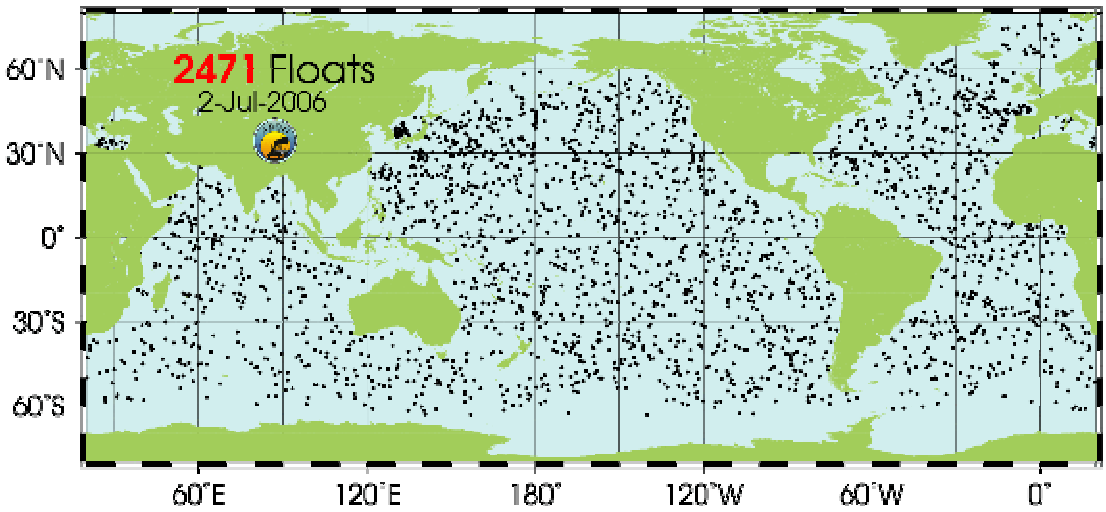

An Argo float is battery-powered and autonomous (Figure 12). A typical measurement cycle is shown in Figure 13. Each float spends most of its time drifting at 2000 m depth, where they are stabilized by a built-in hydraulic bladder. At 10-day intervals, the floats pump fluid into an external bladder and move up to the surface over about 6 hours, measuring temperature and salinity as they rise. When the floats reach the surface they transmit the profile information to orbiting satellites, which also obtain the float's position. The bladder then deflates, allowing the float to sink back down to 2000m, where it drifts until the cycle is repeated. The floats are designed to make about 150 such cycles (Woods Hole Oceanographic Institution, 1999).

Figure 12: The Argo float design.

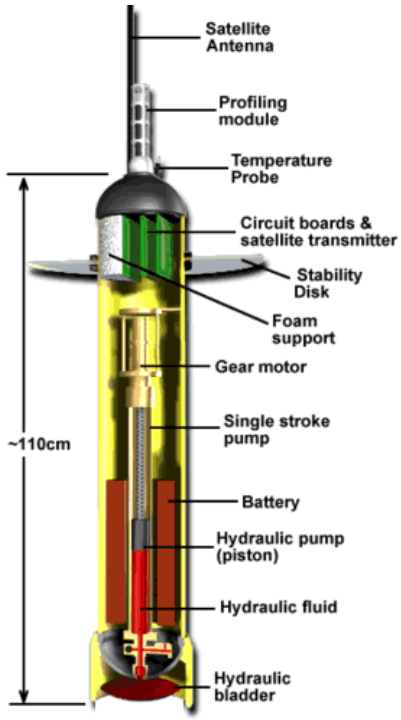

Figure 13: Schematic of ARGO float cycle.

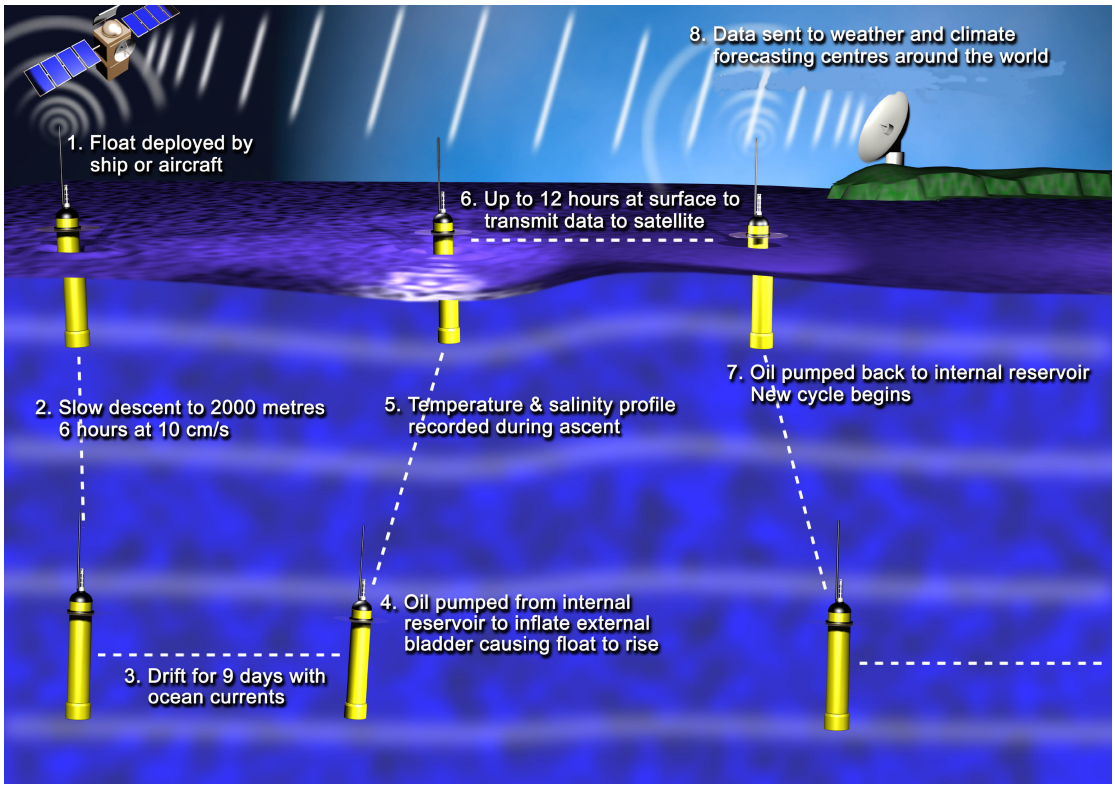

Float data was obtained from http://www.coriolis.eu.org/. We used corrected data, which has been pre-processed to remove any flagged or missing profiles, in netCDF format. However, further processing was necessary in order to ensure only data with sensible pressure, temperature and salinity values were included in our inversion. Additionally, we only used profiles which contained at least 10 measurements to guarantee that bad casts were excluded. Absent data take the value 99999 (see Chapter 5 for more details).

OCCAM Model:

Model details

The OCCAM model is based on the Bryan-Cox-Semtner ocean general circulation model (Webb et al., 1997; Webb et al., 1998). The version we use has a global geographic coverage at a resolution of ¼ degree latitude x ¼ degree longitude. The model contains 36 depth levels, ranging in thickness from 20m near the surface to 255m at 5500m (Table 1). It was run for a 14 year simulation period. The main variables stored are **u**, the horizontal velocity, T the potential temperature and S the salinity. The other variables, P the pressure, **w** the vertical velocity and ρ the density can be calculated from these other values if need be. In general, temperature, salinity and the three components of velocity define the state of the ocean. The temperature variable is stored as potential temperature (relative to a pressure of one atmosphere) because this remains constant under adiabatic changes in pressure.

The horizontal grids

If a global model uses a Mercator grid everywhere, then convergence of the meridians near the North Pole means that the spacing between grid points becomes very small, and at the pole itself you would get a singularity. This requires the model time-step to be small, and requires a large amount of

computation. To overcome this problem, the OCCAM model is split into two parts, called Model 1 and Model 2. Model 1 uses a standard Mercator grid and covers the Pacific, Indian and South Atlantic Oceans. Model 2 covers the North Atlantic and Arctic Oceans and uses a rotated grid, which has its poles on the Equator in the Indian and Pacific Oceans. It is oriented to match Model 1 at the Equator in the Atlantic. A simple channel model connects the two grids through the Bering Strait. The two model grids have a resolution of one quarter of a degree in both longitude and latitude. Figure 14 shows an example of the SSH extracted from the rotated model.

The vertical grid

The model has thirty-six levels in the vertical. These range in thickness from 20m near the surface to 255m at a depth of 5500m. (Webb, Cuevas et al., 1998) (Table 1).

For this project we used the 5-day averaged files from the model 2 grid in the North Atlantic for the ¼ degree resolution model kindly provided by Dr. Andrew Coward, National Oceanography Centre Southampton. We chose the 5-day output as this was easy to match with the Argo float and Jason altimeter data for comparison.

Table 1: Vertical levels in the OCCAM model

OCCAM vertical grid settings. All depths in metres, but note: internally the model uses centimetres

k	**t-box thickness**	**distance between**	**t-pt depth**	**Bottom of t-box**
		t-points		
	(dz)	(dzw)	(zt)	(zw)
0		9.86946		
1	20.00000	20.55911	9.86946	20.00000
2	21.19713	21.92465	30.42857	41.19713
3	22.75355	23.69704	52.35323	63.95068
4	24.76980	25.98805	76.05027	88.72048
5	27.36958	28.93379	102.03832	116.09007
6	30.70166	32.69565	130.97211	146.79173
7	34.93955	37.45820	163.66776	181.73128
8	40.27707	43.42179	201.12596	222.00835
9	46.91741	50.78758	244.54775	268.92576
10	55.05351	59.73280	295.33533	323.97927
11	64.83814	70.37598	355.06813	388.81741
12	76.34513	82.73558	425.44410	465.16254
13	89.52746	96.69041	508.17968	554.69000
14	104.18343	111.95524	604.87010	658.87343
15	119.94538	128.08578	716.82534	778.81881
16	136.30297	144.52066	844.91112	915.12178
17	152.66255	160.65512	989.43178	1067.78433
18	168.43022	175.92725	1150.08690	1236.21455
19	183.09483	189.89180	1326.01415	1419.30937

20	196.28768	202.26245	1515.90595	1615.59705
21	207.80598	212.91698	1718.16840	1823.40303
22	217.60180	221.87305	1931.08538	2041.00482
23	225.74829	229.24868	2152.95843	2266.75311
24	232.39785	235.22084	2382.20711	2499.15096
25	237.74326	239.99061	2617.42795	2736.89423
26	241.98773	243.75842	2857.41856	2978.88195
27	245.32516	246.70897	3101.17698	3224.20712
28	247.92924	249.00381	3347.88595	3472.13636
29	249.94890	250.77921	3596.88976	3722.08526
30	251.50799	252.14711	3847.66897	3973.59325
31	252.70719	253.19770	4099.81608	4226.30044
32	253.62703	254.00263	4353.01378	4479.92747
33	254.33107	254.61818	4607.01640	4734.25854
34	254.86907	255.08824	4861.63458	4989.12761
35	255.27966	255.44681	5116.72282	5244.40727
36	255.59273	127.83037	5372.16963	5500.00000
37			5500.00000	

Figure 14: Example SSH output (in cm) from the OCCAM Model 2, which uses a rotated grid.

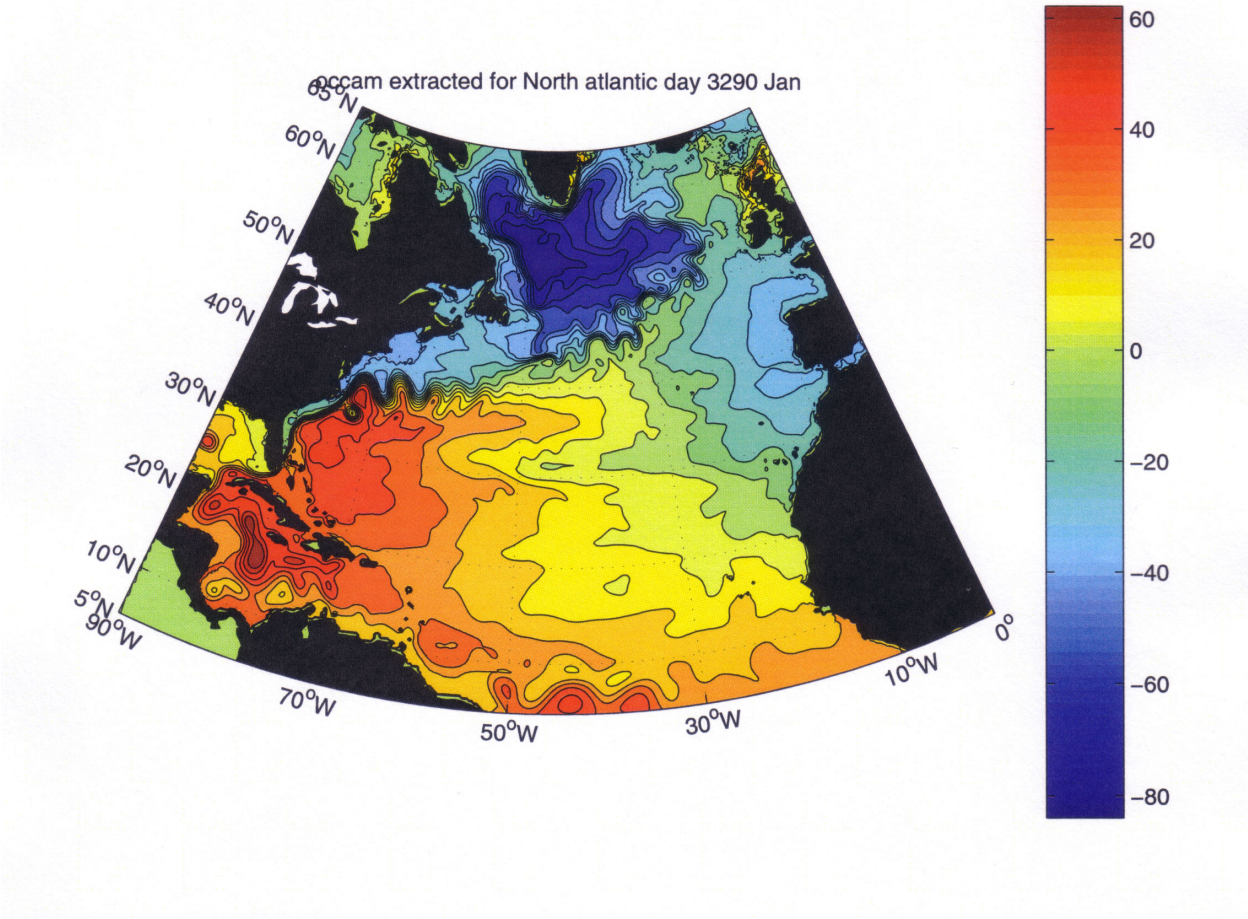

Simulating Argo floats in the OCCAM model

To create a working "model" system we have simulated Argo floats in OCCAM, extracting salinity and potential temperature profiles from the model to apply the Bernoulli function to. The OCCAM model used was the 6 hourly wind forced run in the North Atlantic, which gives 5-day mean average values. The float trajectories on a set level of 1000m were calculated by interpolation of the velocity field in time and space using a predictor/corrector routine (Marsh and Megann, 2002). This routine calculated the motion of a single particle (representing the Argo float) in the model over time. At each 10-day time step this predicted position was then corrected to the nearest grid point in the model. Because the floats are located in the North Atlantic, this routine had to work in the rotated grid model, before converting float positions back to the corresponding latitude and longitude values.

As for the real Argo floats, vertical temperature and salinity profiles were extracted every 10 days along with the latitude and longitude values of each profiling station. These temperature and salinity values are then solved using the Bernoulli function to predict the SSH. Station pairs were obtained for the floats and streamlines are created for these, by seeking crossings of the modified potential temperature versus salinity distribution amongst the eight

nearest neighbouring stations. There is an extra test to check these eight nearest neighbours are all clustered within reasonable distance of each other, and are therefore likely to have the same water properties. From the Bernoulli inverse a set of simultaneous equations are obtained and these are solved by singular value decomposition (SVD). This is outlined in much more detail in the next chapter. Once the slope of the sea surface is known, the barotropic reference velocity may be determined and ocean circulation can be estimated. This surface circulation can later be combined with the dynamic height relative to the surface to calculate the total geostrophic circulation.

The Sea Surface Height (SSH) for the OCCAM model at each of the "float" positions was also extracted for later comparison with the Bernoulli inverse results. Exactly the same method is applied to the "simulated floats" from the OCCAM model, where we know the true solution, as is applied for the "real" Argo floats. The simulated method therefore gives us a clear idea of how well the new method is performing before applying it to the real data, where we do not know the true solution.

To allow comparison, I have used the original positions from Cunningham (2000) as our "simulated float" starting points (Table 2). These are the CONVEX cruise station positions.

Table 2: Simulated float starting positions, given in degrees longitude and latitude

latitude/ longitude	longitude/latitude
329. 39.	336. 39.
329. 42	336. 42.
328. 45.	336. 45.
328. 48.	332. 45.
327. 51.	333. 42.
326. 54.	333. 39.
331. 54.	340. 57.
332. 51.	338. 57.
331. 48.	335. 58.
336. 48.	333. 58.
335. 51.	331. 58.
335. 54.	330. 57.
339. 54.	329. 59.
339. 51.	326. 59.
340. 48.	324. 59.
344. 48.	320. 59.
344. 51.	319. 58.
345. 54.	321. 56.
348. 47.	323. 54.
348. 45.	343. 57.
347. 42.	346. 56.
343. 42.	348. 55.
344. 45.	340. 42.
	340. 39.

340. 45.

Jason Altimetry:

Jason-1 was launched on December 7th 2001. Built around the Proteus spacecraft bus, the Jason-1 satellite carries five instruments: an altimeter, a radiometer, and three location systems. It has been launched into a 1,300-kilometer orbit with a ten-day repeat cycle, identical to that of Topex/Poseidon, which covers 90% of the world's ice-free oceans every ten days (Figure 15). Jason-1 follows on from Topex/Poseidon and continues to provide data of similar quality. Jason-1 is also expected to complement measurements collected by ARGO. In fact the name Argo was chosen to recall the story in Greek mythology of Jason and the Argonauts, to reflect the synergy between Argo and the Jason satellite altimeter missions.

The Jason data is extracted using the RADS (Radar Altimetry Database System) routine, rads2asc, written by Helen Snaith at the National Oceanography Centre. The following command is used:

rads2asc sat=j1 lat=55,60 lon=330,335 ymd=030101,030110 out=jul032 sel=0

Where the latitude and longitude are changed accordingly and the ymd, is the year month and day of the data.

Figure 15 : Jason-1's orbit covers 90% of the world's ice-free oceans every 10 days and is identical to that of Topex/Poseidon

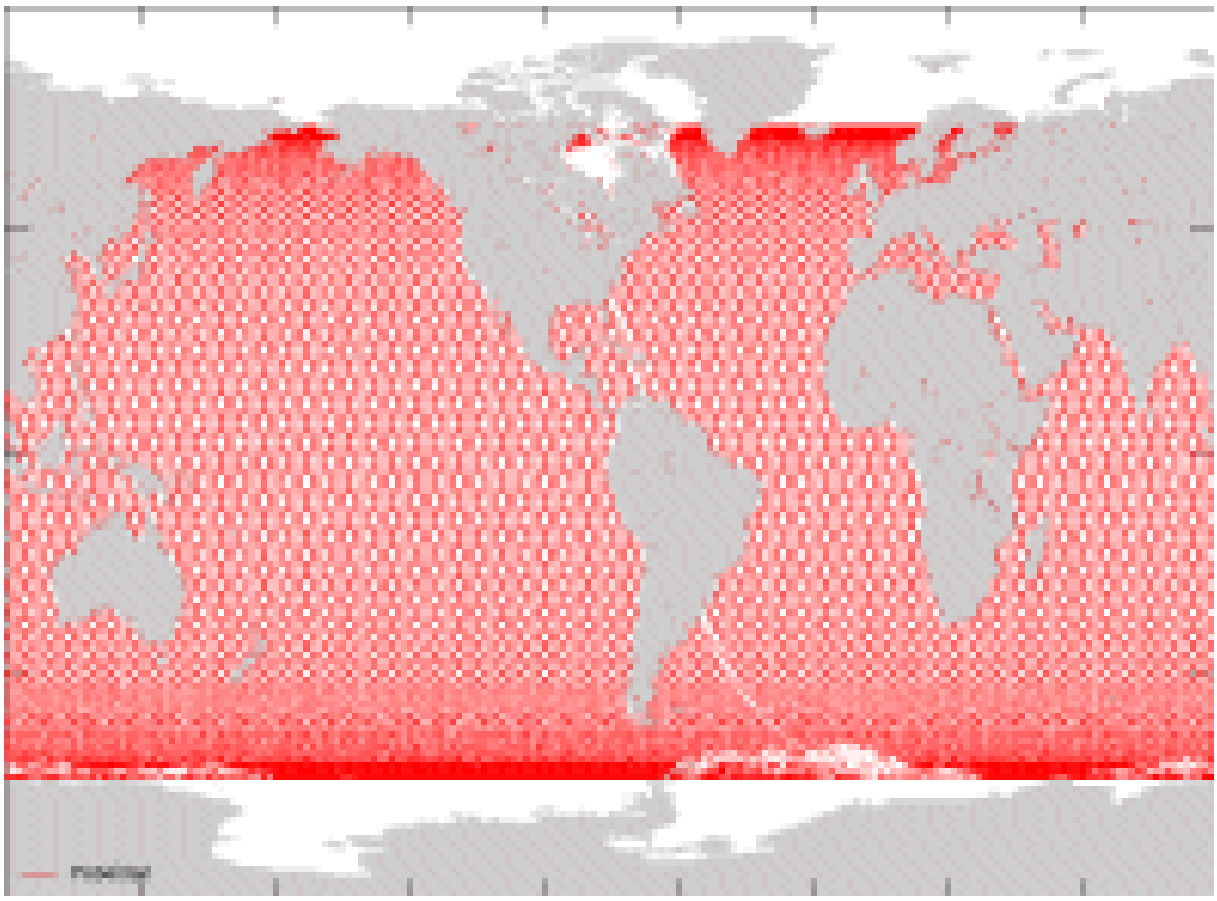

Simulating Satellite Altimetry in OCCAM model

In a similar manner to the floats, satellite altimetry for use in the Bernoulli inverse has been simulated in OCCAM. This was achieved by taking real TOPEX and Jason ground track locations and using these positions to extract SSH values from the model at these locations. The code for the simulated Argo floats was used, but the predictor/corrector routine was turned off to keep the tracks stationary in the model. We simply subtract 10-day snap shots from one another to obtain changes in SSH, ΔSSH.

Figure 16 shows the positions of the floats and satellite altimetry tracks used to extract data from OCCAM in the simulated method. For comparison, Figure 17 shows the positions of the Jason satellite altimetry tracks and the ARGO float positions used for the "real" surface solutions in Chapter 5.

Figure 16. Simulated ARGO floats (blue diamonds) and Jason altimetry (green tracks) in OCCAM.

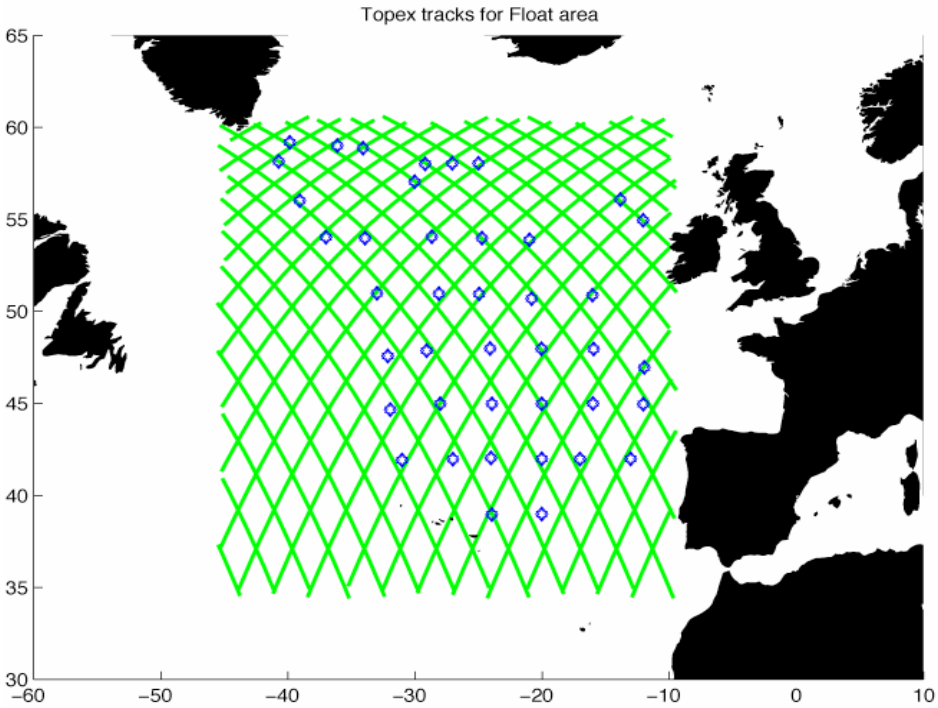

Figure 17: Positions of real ARGO floats (crosses) and JASON tracks (blue lines) for (a) a 1st solution, and (b) a 2nd solution over a larger area.

(a)

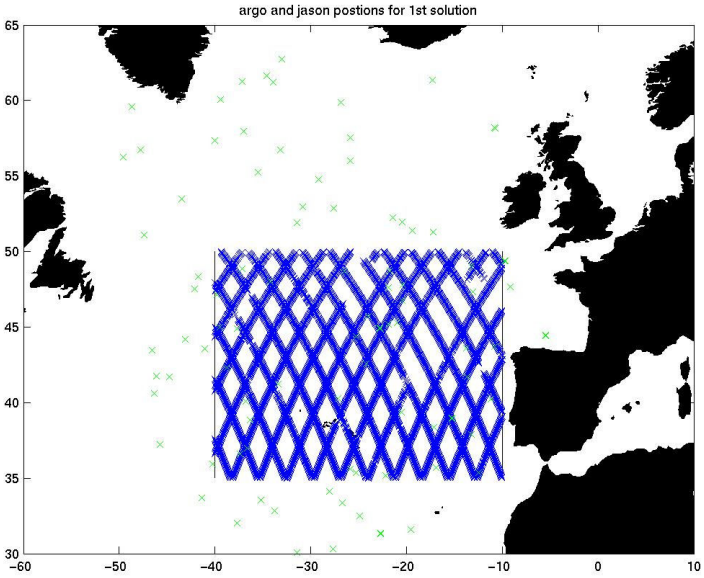

(b)

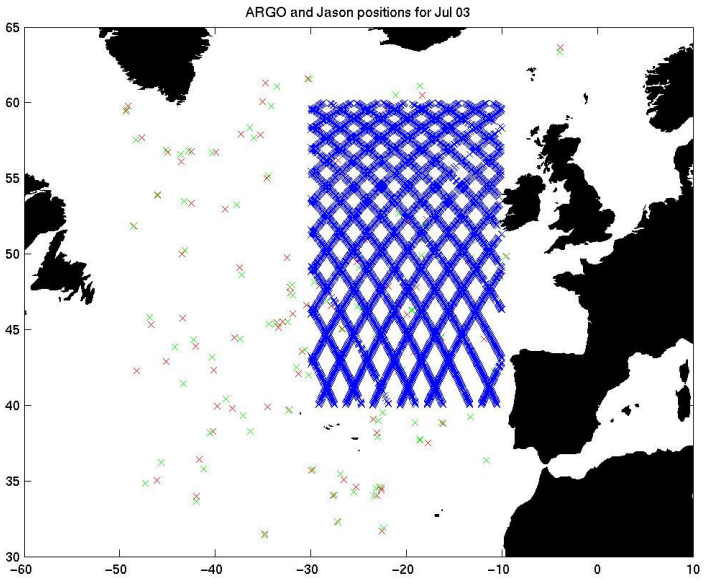

Summary of data processing procedure:

The whole programming process for all the data sets and solutions used in this project is summarised in Figure 18. The starting data sets, shown along the top, are the OCCAM model, the ARGO temperature and salinity profiles and Jason altimetry. To simulate the real world data we obtain temperature and salinity profiles, and the SSH at TOPEX satellite track positions, from the OCCAM model using the routines described in this chapter.

These various data sets are then stepped through the different programming paths described in Chapters 4-6 to obtain our solutions, shown at the bottom of Figure 18. Firstly we obtain point solutions, both with and without the satellite altimetry. Secondly we obtain a surface solution with and without altimetry. Finally we fit a GAM to the model float only point solution.

Figure 18: Flow Chart for data Processing:

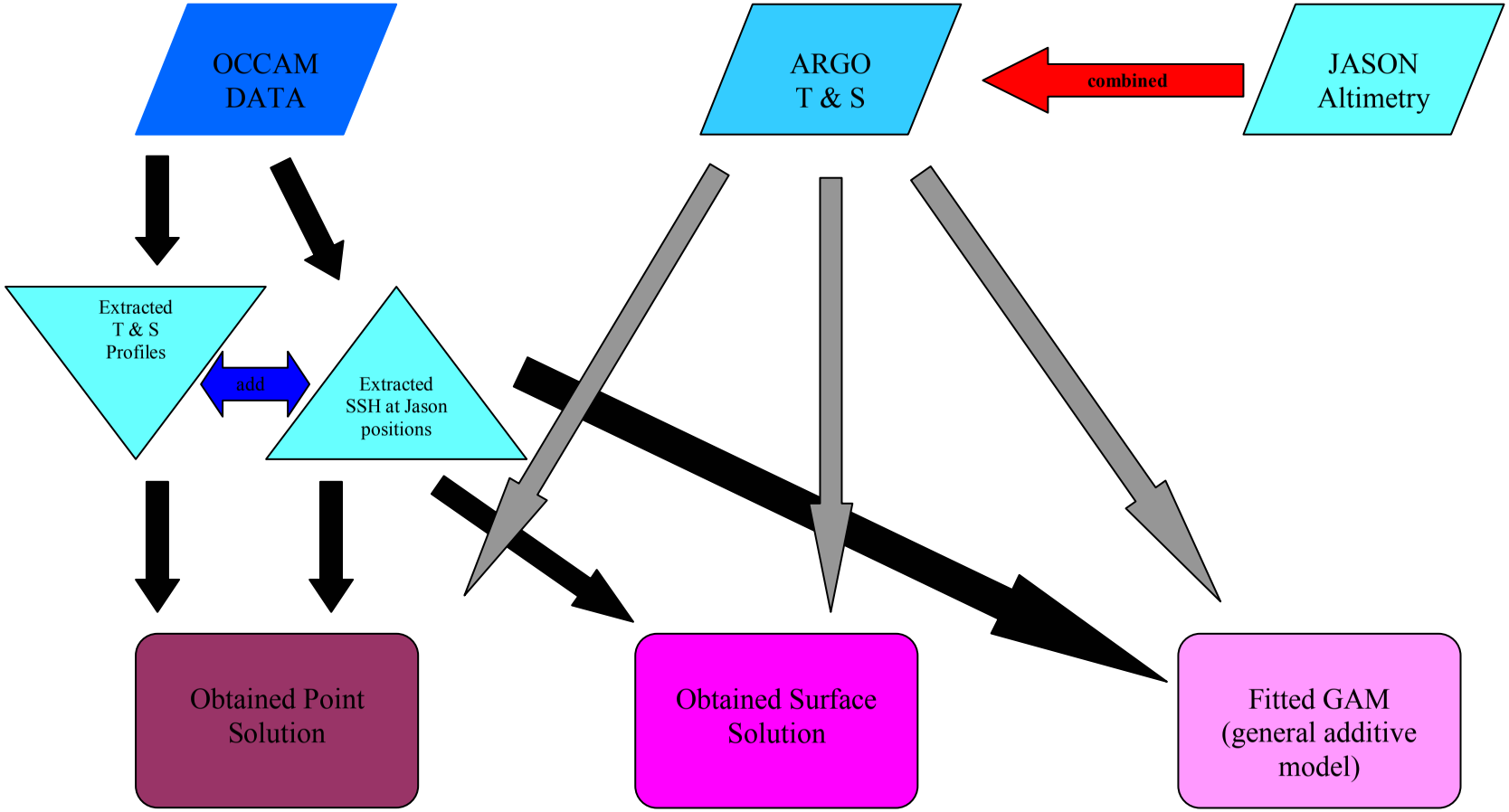

Key:
T: Temperature
S: Salinity
SSH: Sea Surface Height

Acknowledgements for the data used in this project:

OCCAM model dataset:

This was used with kind permission of Dr. Andrew Coward in the James Rennell Division at National Oceanography Centre, Southampton.

ARGO dataset:

These data were collected and made freely available by the International Argo Project and the national programmes that contribute to it. (http://www.argo.ucsd.edu, http://argo.jcommops.org). Argo is a pilot programme of the Global Ocean Observing System.

RADS/Jason altimetry dataset:

RADS data, provided by the Technical University of Delft, (Naeije et al., 2005)

Chapter 4

Background to Inverse Methods

What is an Inverse Method?

According to Wunsch (1996), "the ocean inverse problem, is the problem of inferring the state of the ocean circulation, understanding it dynamically and even perhaps forecasting it, through a combination of theory and observations." In a forward problem we would start with a set of equations that describe the known system and then try to predict what we should observe. In contrast, in an inverse situation we already have these observations and data. What we then wish to achieve is a description of the system producing these observations.

There are three main types of inverse methods used in oceanography, the Beta-Spiral, the Box Inverse and the Bernoulli Inverse methods. When these three methods are compared (Killworth and Bigg, 1988), it can be seen they span a range of length scales. The Beta-Spiral method is fundamentally a local calculation, generating an estimate of the velocity vectors (**u**,**v**) at a

given point or set of points, whereas the Bernoulli and Box inverses can handle a much wider range of data, and aim to give a large scale description of the oceanic circulation. The most popular of these methods is the Box Inverse but this project has chosen to use the Bernoulli solution. This method was first developed by Peter Killworth in 1986 (Killworth, 1986; Grose et al., 1994) and modified in 2000 by Stuart Cunningham (Cunningham, 2000). We work with this modified method, which uses the modified potential temperature and salinity variables. Combination of the Bernoulli inverse with satellite altimetry has only been attempted in one published study, using the original method, in 1994 on the Iceland-Faroe front (Tokmakian, 1994).

This chapter gives a brief background to the other methods, before going into greater detail on the Bernoulli Method used in this study.

The Beta-Spiral Method:

The origins of the Beta-Spiral Method are fully discussed in (Scott and Stommel, 1978). At a given station, the method assumes thermal wind balance in both horizontal directions and buoyancy conservation. The 3D velocity vector at some reference depth provides three unknowns. The horizontal velocity at other selected depths is computed from the thermal wind and vertical velocity. Approximate conservation of density at each of these depths produces an over-determined system of equations for the

reference values (**u**,**v**,**w**), which are solved as a linear least squares problem for example using singular value decomposition (SVD). Conservation of mass between stations can be used to link them together.

The Box Inverse Method:

The development of this method for oceanographic purposes is due to Wunsch (1978). It requires a closed volume of ocean surface surrounded by a set of stations, and assumes thermal wind balance and approximate mass and buoyancy conservation. A reference level for the normal velocity is assumed and all other normal velocities are calculated as offsets from this using thermal wind. Conservation of buoyancy (or temperature) is then applied to each collection of buoyancy ranges. Each conservation equation yields one equation for the collection of unknown reference velocities so that the system is underdetermined. Selecting the optimal solution from the null space of permissible solutions then solves the system: "it is assumed in the method that the evaporation and precipitation are in balance (or negligible), and therefore the amount of water flowing into the box (closed area) must equal the amount of water coming out" (Wunsch, 1978). Because the system of equations is underdetermined we need to add additional information to extract a solution. This is usually done by taking the solution closest to the initial guess.

Bernoulli Method:

In 1986 Peter Killworth produced an inverse method for defining the large-scale ocean circulation (Killworth, 1986). Unlike the other methods, the Bernoulli inverse requires no information about the horizontal velocity gradient. The method is designed for use with widely spaced and vertically sparse data, making in an ideal choice for an array of floats, such as the Argo network. By assuming that density and potential vorticity are conserved on a streamline a set of simulations equations are obtained in terms of the Bernoulli function. These may then be solved by linear regression to give the Sea Surface Height solution to the problem. Unlike other inverse methods, such as the box inverse, we can obtain a unique solution to the problem, rather than a range of values from which we then have to determine the best guess.

Despite these advantages, the box inverse has been much more widely used in the oceanographic community, and has had many subsequent developments as a result. The Bernoulli method lay dormant until Cunningham (2000) modified the method to use modified potential temperature instead of potential vorticity, so that it could be more easily applied to existing oceanographic data. The increasing availability of high-performance computing resources in the last decade has also made it much easier to practically use this method.

How do we obtain Sea Surface height from the Bernoulli function?

In this section, we first explain the general principles behind the Bernoulli method, before discussing modified potential temperature and how this is used as a conserved variable in the Bernoulli function. Then we show how the linear problem is solved, using the singular value decomposition method, to obtain an SSH solution

Figure 19 shows three conserved surfaces (C_1, C_2, C_3). In our case these are three different layers of water with their own unique properties. Conservation means that the flow lines (the narrow lines with arrows in Figure 19) are restricted to their respective surfaces. These flow lines have the properties of the surface that they are on. Where surfaces C_1 and C_2 intersect, the properties of both surfaces must be conserved along the blue line of intersection.

If we then introduce the third surface, C_3, which also intersects the other two surfaces, the properties of this new surface must also be conserved at the line of intersection. The only way that this condition can be met is if surface C_3 is a function of the other two intersecting surfaces, C_1 and C_2:

Equation 2

$$C_3 = fn(C_1, C_2)$$

Figure 19: The figure shows 3 different water layers with their own unique properties. The surfaces are conserved which means that the flowlines (the lines with arrows) have to remain on their respective surface. Therefore the intersection between surfaces (shown in a blue line between surface C_1, C_2 and C_3) is a point at which a streamline must be conserved for all three surfaces.

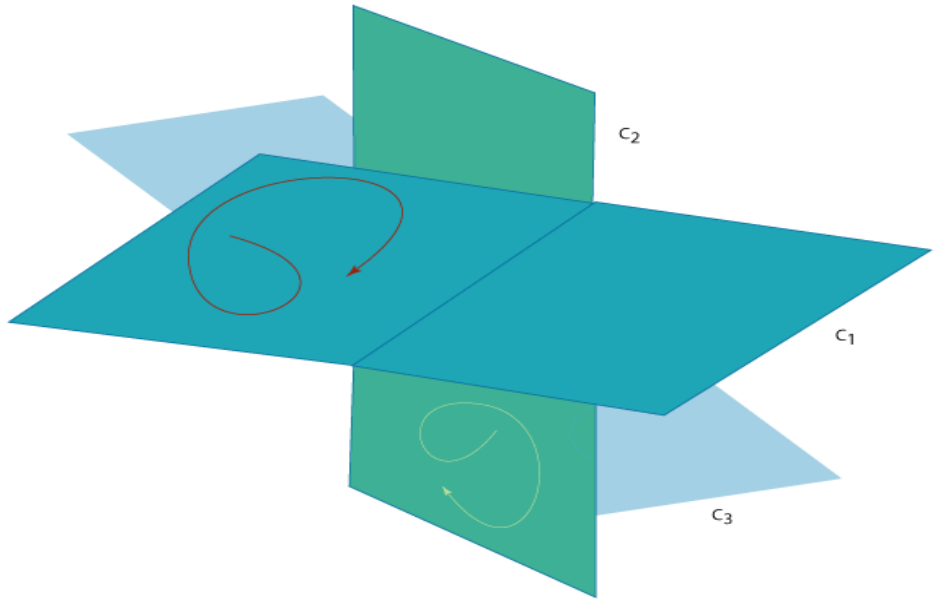

The conserved surfaces in Figure 19 can represent any conserved function or variable (Bernoulli function, Montgomery function etc.). In our case the Bernoulli function is used. In the original Bernoulli inverse of Killworth (1986) density and potential vorticity were used as the conserved variables, C_1 and C_2. The third surface C_3 was the Bernoulli function. In this project we instead

use salinity and modified potential temperature as our conserved variables, following the method of Cunningham (2000).

We now take profiles at two stations or float positions and extract the temperature and salinity through the water column, as in Figure 20 below. The temperature is later converted to modified potential temperature, as explained later in this section.

Figure 20: Salinity and temperature profiles at two stations. Values are extracted at depths Z_1 and Z_2, indicated by the dark blue horizontal lines. These are the same Z_1 and Z_2 used later in equation 3.

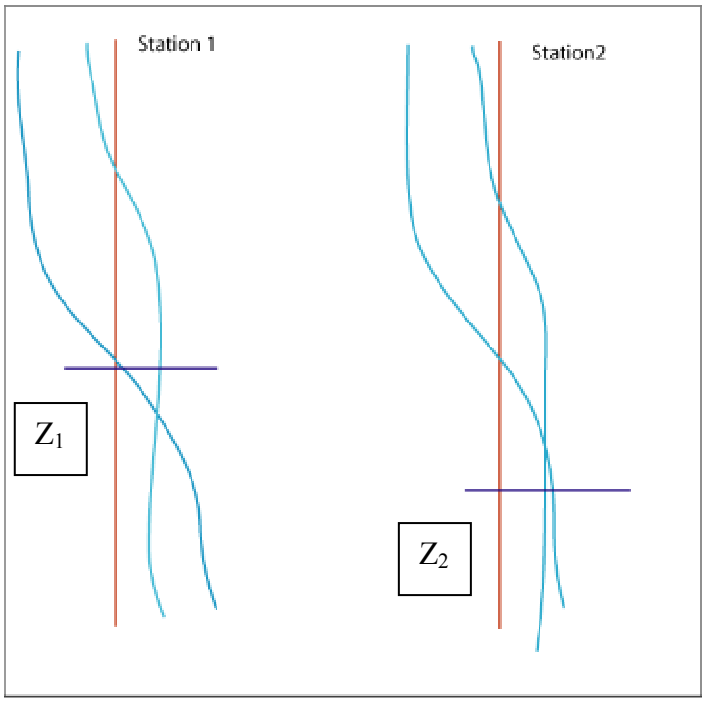

These temperature and salinity profiles can also be plotted against each other as in Figure 21, where C_1 and C_2 are modified potential temperature and salinity. At depth Z_1 in profile 1, and depth Z_2 in profile 2, the temperature and salinity values for the two profiles intersect, forming a crossing point.

From our earlier discussion and equation 1, a function of these conserved temperature and salinity variables, i.e. the Bernoulli function, is also conserved between these points.

Figure 21: The functional relationship between the two conserved variables C_1 and C_2 .S_1 and S_2 are the profiles extracted at the two stations in figure 2. The blue dot denotes the crossing point of these two stations.

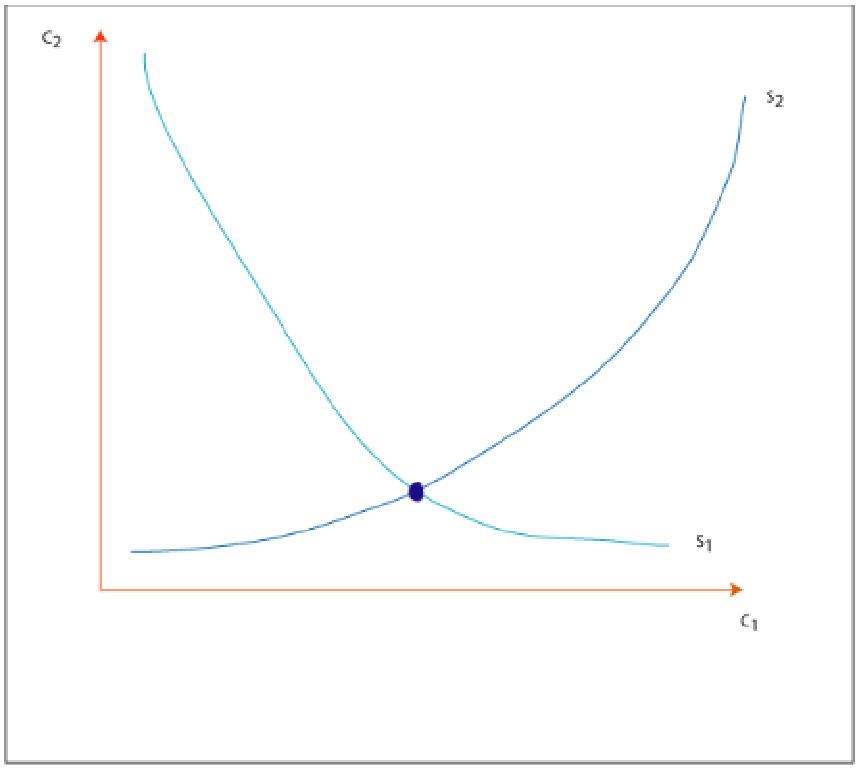

From Figure 21 we now have the following equation:

Equation 3 $$C_3(Z_1) = C_3(Z_2)$$

Where Z_1 and Z_2 are the depths at our two stations or float positions. A crossing point between the two stations S_1 and S_2 has been obtained. We now expand the equations to include the Bernoulli function.

The Bernoulli function can be expressed as:

Equation 4 $$B = P + \rho g z$$

Where P is the pressure and the ρgz term is the variation of potential energy within the water column.

If we take equation 4 and integrate this function from the surface to depth z, we can obtain the following new equation:

Equation 5 $$B = B_0 + \int_0^z g\rho dz$$

As we are integrating from the surface, we have replaced P with B_0, which is the value of the Bernoulli function at the surface. This can also be written as:

Equation 6 $$B_0 = \rho_0 g \eta$$

where η is the unknown Sea Surface Height (SSH) and ρ_0 is the density integrated from the surface. The second term in equation 5, $\int_0^z zg\rho dz$, can be

obtained from the profile at each station position. Hence for a series of station points we obtain a set of simultaneous equations for an over-determined system in which the only unknown is the SSH.

In summary we have a series of simultaneous linear equations in the conserved variables, density and salinity, that we can solve for sea surface height. These can be solved using standard methods such as SVD. The details of this solution are given later.

Modified Potential Temperature:

We now explain how the conservative variable, modified potential temperature, which we use in this project is obtained from the temperature profile, according to the method of (Cunningham, 2000).

Ideally to meet the conditions explained above we need to choose variables that are conserved when water parcels are mixed, and are independent of changes in pressure. For example, salinity remains unchanged by physical processes in the ocean and only depends on the chemistry of the water, hence it is said to be conservative. In oceanography potential temperature (θ) is often used as though it is a conserved variable like salinity. However, (McDougall and Jackett, 2000) show that mixing fluid parcels from the real ocean leads to a maximum production of θ of about –0.4°C, meaning that θ is not truly conserved. However, it has been shown by (Macdonald, 2003) that potential enthalpy is more conservative than potential temperature by two orders of magnitude. Potential enthalpy is the enthalpy that a water parcel would have if raised adiabatically and without exchange of salt to the sea surface, where enthalpy is defined as the sum of the internal energy, U, plus the product of the pressure and the volume. U, is the sum of the total kinetic energy due to the motion of molecules, and the total potential energy associated with the vibrational and electric energy of atoms within molecules. Although enthalpy is a quantifiable state variable, the total enthalpy of a

system cannot be measured directly. The enthalpy change is measured instead.

Equation 7 **H = U + PV**

Where H is the enthalpy, U is the internal energy, P is the pressure and V is the volume. The enthalpy change is calculated from the final enthalpy of the system minus the initial enthalpy.

A simple linear combination of potential enthalpy and salinity gives us a new variable, modified potential temperature (Θ), also referred to as conservative temperature. This gives us (from McDougall and Jackett, 2000):

Equation 8 $$\Theta(S,\theta) = \frac{H(S,\theta,P=0)}{c} + 2.76664\times10^{-3} S$$

Where c is the specific heat capacity of water and the constant term, 2.76664×10^{-3} scales the value so that at 0°C we have $\Theta(0,0)=0$ and similarly at 20°C we have $\Theta(35,20)=20$, (Cunningham, 2000).

We now have a new functional relationship, which allows us to transform the Bernoulli function into a new variable E:

Equation 9 $$E = F(\Theta, S)$$

Solving the modified Bernoulli function:

Imagine we have a similar situation to that shown in Figure 21, but with three stations instead of two. Suppose a streamline exists from station one to station two and another streamline exists from station one to station three. We know the Bernoulli function, modified potential temperature and salinity are all conserved along these streamlines. We can now obtain a set of simultaneous equations for each pair of stations. These simultaneous equations are equations 10, 11, 12 and 13 below. Stations one and two intersect at depths z_1 and z_2, whereas stations one and three intersect at depths z_3 and z_4.

Equation 10 **Θ1(z1)=Θ2(z2)**

Equation 11 **S1(z1)=S2(z2)**

Equation 12 **S1(z1)=S2(z2)**

Equation 13 **Θ1(z3)=Θ3(z4)**

Equation 14 **S1(z3)=S3(z4)**

We have transformed B, the Bernoulli function into a new variable E (Equation 10), which is a linear combination of the two conserved variables B-gη and Θ, the potential temperature. The new variable, E, is itself conserved except for the unknown SSH contribution. We now have the equation:

Equation 15 $$\mathbf{E = B - B_{corr}}$$

B_{corr} is a scaling term added for numerical reasons, without it we end up subtracting two very small numbers (Cunningham, 2000).

Equation 16 $$\mathbf{B_{corr} = -393.4 - 3987.6\,\Theta}$$

We now have the following new simultaneous equations for the problem using this new variable E and our conserved variables Θ and S:

Equation 17 $$\mathbf{E1(z1) + g\eta 1 - E2(z2) - g\eta 2 = 0}$$

Equation 18 $$\mathbf{E1(z3) + g\eta 1 - E3(z4) - g\eta 3 = 0}$$

Where E is the Bernoulli function in the new modified form from equation 15 at our crossing points for the four simultaneous equations 11-14. g is acceleration due to gravity and η is the unknown SSH that we wish to determine. We can rearrange equations 17 and 18 to the following format:

Equation 19

$$g(\eta_1 - \eta_2) = -\{E_1(z_1) - E_2(z_2)\}$$

Equation 20

$$g(\eta_1 - \eta_3) = -\{E_1(z_3) - E_3(z_4)\}$$

For *n* stations and *m* crossings the rank of the problem is *n* -1 since one value of the SSH may be chosen. Generally there are many more known crossings than unknown station SSH's, *m*>*n*, so that the system of linear simultaneous equations is an over-determined problem. In the matrix solution seen later in this section, we rearrange this equation by dividing by g, so that only the unknown SSH which we wish to solve is on the left hand side. It should also be noted that for simplicity the Bernoulli function is still referred to as B in our matrices as it is more familiar and less easily confused. However, this is actually the modified Bernoulli function E.

Equations 19 and 20 are solved using the Singular Value Decomposition (SVD) method, which is explained in the next section

Singular Value Decomposition Method (SVD)

Singular Value Decomposition is a very powerful method for dealing with sets of equations or matrices that are either singular, or numerically very close to

singular. SVD allows us to diagnose the problems in a given matrix and can provide a numerical solution to a linear regression problem.

The least squares problem for the Bernoulli inverse method can be written in matrix form (Lawson and Hanson, 1974) as:

Equation 21 $$\mathbf{Ax} = \mathbf{y}$$

where **A**, the design matrix, is a real matrix with *m* rows and *n* columns. Here *m* is the number of crossing points and *n* is the number of stations or floats in the problem. **x** is the real *n*-vector of unknown SSH that we wish to solve. The new function E lies on the right hand side as the Bernoulli differences in a real *m*-vector **y**.

The solution to equation 21 is:

Equation 22 $$\mathbf{x} = \mathbf{A}^{-1}\mathbf{y}$$

However inverting the matrix **A** would be computationally very inefficient. The following equations 23-28 show how a solution is obtained using matrices and the SVD method, which eliminates these computational difficulties.

Any matrix (m×n) where the number of rows is greater than the number of columns can also be written as:

Equation 23 $$\mathbf{A} = \mathbf{U}S\mathbf{V}^T$$

The matrices **U** (m×m) and **V** (n×n) are orthogonal, which means that the inverse of these matrices equals their transpose. **S** (n×m) is the matrix consisting of a diagonal of singular values and zeros everywhere else.

Equation 24 $$\mathbf{U}^T.\mathbf{U} = \mathbf{V}^T.\mathbf{V} = \mathbf{I}$$

Where **I** is the identity matrix. If all the eigenvectors of the symmetric design matrix $\mathbf{A} . \mathbf{A}^T$ exist then,

Equation 25 $$\mathbf{U} . \mathbf{U}^T = \mathbf{I}$$

And similarly for **V**

Equation 26 $$\mathbf{V} . \mathbf{V}^T = \mathbf{I}$$

The natural inverse of **A** is $\mathbf{A}^{-1}$, so we can now rearrange equation 23:

Equation 27 $$\mathbf{A}^{-1} = \mathbf{V}S^{-1}\mathbf{U}^T$$

Where S^{-1} is the inverse of the singular values. We can now substitute for A^{-1} back into equation 22:

Equation 28 $$\mathbf{x} = \mathbf{V}\mathbf{S}^{-1}\mathbf{U}^T\mathbf{y}$$

Where **x** is the unknown SSH we wish to solve for and **y** the differences of the new Bernoulli variable, E for each station pair (the right-hand side of our equations 19 and 20).

In Figure 22 below a schematic of the matrices we wish to solve in this problem are shown. On the left hand-side we have the vector of Bernoulli differences y. On the right hand-side we have the design matrix A, which is a matrix of ones and minus ones denoting crossing points, and zeros where no crossing is obtained. Each crossing pair will be represented by a one and a corresponding minus one, as a result of us using the Bernoulli difference function. The x vector is the unknown SSH we wish to solve for. All the matrix dimensions are shown, where n is the number of stations or floats in our problem and m is the number of crossings that have occurred between these stations. The Bernoulli method assumes a constant single water mass. In practice because we are solving across a larger basin there are a number of water masses involved. To reduce the number of crossings between different water masses we restrict ourselves to local crossings. For this reason only the eight nearest neighbouring stations are checked for crossings, so that only crossings likely to be within the same type of water mass are used in the solution.

Figure 22: A schematic of the matrices to be solved for the problem.

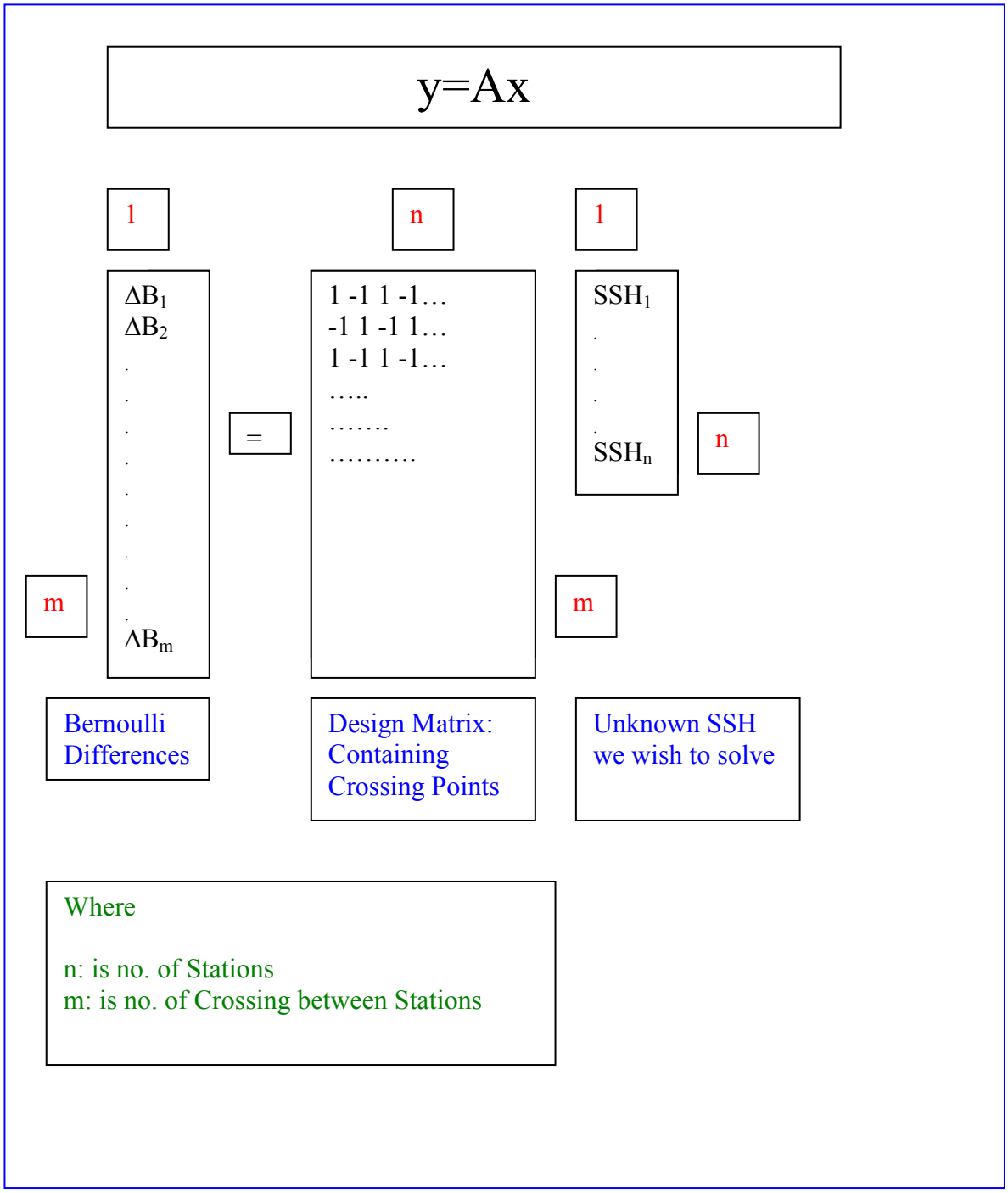

Results for inverse of OCCAM Model data:

Before moving on in the next chapter to the improvements we have made to this method by fitting a surface solution, we will examine our simulated floats in the OCCAM model, and use the extracted profiles of temperature and salinity from the model to produce a "point" solution.

Simulated ARGO floats in OCCAM:

The following figures demonstrate the use of the predictor/corrector routine to track the simulated Argo floats as they move in the OCCAM model, as outlined in Chapter 3. These plots show how the position of the floats changes over an increasing number of days.

Figure 23: Initial positions of the floats.

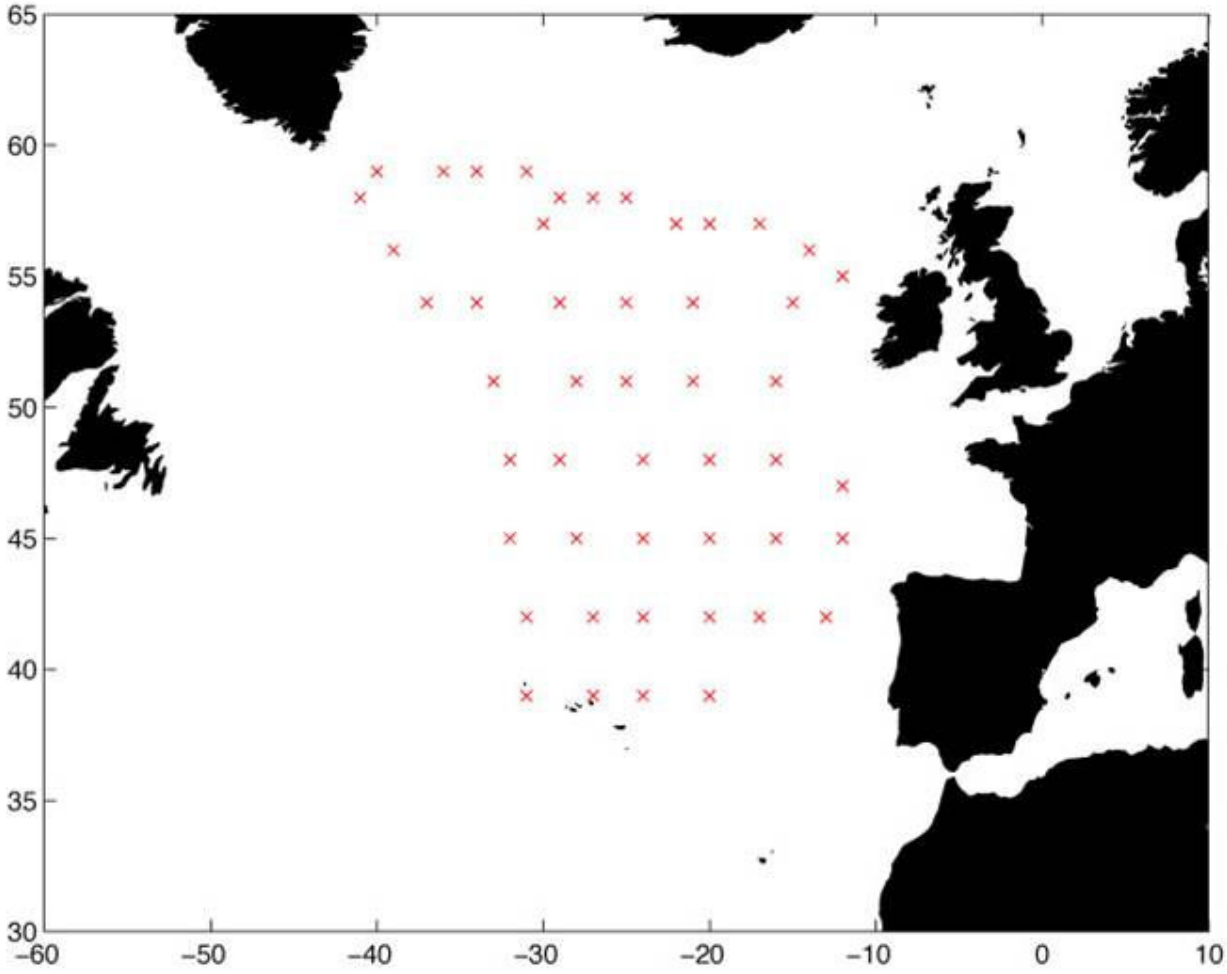

Figure 24: Float positions after drifting in the model for 25 days. The blue X marks the initial position and the red trail the motion to new locations.

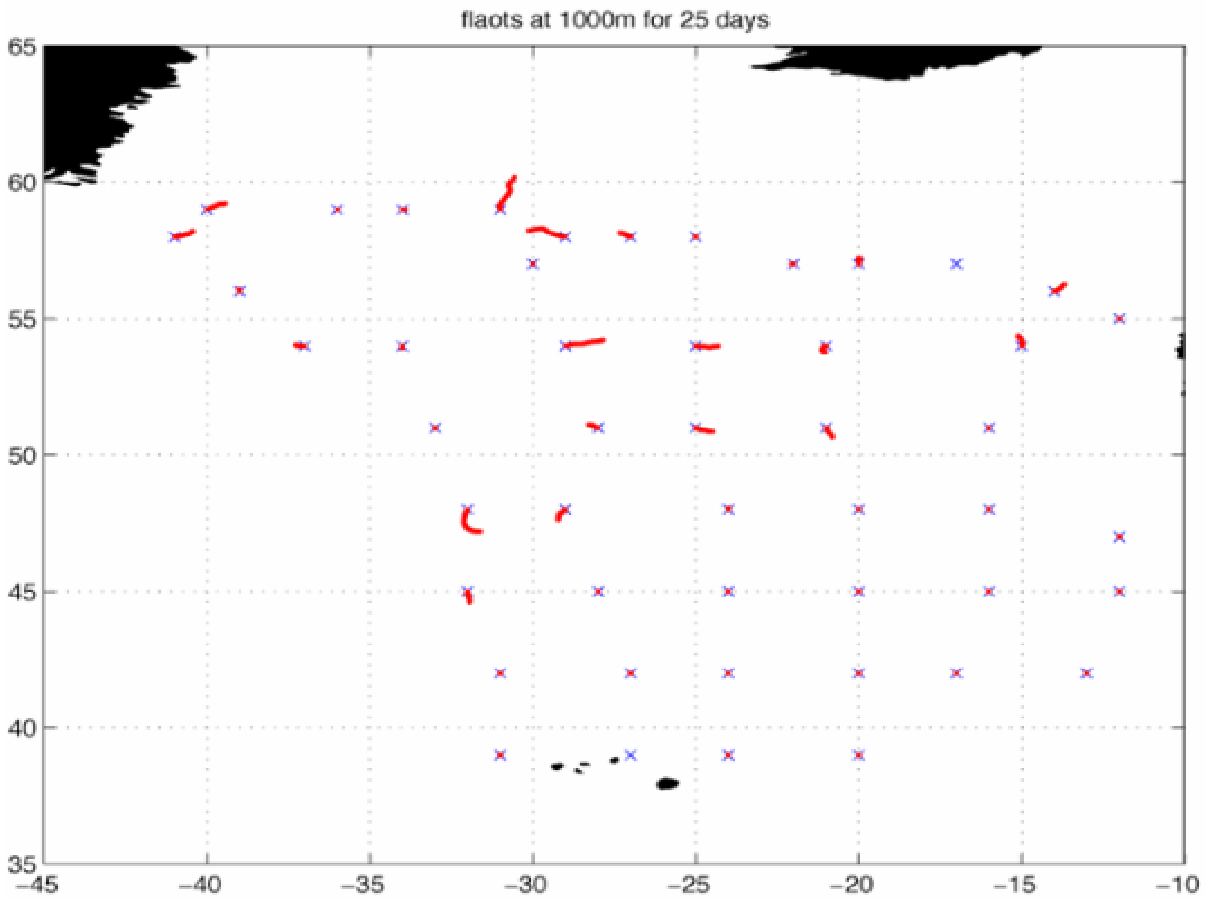

We can see that one or two of the floats (for example the float at approximately -27° W, 39° N) have not moved because they have hit topography (Figure 4, which plots these float locations onto a bathymetry map of the North Atlantic, shows that this float intersects the Mid-Atlantic Ridge). These floats have been omitted from the solution.

Figure 25: The floats after 100 days of projection. Blue trails mark motion of the floats from their starting positions (crosses)

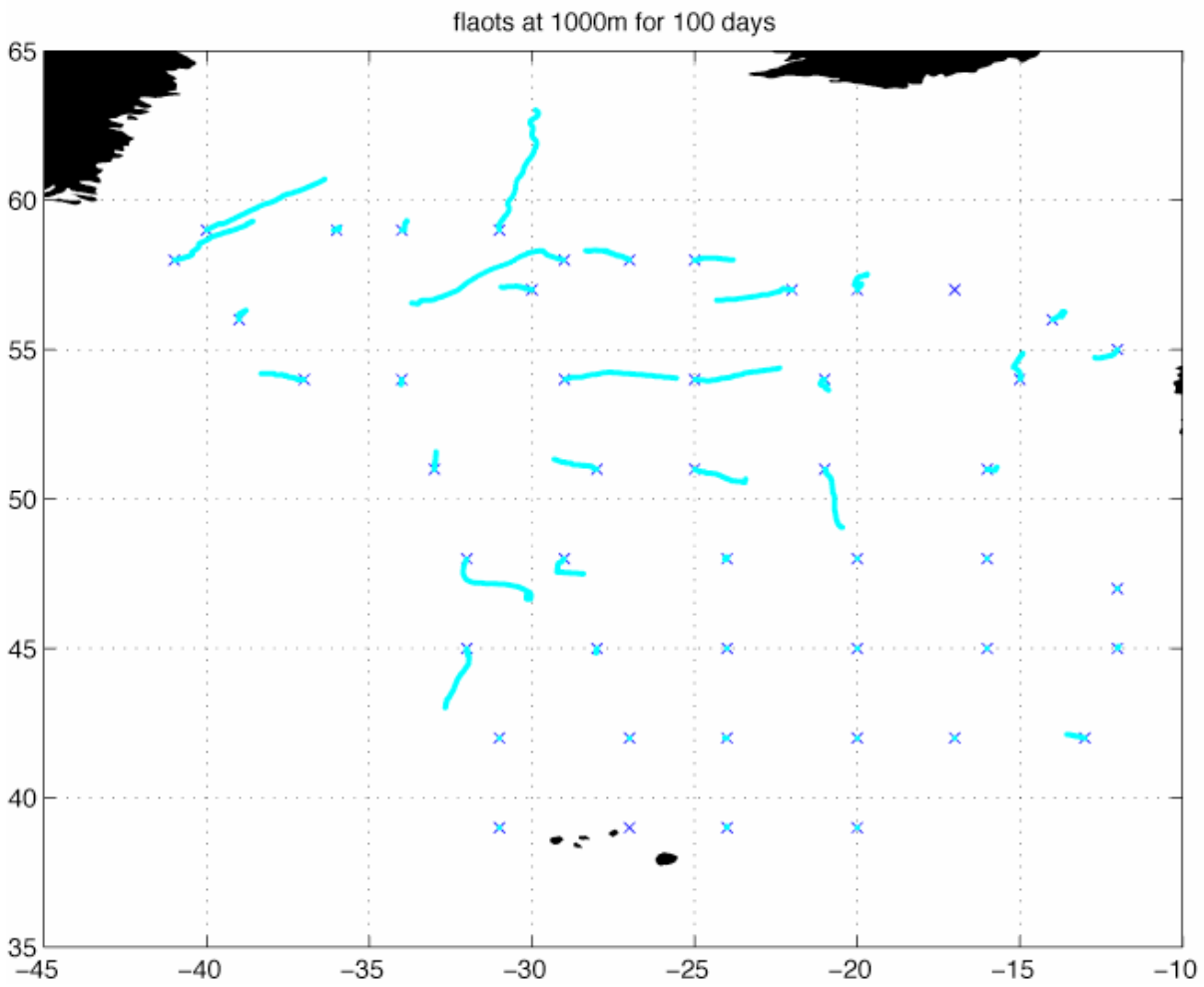

This figure shows that even after 100 days, many floats have hardly moved. Though we can accept that some of the floats will not move due to the obvious constraints of the topography in the bottom middle of the map, this does not explain why many other floats appear not to move at all either. We became concerned about this and decided to look at the actual velocity fields for some of these locations in the OCCAM model, to try and discover what was happening.

Figure 26: U Velocity field extracted from OCCAM. Velocities in ms^{-1} (vertical axis), extracted from the OCCAM model at different levels, are plotted for each float position (numbered along the horizontal axis).

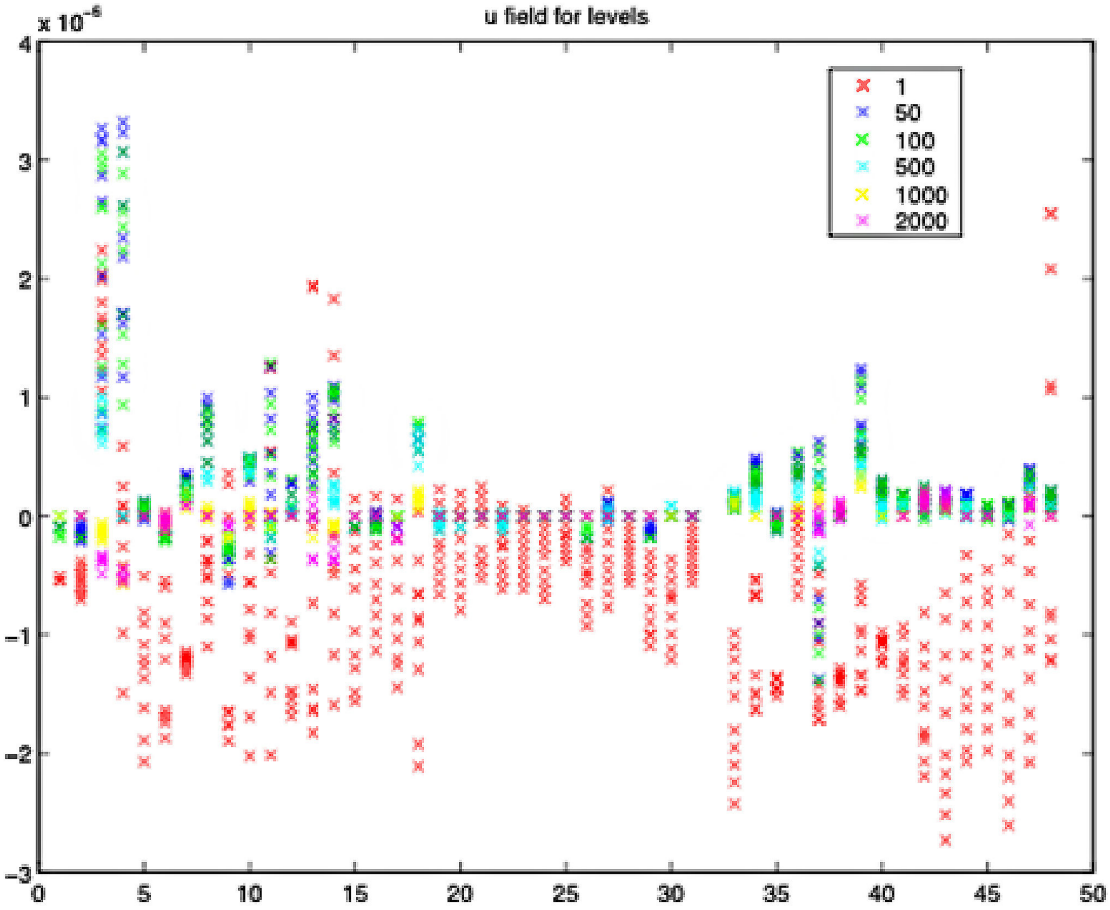

Figure 27: V velocity field extracted from OCCAM.

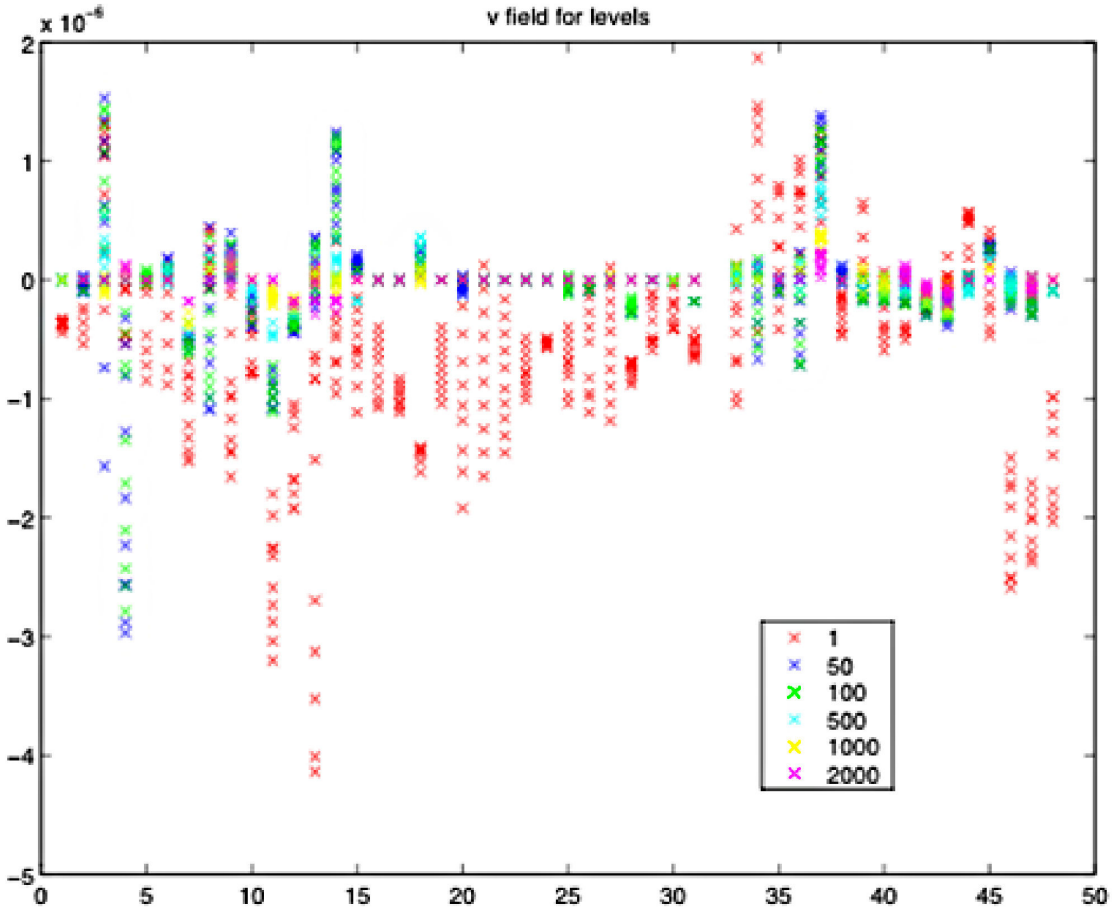

These figures may be a little difficult to interpret at first. What we have done is to extract the velocity field directly from OCCAM at each float location during the period of simulated motion. We have done this for several depth levels of the model: 1, 50, 100, 500, 1000 and 2000 m. We would expect the bottom levels to have a lower velocity in both U and V, and the surface velocities to be higher. The velocity is shown by the vertical distance from the zero axis. What we see from this figure is that the deep floats, at 2000m are hardly moving because the velocities are so low. The floats higher in the

water column are moving, though a certain number had obviously hit topography during our simulation. To reduce this problem we raised the drifting level from 2000 m to 1000 m. We also concluded from this analysis that the extremely low velocities observed at lower depths in the OCCAM model, of the order of 10^{-6} ms^{-1}, are so small that rounding errors might be an issue when writing the profiles to a file, hence we increased the number of significant figures for the temperature and salinity file outputs from our program.

It is not clear why OCCAM has such small velocities at depth. One possibility is that the run we use is not fully spun up after 14 years. This problem does not appear to have been noted by other people. This run with seasonal forcing has been used extensively. By moving our floats to 1000m we produced simulations that were suitable for our purpose so we did not pursue this odd behaviour in OCCAM. Because we can prove that our simulated floats were moving correctly within the model, these small changes to our program were sufficient to allow us to move on the main focus of the project, applying a Bernoulli inverse to this data set.

Extracting temperature and salinity profiles from OCCAM:

In order to apply the Bernoulli method we need to extract temperature and salinity profiles to mimic the ARGO floats. We then obtain the crossing points for the Bernoulli equations by plotting the temperature versus salinity. Below we have plotted just two station profiles (Figure 28) and then all the profiles extracted from the model (Figure 29).

Figure 28: Profiles of extracted salinity and temperature for two simulated floats plotted together. The blue line uses potential temperature extracted from the model; the green line uses the modified temperature for our method.

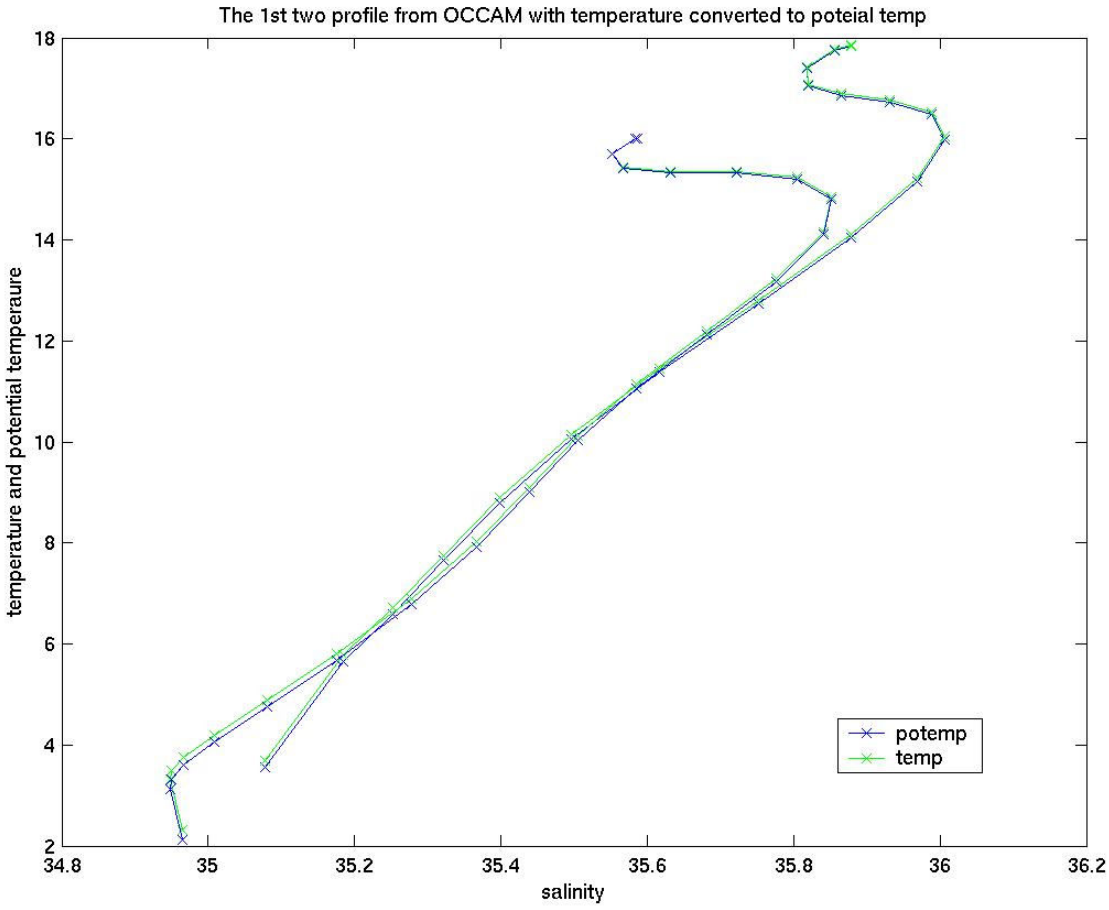

We can see from Figure 28 that these two stations have in fact got more than one crossing point between them. This is a clear example of how this problem is over-determined, with far more crossing points than stations. This graph also shows that there is a good match between the potential temperature extracted from the model (blue line) and the converted temperature for our method (green line).

Figure 29: Temperature and salinity of all 48 extracted profiles plotted against one another. The different North Atlantic water masses are also indicated by their expected temperature and salinity properties.

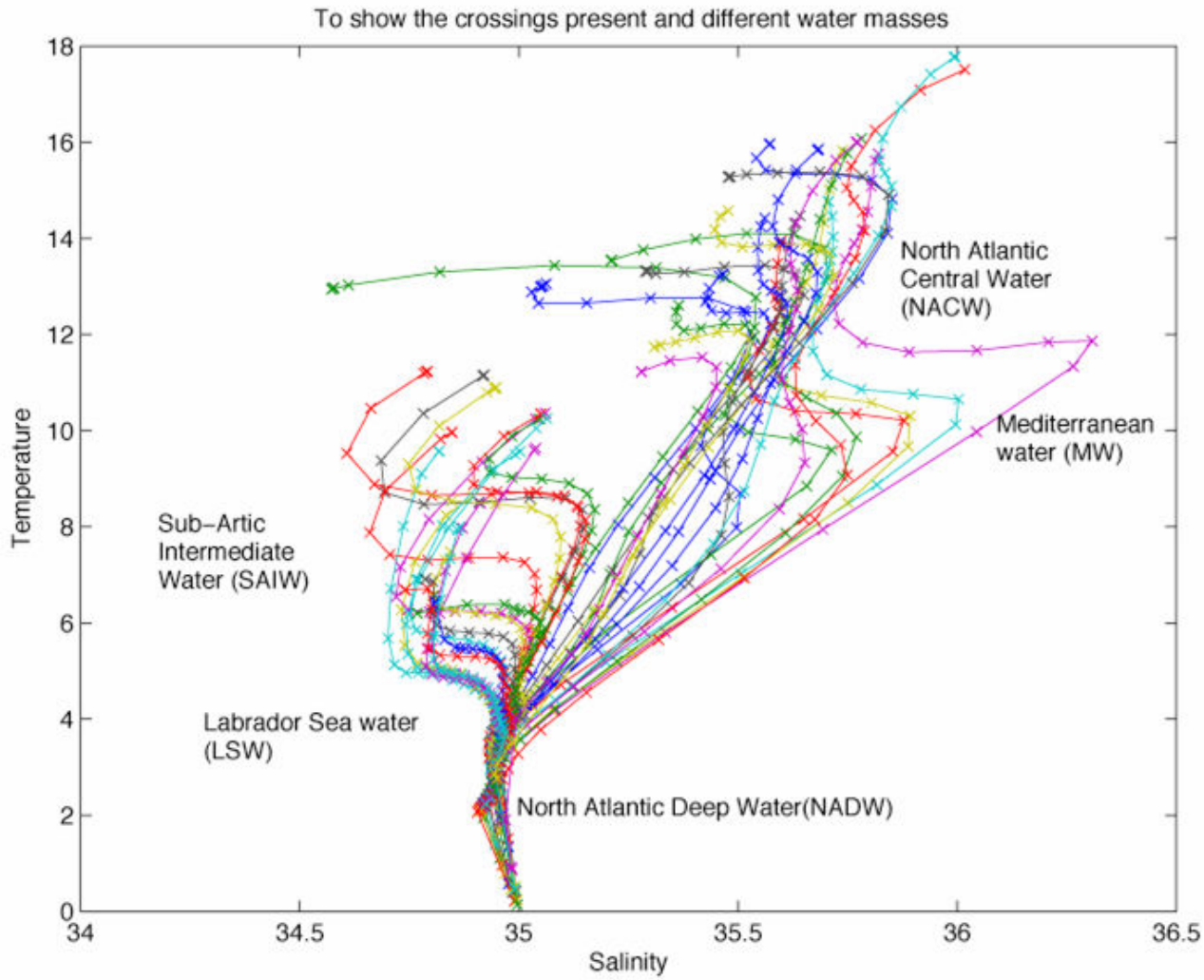

We are now ready to go on and apply an inverse calculation to this data set.

Results for the original Bernoulli point solution method and comparison with OCCAM:

In this section we use the simulated floats in OCCAM to obtain a Bernoulli inverse "point" solution for the SSH. Because we have simulated the ARGO floats in a model, we can also extract the "true" SSH at each of the float positions and do a comparison with the SSH obtained from the inverse.

First of all we do a quick comparison between the "point" solution method of (Cunningham, 2000) and that of the extracted SSH from the OCCAM model. The OCCAM data is shown in Figure 30. These plots clearly show some of the expected features discussed in Chapter 2. The higher (red/orange) SSH in the south west is associated with the Gulf-Stream/North Atlantic Current, and the subpolar gyre is clear as a region of lower (blue) SHH in the north west corner. The eastern Atlantic has much less variable topography, but moderate to high SSH, as expected.

Figure 31 shows the SSH "point" solution obtained between the same float locations using the Bernoulli inverse method, as outlined at the beginning of this chapter.

A matlab contouring routine has been used on both of these figures for comparison. We also present the point solutions without contouring as scatter plots in Figures 32 and 33.

Figure 30: The 1st six ten-day snap shots of SSH (in m relative to an arbitrary reference point) extracted from OCCAM. The black X's denote the positions of the floats. T_0 is the first 10 day snapshot, T_2 is 20 day snap shot and so on.

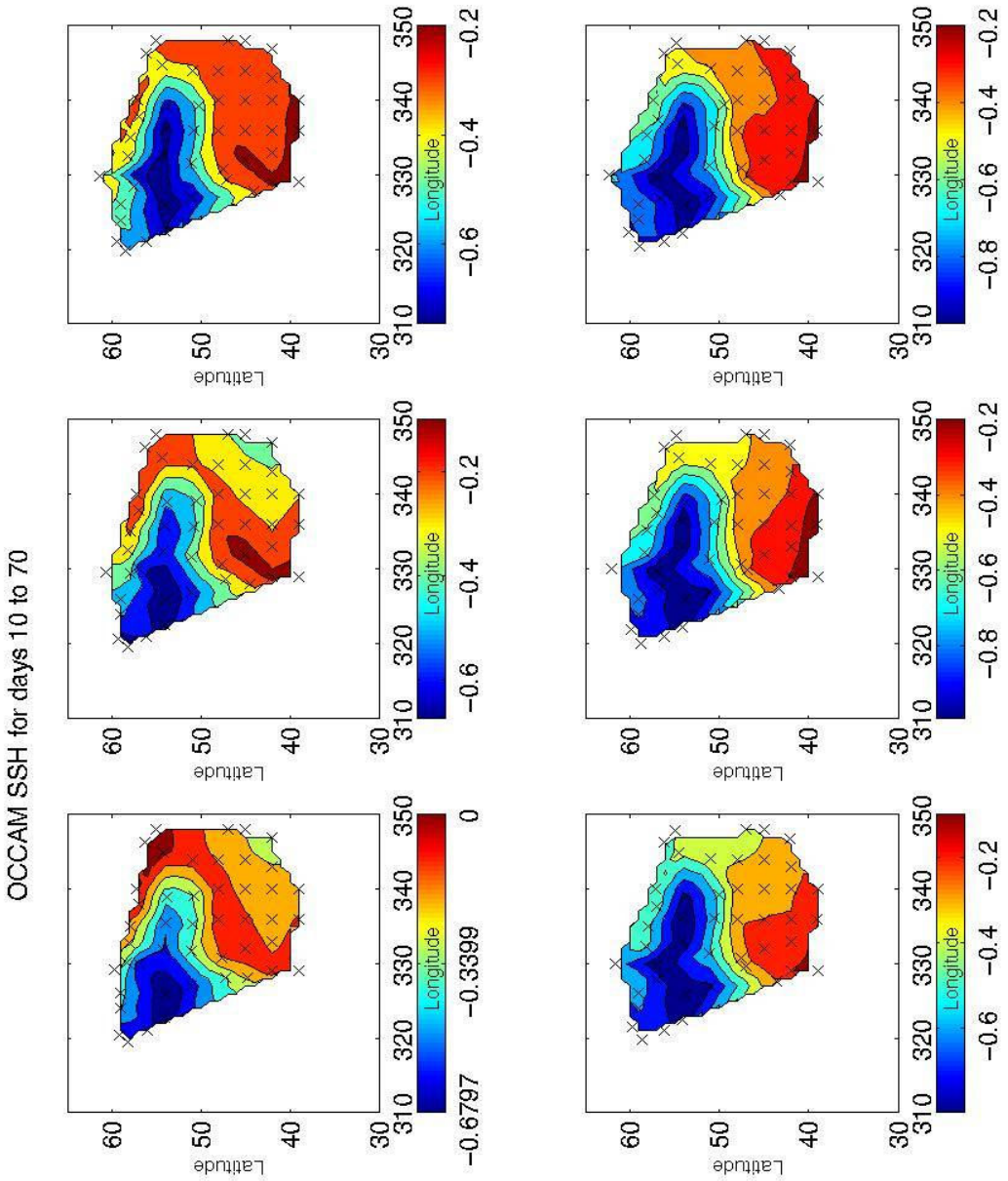

Figure 31: The same seven ten-day snap shots of SSH (in m relative to an arbitrary reference) solved using Bernoulli inverse.

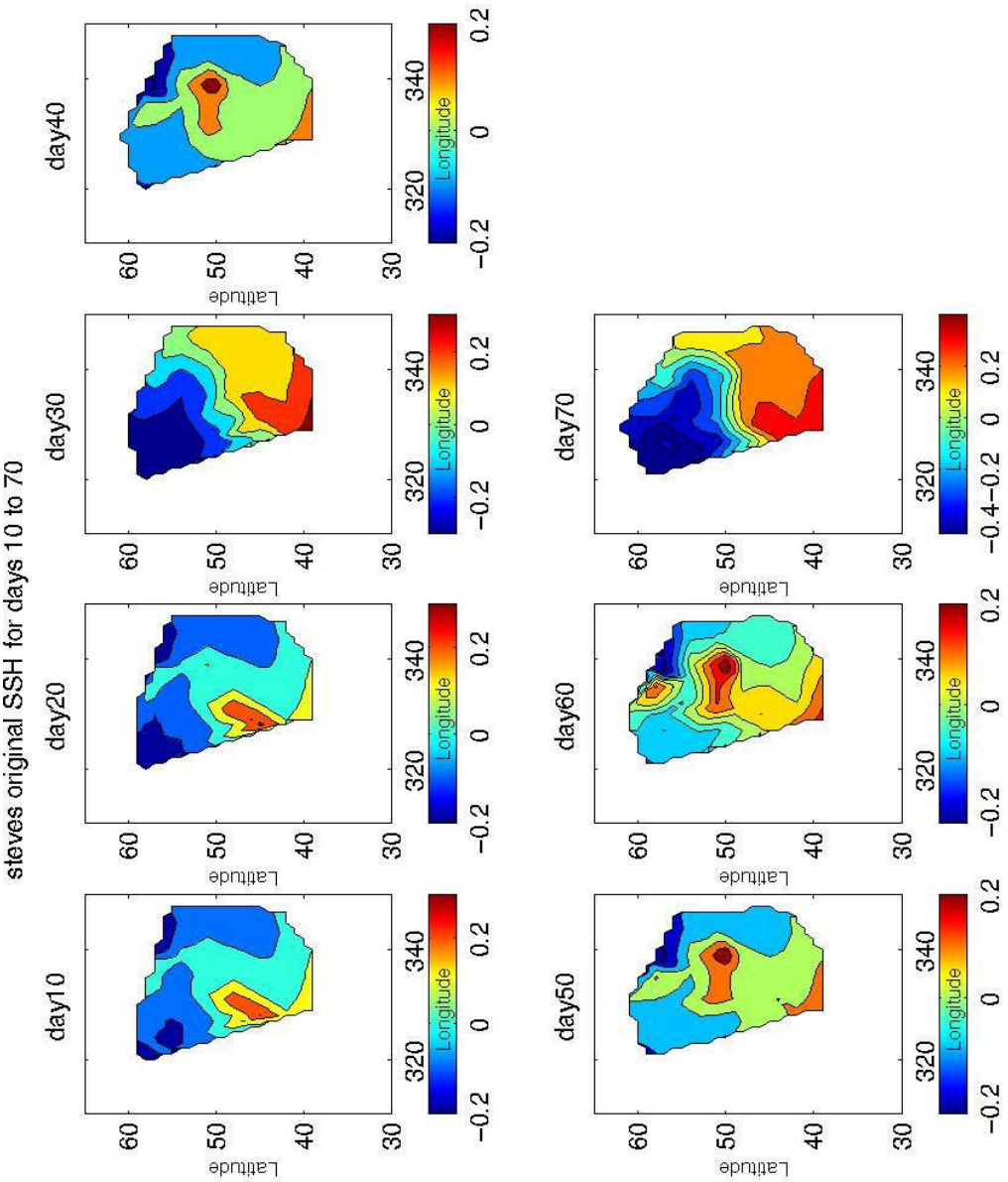

Figure 32: Dot plot for the first of the six ten day snap shots of SSH in Figure 30 extracted from OCCAM. SSH values are in cm; the mean SSH signal has been calculated and subtracted from each value.

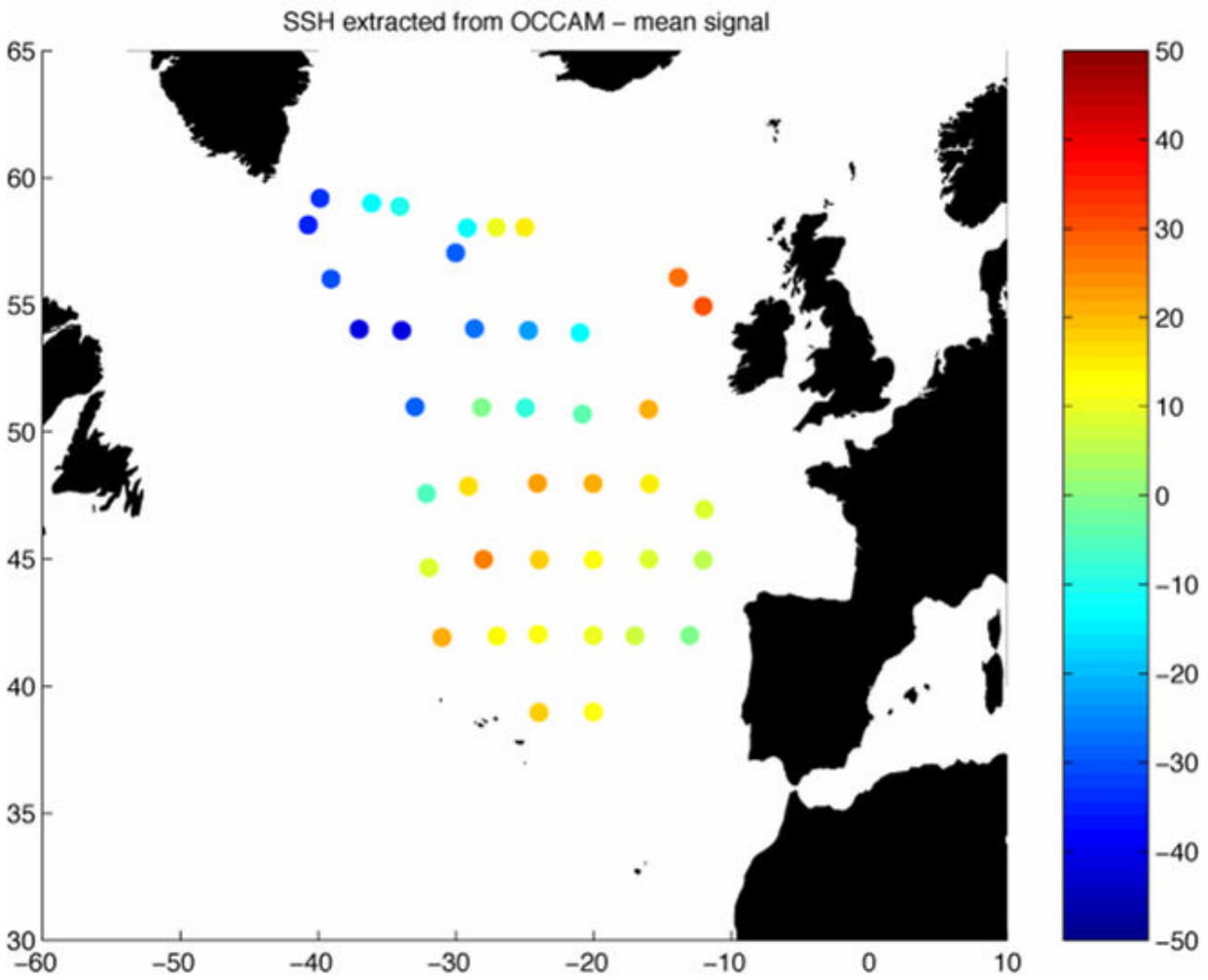

Figure 33: The first of the six ten day snap shots obtained from the Bernoulli solution displayed using a dot plot. SSH is in cm, and again the mean signal has been calculated and subtracted from the solution.

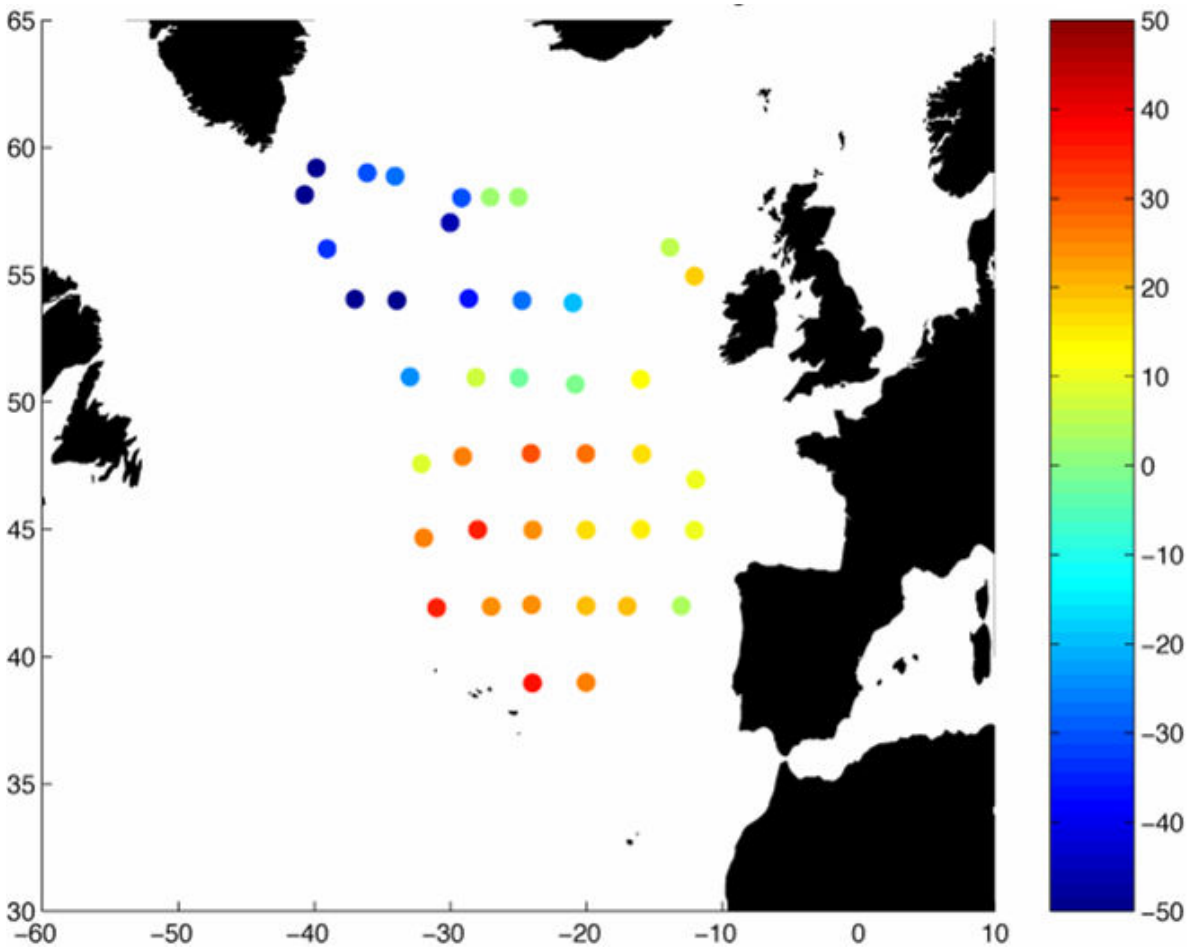

When we compare these two dot plots (figures 32 and 33) we can see that the magnitude of the Bernoulli obtained SSH is slightly higher than that of the extracted OCCAM SSH, but in general there is a very strong similarity between the two data sets. We can see the low sea surface height region to the North West in both figures and similarly the high sea surface height in the South. Going beyond this geographical comparison we have plotted the expected SSH from OCCAM against the SSH obtained from the Bernoulli solution in a

scatter plot, figure 34. If the solution was perfect we would expect to see a cluster of points along a diagonal from the origin. The solution is not perfect but we do have a general linear trend across the plot. A value of 0.34 was obtained for the correlation coefficient. This is very low and illustrates the poor fit. However despite this poor fit, we can see the main oceanographic features that we would expect for the region, the North Atlantic Current and the sub-polar gyre, though these are easier to see in the 2-D plots. We discuss how successfully these features are reproduced by our solution in more detail in Chapter 5.

Figure 34: The expected SSH solution extracted from OCCAM plotted against the solution obtained from the Bernoulli method.

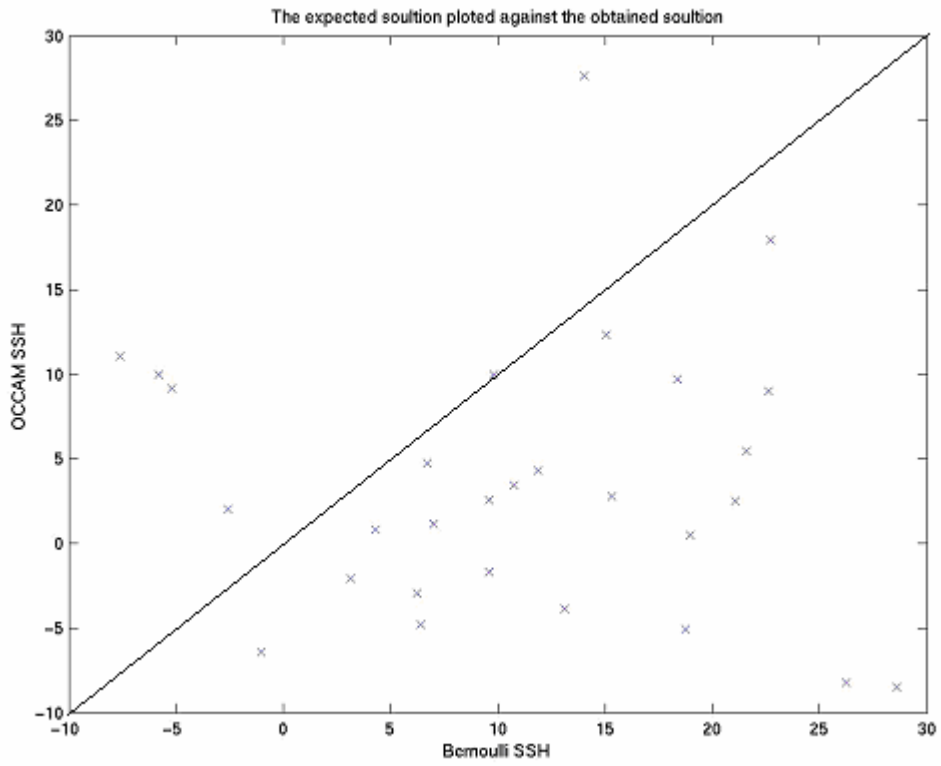

For a more comparison of these results we have plotted two line graphs. Figure 35 plots our "point" solution (blue) with the OCCAM SSH (red). We can see that the shape of the "point" solution is similar to the expected answer (the OCCAM SSH), but that there is an offset. The two surfaces appear to have different reference levels. Figure 36 compares the "point" solution (red) to the OCCAM SSH minus the mean signal (green). This removes the offset, and we see that our "point" solution is in good agreement with the OCCAM SSH, though some detail is lost at small length scales. Looking at figure 36 we can see that both the red and green curve rise to a maximum at ~20 and have a minimum at ~40, rising again towards the end of the plot. Although this general shape is common there are discrepancies in detail. For example at ~5 and ~12, where the OCCAM (green) signal has spikes. It should be noted that the sign of the OCCAM SSH is flipped between these two figures, because there is an arbitrary sign in the solution.

Figure 35: one time step of OCCAM compared with the same "point" solution for the same time step. The red line is the OCCAM SSH extracted at the solution points and the blue is the "point" solution. Vertical axis is SSH in cm, horizontal axes shows float number.

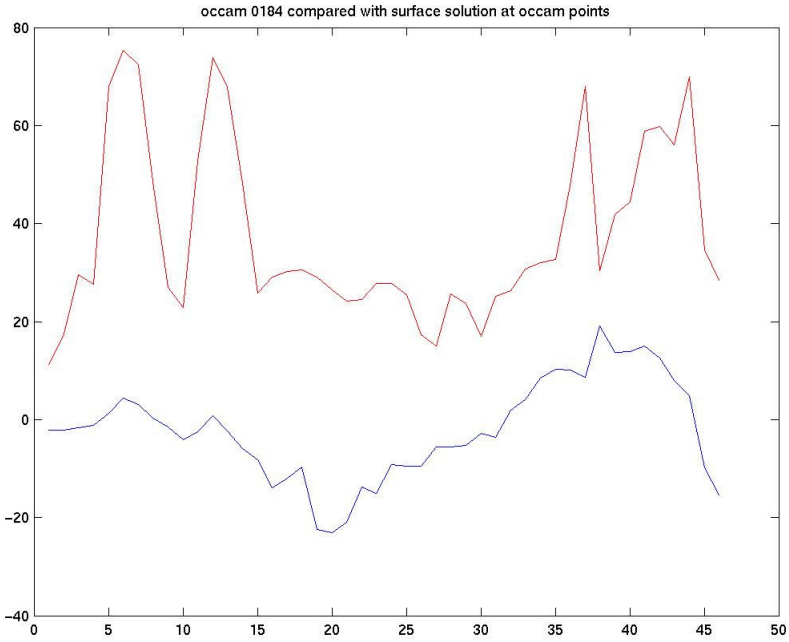

Figure 36: The solution (red line) and the extracted data (green line) at the same time step but with the mean signal subtracted from the OCCAM SSH. Note the change in sign. Axes as in Figure 34.

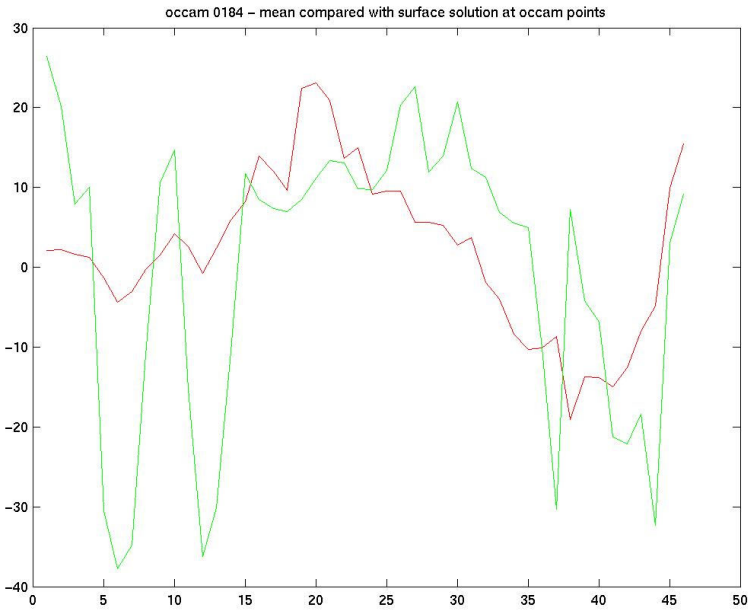

Figure 37 is a simple line plot of the SSH calculated at the simulated float locations using the "point" inverse method for the 1st five ten-day snap shots shown in Figure 31. Variations in SSH are in metres rather than centimetres as in Figure 36. This plot gives us a clear idea of the expected magnitude of the SSH signal (between ± 0.4 m), which is useful when we move on to our surface solution. We have also marked the errors obtained from the Bernoulli solution using the SVD linear regression method. We can see that the typical error is ~ ±0.05 m, which is small in terms of the overall signal.

We have also obtained a mean square error value for how well the inverse solution compares to the extracted OCCAM SSH (we discuss how this is calculated in Chapter 5, where we discuss in detail all of the mean square error calculations for our different solutions). We obtained a value of 681 cm^2. The square root of this value, the standard deviation, is 29 cm, which is rather large. We will see in Chapter 5 that this value for the "point" solution is smaller, and indicates a better result, than the simple 6th order polynomial surface solution we obtain using the floats only. However, the value is very close to that obtained by our later 7th order polynomial surface fit and our 6th order polynomial surface solution combining the satellite altimetry.

Figure 37: Line plot of point solution obtained from Bernoulli inverse for the 1st five ten day snap shots in Figure 31. Vertical axis is SSH in m, horizontal axis is float number.

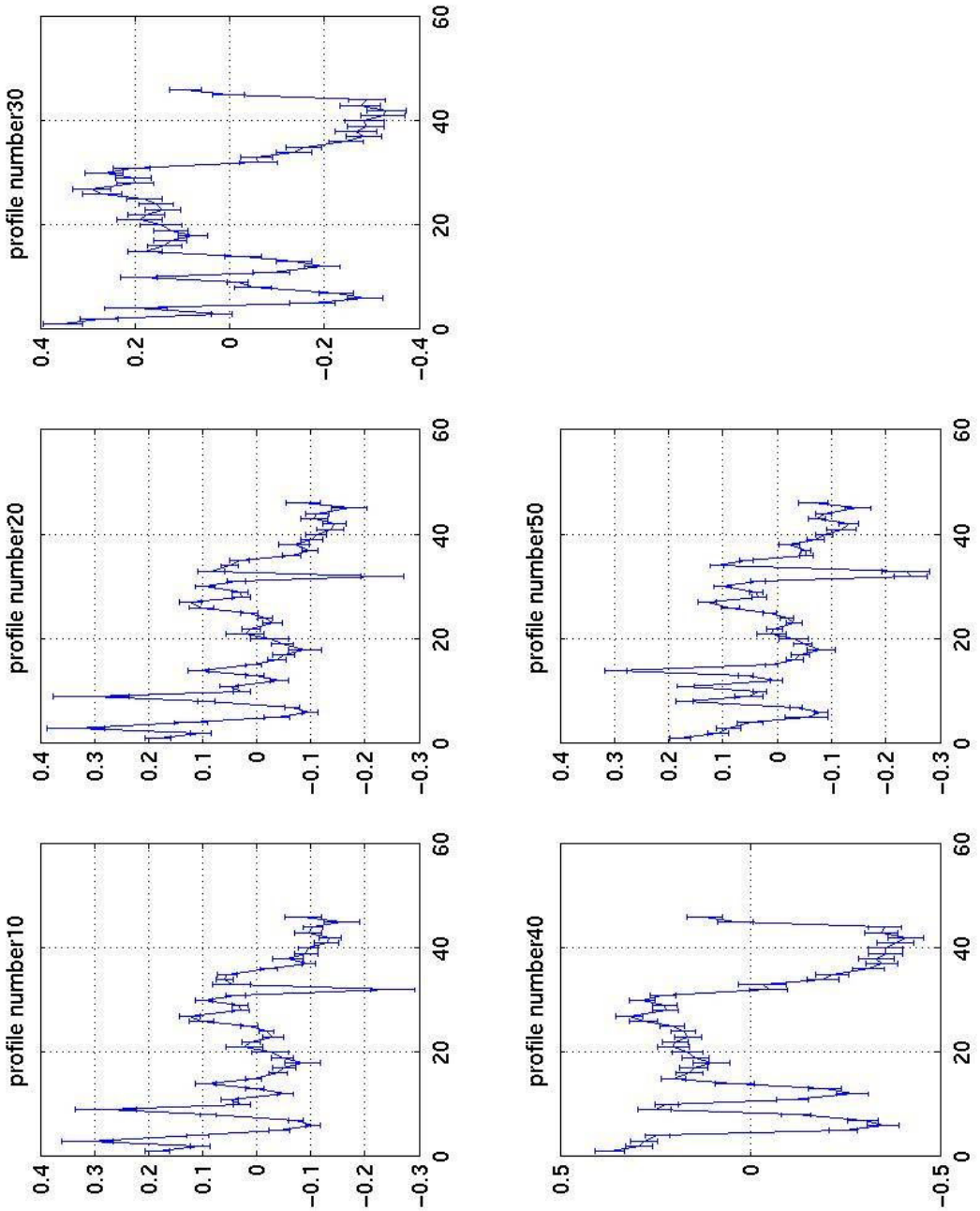

At this point in the project we have now examined the simulated floats in the OCCAM model and their temperature and salinity profiles. We have managed to reproduce the earlier work of (Cunningham, 2000) effectively by applying a "point" solution of SSH to these data. We have seen a strong similarity between the extracted SSH of the model and that produced using the Bernoulli inverse method. We are now ready to move on and examine the new developments of the method, the addition of satellite altimetry and surface fitting.

Chapter 5

Improving the method with the addition of satellite altimetry:

The discussion so far has focussed on the use of simulated ARGO float data, which record temperature and salinity profiles every 10 days. These profiles can be used by the Bernoulli inverse to obtain the SSH for each 10 day snapshot between the ARGO float locations. This is a new application for the Bernoulli inverse, which in the past has been largely been applied to model data only (Bigg, 1986; Killworth, 1986; Killworth and Bigg, 1988; Tokmakian, 1994; Cunningham, 2000), although Cunningham (2000) did apply the method to some CONVEX CTD data. Prior to this study, it has never been applied to such a variable and real time data set as is represented by ARGO.

In order to advance and improve the solution we wish to constrain the problem further with the introduction of satellite altimetry data. The SSH from the inverse solution of the ARGO floats will be combined with the differences in SSH, ΔSSH, obtained from satellite altimetry to map a sea surface elevation for a given region (in this study, the North Atlantic) to study large-scale geostrophic currents.

The only previous study to combine altimetry and the inverse method was by (Tokmakian, 1994). The inverse method was used to obtain a set of Bernoulli values, B_1 and B_2, for each of two surveys of a region. The changes in SSH between the two surveys, $\Delta\eta$, were known from the altimetry. Therefore the difference between B_1 and B_2 was equal to $\Delta\eta$. The inverse solutions were found using a weighted least squares method, and the stations that had coinciding altimetry data were weighted more than the stations without, and hence the solution was forced towards the a priori altimetry data values. This study showed that with the use of satellite altimetry the Bernoulli inverse method does produces a valid geostrophic velocity field. It also demonstrated that the use of the altimetry data in the inverse method did not just help to constrain the SSH at the locations of the altimetry but also at other locations, for example 63.7˚ N, on profile C in Figure 38.

Our study differs from that of (Tokmakian, 1994) because we do not use the altimetry simply as a priori information for the inverse method. Instead, we combine the altimetry directly into the solution matrices to be solved as a linear regression solution by the inverse. A further advance is the solution for a paired parametric surface solution over two time steps of float data with the difference in altimetry between these two time steps. These developments are described in more detail later in this chapter.

Figure 38: Differences in dynamic height between two surveys for altimeter height data (dash-dot line), a traditional geostrophic calculation referenced to 800m (solid line), and an inverse model with (short dash) and without (long dash) altimeter data. Altimetry locations are indicated at points where the inverse method and altimetry lines exactly intersect. From (Tokmakian, 1994)

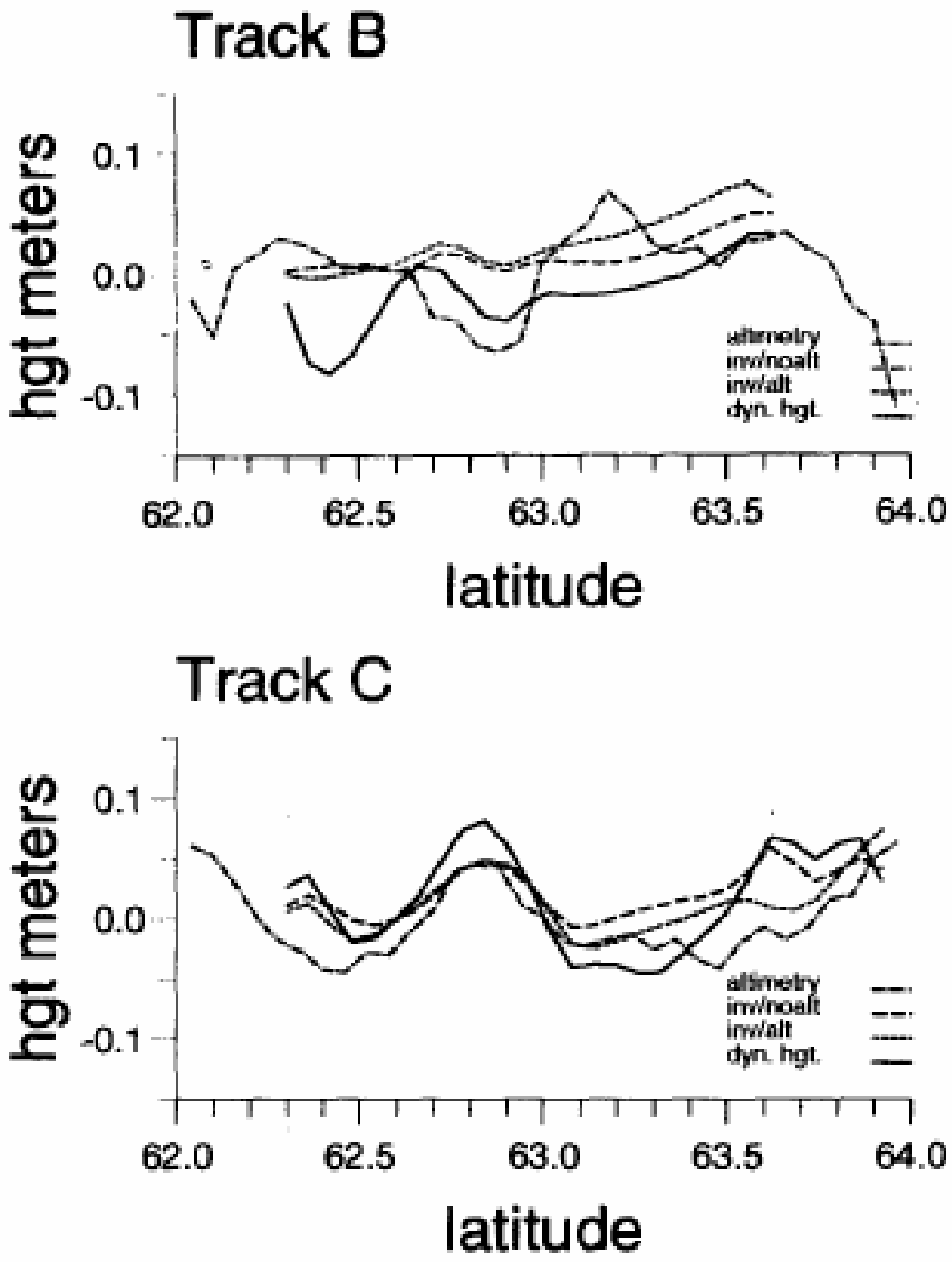

Problems with combining altimetry and moving to a surface solution:

It is difficult to combine this sea surface height solution for the floats with the satellites because the float solution is an absolute sea surface height. By comparison the satellite altimetry gives us a measure of the sea surface relative to the reference ellipsoid. As we explained in Chapter 1, for this reason we are unable to use altimetry on its own to calculate absolute surface currents.

So the altimetry data is not an absolute measurement, and cannot easily be combined with float data in the inverse method. The array of float points and the distances between them are also changing, because the floats are drifting to new locations every ten days. This means that the floats form a highly irregular non-stationary grid, which makes their integration with altimetry even more complex.

One solution to these problems would be to interpolate the inverse solution for the floats on to a standard grid to compare snap shots at different times. However, we would still be left with the problem of combining the altimetry into the solution. We would still have the difficulties of combining the differences in SSH from the altimetry with the absolute SSH calculated from the inverse of the float data.

Therefore, rather than using interpolation techniques we have opted to solve for a parametric surface solution. So rather than solving for a point SSH solution we obtain the surface fit parameters for the whole region of interest. This is potentially of great advantage because we can now fit any basis function of any complexity to the problem. In the next section we explain the new surface method in detail and show how the matrices are modified to solve for the surface parameters (α) rather than the absolute SSH between the station or float locations.

Improving the method by surface fitting

In the preceding chapter we have outlined the theory behind the Bernoulli inverse method and seen the results obtained for the "point" solution method. This section moves on to explain how we enhance this method to obtain a "surface" solution. First we discuss some background to surface fitting, and show how this approach changes the equations for the problem given in Chapter 4.

Our main reason for obtaining a surface solution rather than a "point" solution is to be able to solve for the SSH for a whole region of interest. With a "point" solution we are only able to solve for the SSH at a set number of stations or float positions, whereas with the surface solution we solve for the parameters

of the surface fit for a whole region, giving us SSH values at any point in that region.

Surface fitting is an attractive method for interpolating small numbers of observations because an interpolation can be produced for an entire region even in the absence of any other background knowledge to constrain the solution. It also is possible to account for observational errors through cross-validation (especially when using GAMS; see Chapter 6). However there are also disadvantages. There can be no incorporation of information from a background field, hence we ignore any prior knowledge we may have. We must also be aware of the risks of under fitting, over fitting, or using the wrong set of functions. If the data is under fitted, by not having enough terms in the polynomial expansion, important details in the dataset may be unresolved. If, on the other hand, we over fit the observational data, by using too many polynomial terms, the solution may display features which have no real significance. Surface fitting can also be computationally expensive when large numbers of observations are considered.

In our case, surface or function fitting is used to find the parameters that best describe the set of ARGO and Jason data we have for the North Atlantic. In this case we wish to extrapolate beyond the observation points we have to obtain a much larger picture of SSH in the North Atlantic region than the one we can simply obtain at our observation points. This method will also allow for the easy comparison between different time snap-shots, which is difficult

to achieve with a simple ”point” solution because the “points” (the ARGO floats) move about randomly with respect to each other over time.

From chapter 4 we have seen how a “point solution” is obtained for the sea surface height by solving the Bernoulli equations. We had the following equation 19:

Equation 29 $\mathbf{y} = \mathbf{A}\mathbf{x}$

Where **x** was the unknown SSH we wished to solve for. In this section we move on to explain how we obtain a surface fit by solving the modified equation:

Equation 30 $\mathrm{y} = \mathbf{A}\mathbf{B}\alpha$

Where **A** is the design matrix of crossing points. As in equation 19, this matrix has *m* rows and *n* columns, where *m* is the number of crossings and *n* is the number of stations or floats in the problem (see Chapter 4).

y is a vector of the differences in the Bernoulli function, with dimensions 1 by *m*. Thus we have a Bernoulli difference for each one of our station pairs with a crossing point.

B is a new position matrix. This contains the latitude and longitude positions of the floats and (when used) the satellite ground tracks. This matrix has *n* rows and *a* columns, where *n* is the number of points we have in the solution, the number of floats plus satellite altimetry points, and a is controlled by the order of our polynomial fit. It corresponds to the number of parameter terms in the equation. So in column one we have a column of ones for the first term, in column two latitude, column three longitude and so on. All of the expansion terms for the 6^{th} and 7^{th} order polynomial are listed in Table 3.

The last term α, are the surface fit parameters which we now solve for instead of the earlier unknown SSH in equation 19. This solution gives us the parameter fit for the surface over our whole region of interest. We then simply evaluate our polynomial equation using the α terms and relevant latitudes and longitudes to obtain the SSH for this whole region.

Given an n^{th} degree polynomial, the roots can be found by finding the singular values of the matrix. This is still a linear problem so we can solve it in the same way as already outlined in Chapter 4, by using the SVD method to find the eigenvalues.

The Polynomial structure and surface fitting:

Bearing in mind that we could take any basis function of any complexity to fit to our problem, we have chosen a polynomial fit. We have made this choice because it is computationally simple, can be generalised easily and there are previous examples of polynomials being used in this manner. One of the best known of these examples is (Panofsky, 1949), which was the first published attempt to fit a mathematical function (in this case a 3^{rd} order polynomial) to two-dimensional meteorological data, across areas of the order of 10^6 square miles (eastern North America). Surfaces were defined by means of two-dimensional polynomials for each sub-region of the study area. These surfaces were joined smoothly at the edges of each sub-region. Panofsky states that a field of 10 observations can be fitted accurately by a third-degree polynomial, with no smoothing of the data. He also states that though the polynomial cannot be expected to fit eddies in the data it should represent the large scale features of the field to be analysed.

Polynomials are a popular choice as a fitting function, but we must be aware of the problems of using them. There is a tension between describing too little, using a function that does not have enough flexibility to follow the data, and too much, using a function that is so flexible that it fits noise or produces artefacts in the original data.

Any reasonable model with N free parameters should be able to exactly fit N data points. The goal of fitting is usually to be able to interpolate or extrapolate. Extrapolation should only be carried out with great care as the polynomial is not constrained outside the data. If there is any noise in the data, a model that passes through every point is carefully fitting details of this noise and does not generalize the meaningful patterns of the data. On the other hand, if too few parameters are used, the model may be forced not only to ignore the noise but also to miss the meaningful variation as well. Successful function fitting requires a balance between *overfitting*, where there are model mismatch errors because the model is also incorporating noise, with *underfitting*, where there are model estimation errors due to too few parameters in the model. These ideas are illustrated Figure 39 below.

Figure 39: Figure showing how the function relates to the system it is trying to describe. Light green line shows how the errors for an originally underfitted function decrease as the model complexity increases, but past a certain point increasing complexity leads to an increase in error due to overfitting. Taken from (Gershenfeld, 1999)

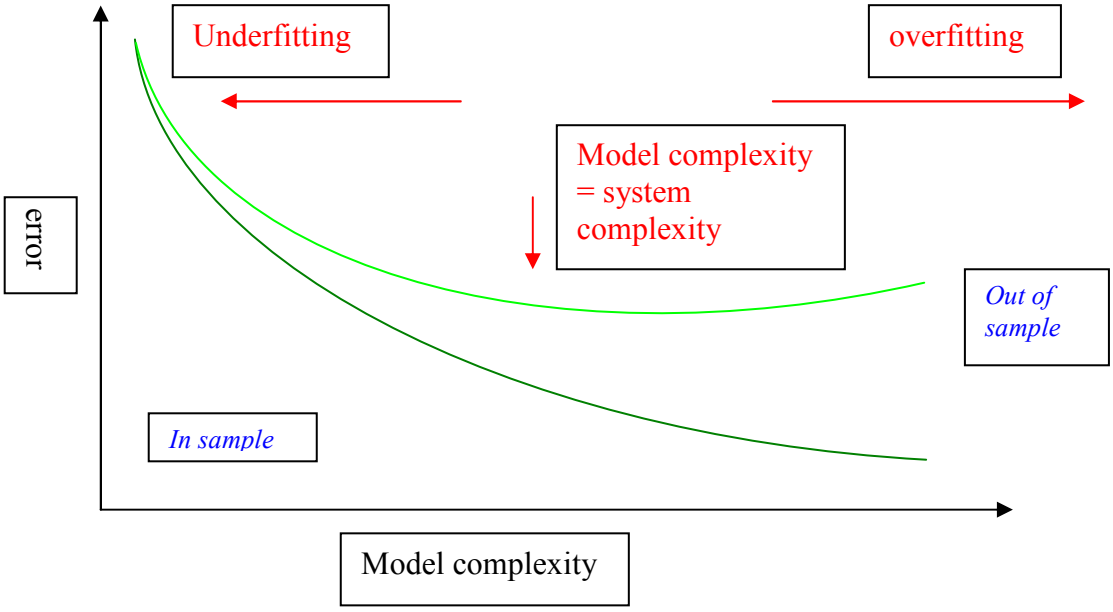

In our case we have chosen to fit a 6^{th} order polynomial to the data. For comparison, we later fit a 7^{th} order function to see what difference, if any, is made to the solution. A further test of this method is made in Chapter 6, where we fit a generalised additive model (GAM) to the "point" solution we obtained in Chapter 4. This allows us firstly to assess how well a polynomial fit describes the data, and secondly to see whether it is better to solve for a surface solution, or to obtain a "point" solution and then fit a surface to it.

Our model dataset consists of approximately 48 Argo floats simulated in the OCCAM model, and in the case of the real time data we have information from approximately 115 floats every 10 days to fit a function to.

We apply a polynomial equation of the form:

Equation 31 $\alpha_0 + \alpha_1 x + \alpha_2 x^2 + ... + \alpha_n x^n$

This generalises to a bivariate polynomial form with two variables.

Equation 32

$$a_{nm}x^n y^m + \ldots + a_{22}x^2y^2 + a_{21}x^2y + a_{12}xy^2 + a_{11}xy + a_{10}x + a_{01}y + a_{00}.$$

Where our two variables are latitude and longitude positions of the floats and the satellite altimetry.

The terms for the expansion of the polynomial up to the 6th and 7th orders are shown in Table 3. Figure 40 shows an example polynomial fit to some OCCAM SSH data. It can be seen that the fit captures most of the variability in these data.

Table 3 : Terms for the 6th and 7th order bivariate polynomial fit:

Term	Order
1	
X	
Y	End of 1st
X^2	
XY	
Y^2	End of 2nd
X^3	
X^2Y	
XY^2	
Y^3	End of 3rd
X^4	
X^3Y	
X^2Y^2	
XY^3	
Y^4	End of 4th
X^5	
X^4Y	
X^3Y^2	
X^2Y^3	
XY^4	
Y^5	End of 5th
X^6	
X^5Y	
X^4Y^2	
X^3Y^3	
X^2Y^4	
XY^5	
Y^6	End of 6th
X^7	
X^6Y	
X^5Y^2	
X^4Y^3	
X^3Y^4	
X^2Y^5	
XY^6	
Y^7	End of 7th

Figure 40: An example of a polynomial fit to some SSH data extracted from the OCCAM model, in this case a simulated single TOPEX/Jason track. Vertical axis is SSH in cm, horizontal axis is data point number.

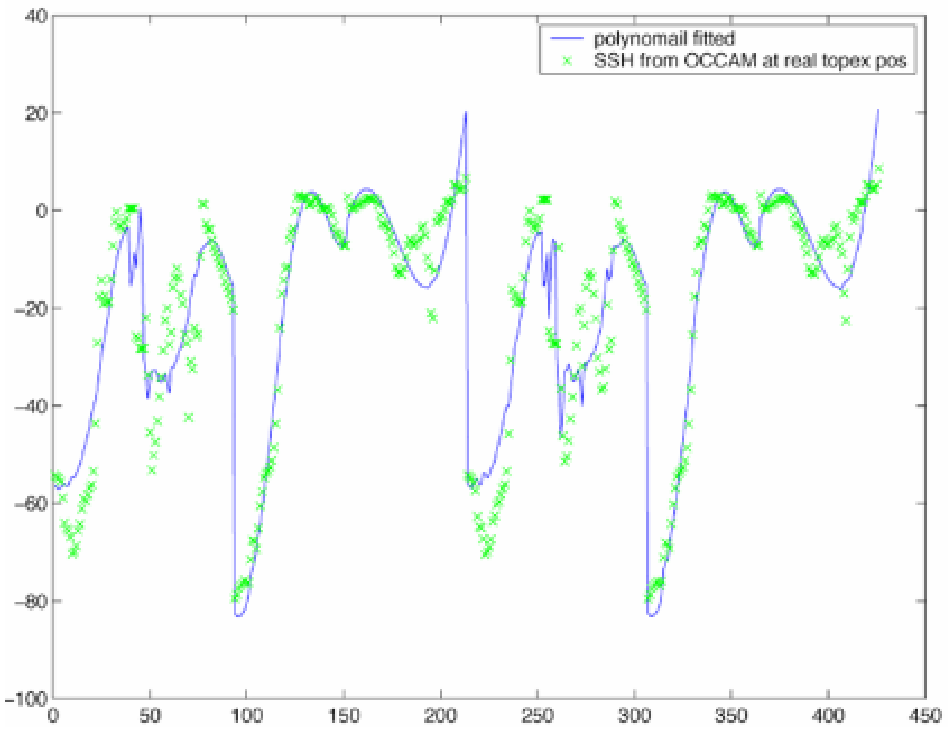

Our approach to the problem:

Having outlined the principles behind surface fitting, and particularly the use of polynomials, it is now time to move on to explain how we have modified the Bernoulli inverse to produce a surface fit.

The easiest way to understand the method is go back to our modified equation:

Equation 33 $\mathbf{y=AB}\alpha$

And examine the construction of the new matrices required to solve the problem. These are shown in Figures 40 and 43 below. We have approached the problem in stages to gain an improved understanding of how well the method is performing. Firstly we solve for a surface solution using the float data only, before incorporating the satellite altimetry into the problem.

Obtaining a float only solution:

First we apply the surface fit to one time step of simulated float data. We have extracted the "real" SSH from the OCCAM model at the same time as our simulated temperature and salinity profiles. This is the solution that we expect to be able to replicate. The matrices for this solution are shown in Figure 41.

One of the advantages of using matrices is that it is very simple to include or exclude part of the matrices in the solution. In Figure 41 we divide the matrices so that the upper parts describe the floats, with the satellite components in the lower parts. Therefore, for the float only solution we just exclude the lower part of the matrices which contain the satellite components.

As in the earlier "point" solution method described in Chapter 4, the vector y on the left hand side of the equation is the difference in the Bernoulli function between two crossing points obtained from our simultaneous equations. On the right-hand side, we have the design matrix **A**, the crossing point matrix. As described in Chapter 4, this matrix is constructed from the crossing points between pairs of streamlines. The matrix contains a set of ones and minus ones, with each one corresponding with a minus one for the crossing pair, because we are looking at the difference in the Bernoulli function for each pair.

For the surface solution we now have an additional **B** matrix. This is the position matrix and contains the latitude/longitude terms from the polynomial equation. As described in the previous section, in column one we have a column of ones for the first term, in column two latitude, column three longitude and so on. The expansion terms for the 6^{th} and 7^{th} order polynomial are listed in Table 3.

The last term in the equation is the vector α , which denotes the parameters of the surface fit, and is replacing the height between the points, h, which is solved for in the "point" solution.

Adding altimetry to the problem:

As we can see from Figure 40, when we wish to include the altimetry we simply add the bottom sections of the y, **A** and **B** matrices described above. On the left hand side of the equation we add an extra section to the bottom of the Bernoulli difference vector y, which contains the changes in SSH from the satellite altimetry. On the right-hand side, the altimetry part of the design matrix **A** is made up of a diagonal of minus ones, and the **B** matrix is expanded so that it contains the latitude/longitude terms for both the float positions and altimetry. We only need the positions of the altimetry for one time step as the ground tracks are assumed to remain constant.

Figure 41: Matrices for the new surface fit.

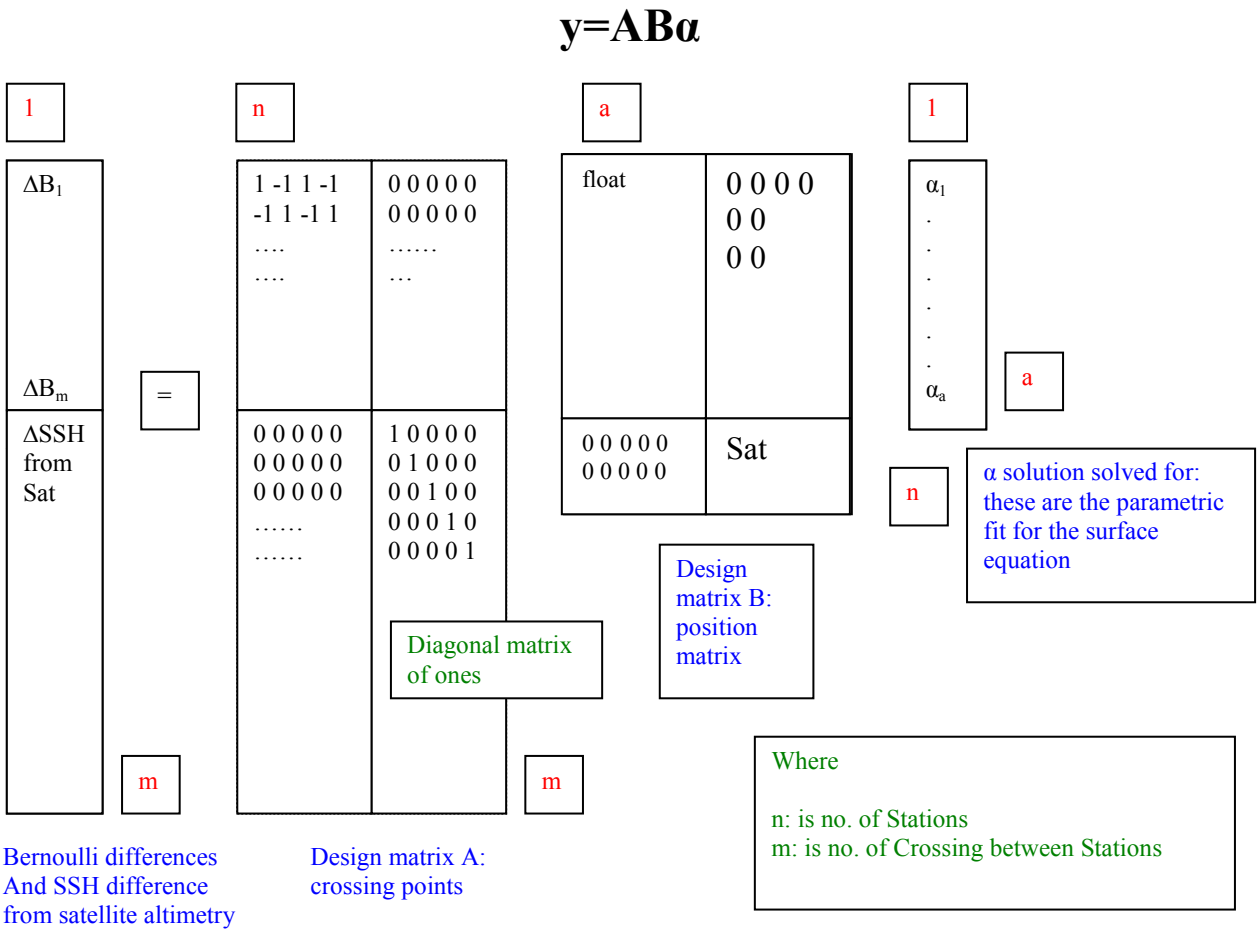

Results of a Simple surface solution for one time step:

The inverse has now been modified to solve for alpha parameters of a surface fit instead of SSH. We are now ready to calculate a surface solution for the whole North Atlantic region, by applying a simple low order polynomial fit to the data. At this stage we are still using the OCCAM model output rather than real ARGO or Jason data sets. Figure 42 shows the alpha parameter estimates for two separate single time step solutions. Note that this is not a SSH solution, the vertical axis of the figure denotes the value of alpha and the horizontal axis each of the polynomial terms listed in Table 3.

The alpha parameters were very small when the solution was first run, because the SSH variations being fitted to were very small in relation to the dimensions of the surface. For computational reasons we decided to put a scaling factor directly in to the solution code so that, when building the position matrix B, the latitudes and longitudes were scaled to fit on a unit square. We write out these scaling factors with the solution and then use them to rescale the heights to a new latitude and longitude grid.

Figure 42: Example of an α parameter solution for a surface fit, obtained for two separate single time steps. Vertical axis denotes the value of α for each of the polynomial terms listed in Table 3 (horizontal axis).

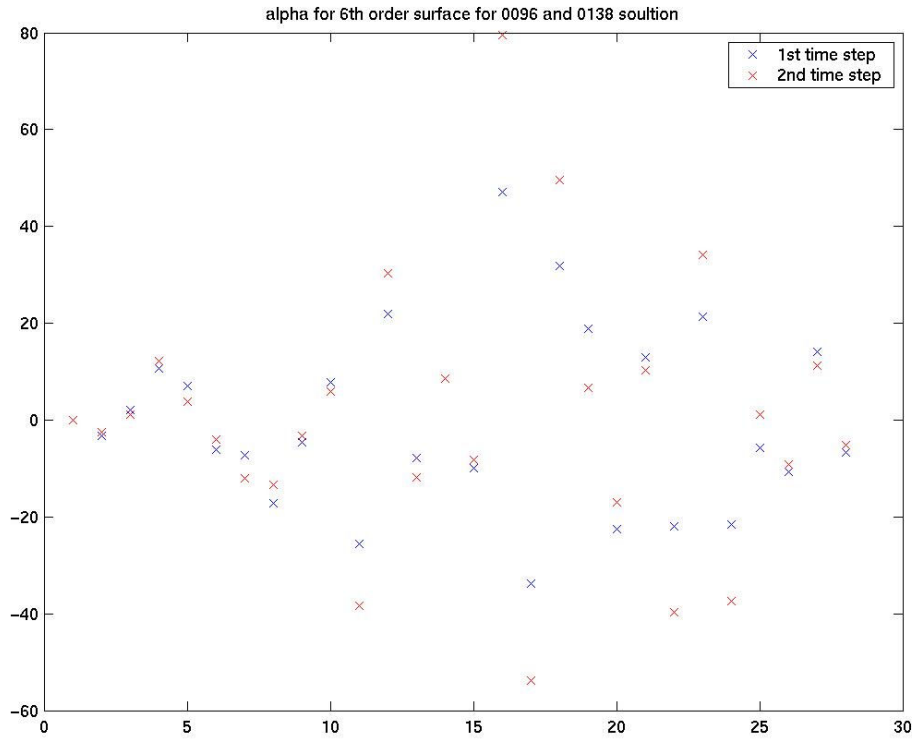

This α solution is then converted to a SSH solution by multiplying out the alpha terms in the polynomial to obtain a surface solution for the whole region of interest

Figure 43: A 1-dimensional profile of surface solutions obtained for the whole region. The vertical axis is SSH in m and the horizontal axis is distance along the profile Each of the coloured lines represents a single step solution at different times in the OCCAM model.

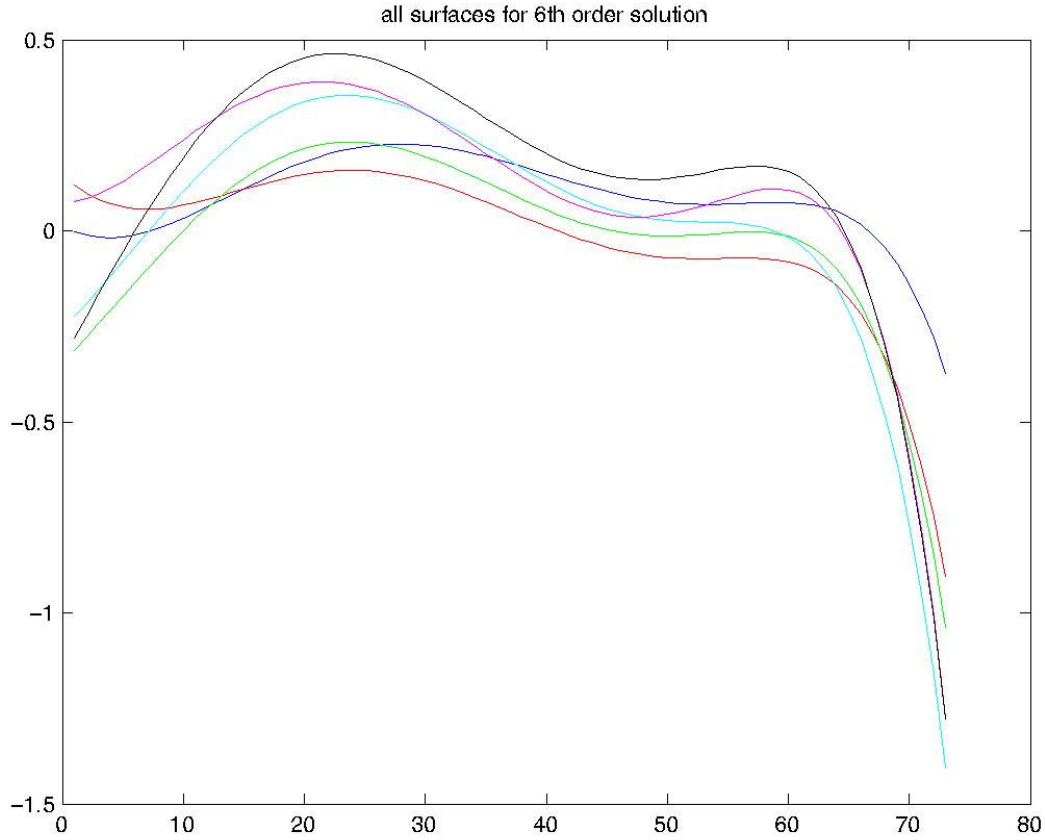

In figure 43, we can clearly see the smoothing effect of applying a low order polynomial to the data. The different solutions indicate changes in the SSH with time, but this 1-D representation does not give us a particularly clear idea of the oceanographic features in the data. In later representations we plot our solutions in a 3-D way with geographical information, by applying a standard grid to the data and using Matlab routines. Meshgrid was used to create the following standard grid:

- Latitude: from 30.25 to 60 degrees in 0.25 degree steps.

- Longitude: from 320 to 350.5 degrees in 0.255 degree steps (due to a constraint in Matlab, the matrices need to be of the same size, so we use a 0.255 degree step rather than 0.25).

The griddata routine was then used to place our datasets onto this standard grid. By applying the same standard grid to both the surface solution and the extracted OCCAM SSH, we could easily compare our solution with the expected results.

In summary the polynomial coefficients were very small and in figure 42 we can see there was little change between the first and second time step. When a number of time steps were plotted in figure 43 as a 1-Dimensional surface plot the smoothing effect of the polynomial function can be clearly seen this will obviously reduce accuracy as we know that the OCCAM model has variability on all space scales.

We now move on to solving for paired time steps rather than single time step solutions.

Obtaining a paired solution rather than a single time step.

We still have two problems with our method at this point.

1. We have not overcome the problem of combining the ΔSSH values from the satellite altimetry with the absolute SSH values of the Bernoulli float solution, which move relative to the satellite tracks.

2. We still do not know the contribution of the geiod to the problem. As we discussed in Chapter 1, it is impossible to separate out the mean flow field without knowing the value of the geoid. However, due to the irregular nature of the ARGO array it is not possible to use a traditional approach to the problem, where we estimate the geoid from surface observations made at the same time and location as the satellite pass. The ARGO array is too sparse and irregular and we would need to match up the times of both the floats and the satellite track passes.

To overcome these difficulties we have opted for a paired solution, using two sets of float data, taken ten days apart. The difference in altimetry between these two time steps is then used in the inverse. Because we now have information about ΔSSH from the ARGO floats, we can incorporate the satellite data into our solution for absolute SSH. The new matrix arrangement for this paired solution is shown in Figure 44. The difference from Figure 41 is

that we have now added extra sections to the matrices for the second float data set. We now solve for two sets of α solutions, one for each time step.

As with the single time step solution we can very easily produce a float only solution by simply turning on and off parts of the matrices to obtain solutions with and without the altimetry. We now move on to present some results using these new matrices to solve the method.

Figure 44: Matrices for float pair surface solution

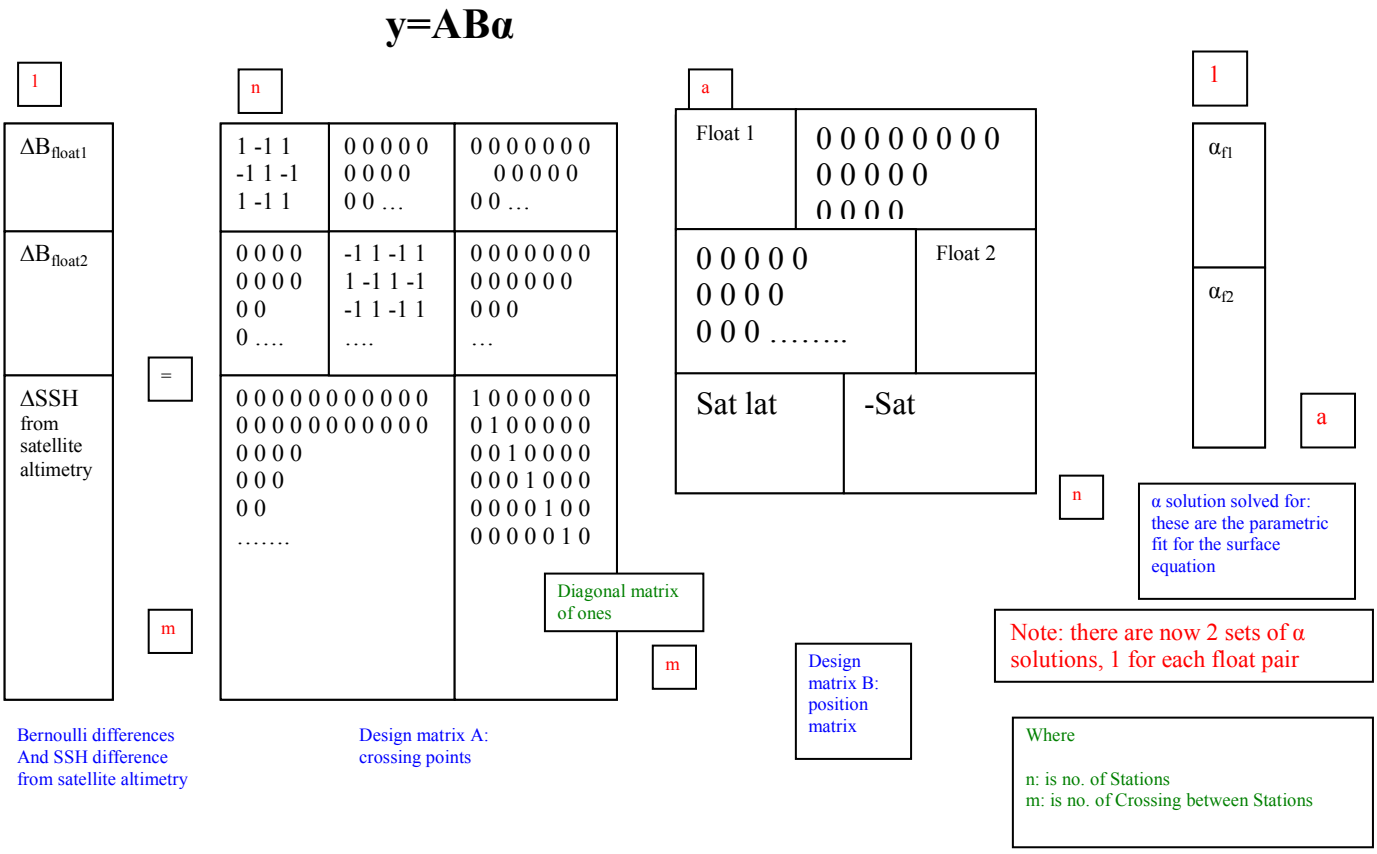

Results of Surface solution for the paired floats solution:

Figure 44 shows a 6th order surface solution for OCCAM paired float data only, in the form of a dot plot similar to the solutions presented in Chapter 4 (Figures 32 and 33), although the float positions are different due to this solution being from a later time step. The latitudes and longitudes are scaled to fit on a unit square, for the reasons discussed in the previous section.

Figure 45: Dot plot of 6th order fit for floats only solution. The axes are the scaled latitude and longitude. The colour scale represents SSH is cm.

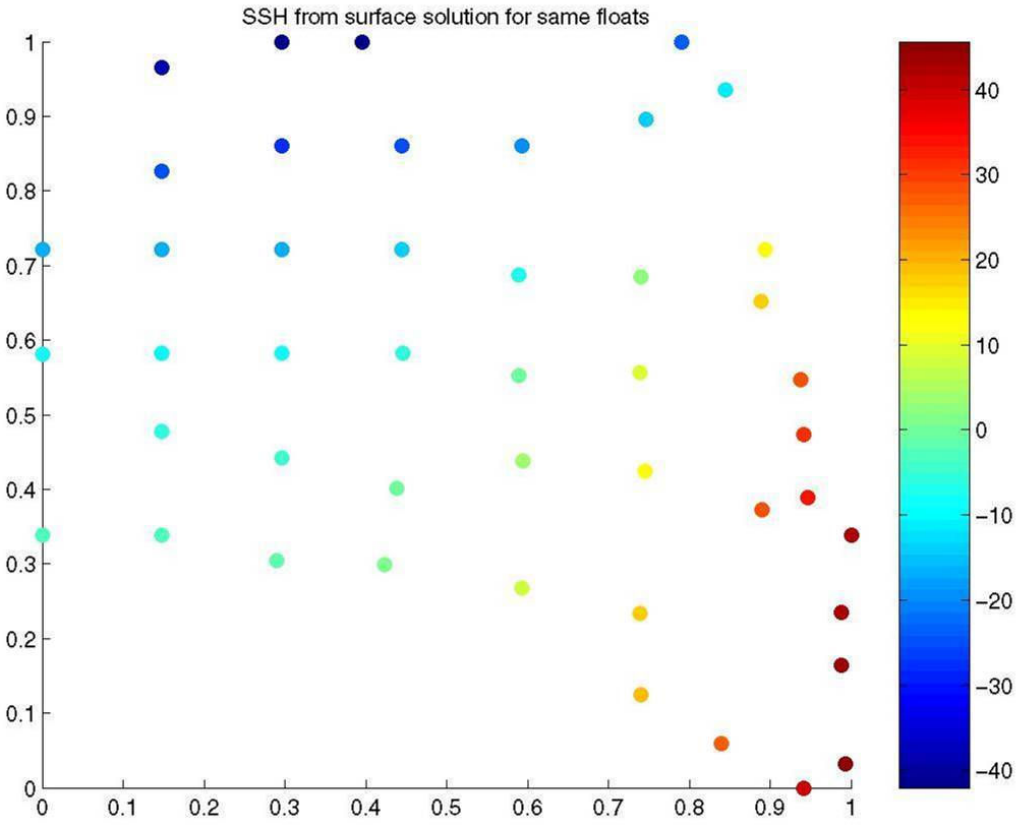

Figure 46 plots the expected SSH values, directly extracted from the OCCAM model. A comparison with Figure 44 shows that the broad features of the OCCAM SSH have been reproduced by our surface solution, with low SSH values in the north west and higher values in the south east. However, we can see the smoothing due to our use of a low order polynomial. Some of the smaller-scale variation in the OCCAM SSH appears to have been lost in our solution.

Figure 46: Dot plot of SSH from OCCAM extracted at the same positions as the floats above. The axes are the scaled latitude and longitude, with SSH in cm.

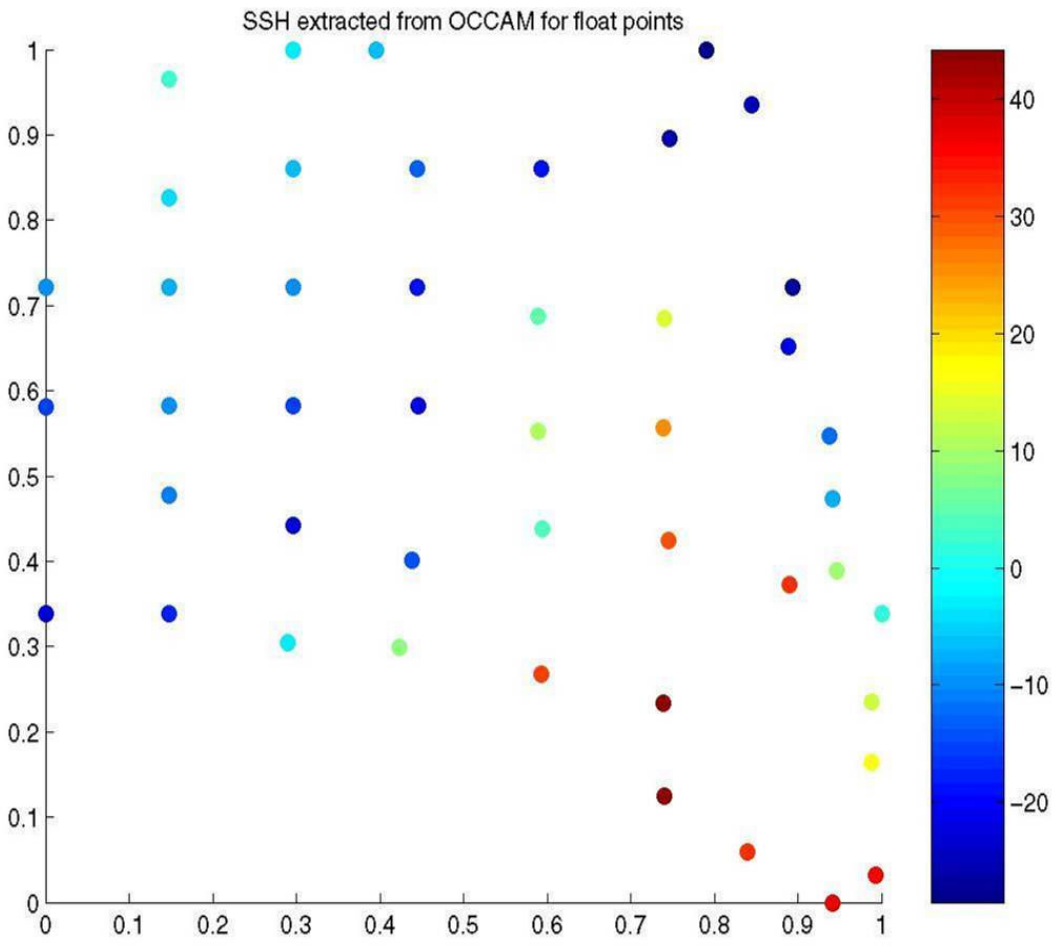

Figure 47 shows a 2-D image plot of our float-only solution, which allows us to more easily compare the features reproduced by our solution to the oceanographic features that we expect to see in the North Atlantic. The sub-polar gyre is clearly indicated by the region of low SSH in the north; the increased SSH values in the east are also a result of the wind-driven circulation (see Chapter 2). We do not see high SSH values in the south west as we did in the point solutions for Chapter 4, but this feature is not seen in the OCCAM SSH plot either. This is probably because of the different distribution of simulated floats used in this solution, which does not include any floats from the southwest North Atlantic. At this point we had removed some simulated floats which were problematic, because of the low velocities in the OCCAM model (see Chapter 3).

Figure 47: The 2-D image surface solution for the same time step using only the float data.

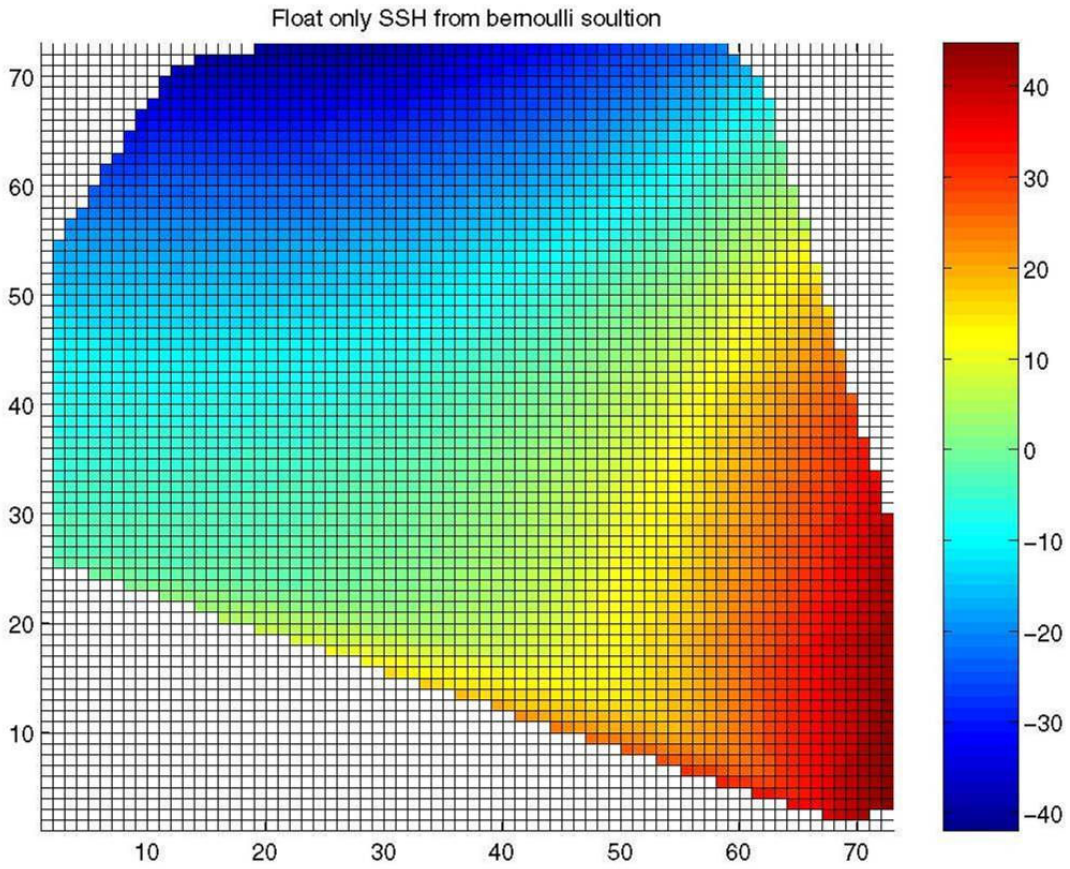

There are two further ways of comparing our solution with the OCCAM SSH, firstly by looking at the maximum and minimum range of the SSH signal, and secondly and more accurately by examining the mean square error calculations.

If we compare the SSH signal for our solution with the original OCCAM SSH, our solution has a range of ±40 cm, while the OCCAM SSH had a

maximum/minimum range of ± 50 cm. The smoothing effect of the low-order polynomial also appears to have reduced the maxima and minima of the solutions. In terms of the Root Mean Square Error (see later for details of the calculation) the difference between this solution and OCCAM is 46.8cm but the "point" solution has a RMSE of 29.1cm. However this comparison is unfair as the surface solution RMSE is calculated over the whole field whereas the point solution can only be calculated at the float positions.

The following figures compare our paired float solution with the OCCAM model in two ways. **Solution A** (Figure 48) plots the difference between the surface solution obtained for the first time step only, and the SSH extracted from OCCAM with the mean signal removed. For **Solution B** (Figure 49) we have plotted the difference between our paired surface solutions and the changes in the OCCAM SSH over the two time steps.

We would expect solution A to be better than solution B (solution B becomes relevant later, when we consider the effects of adding satellite altimetry to our solution). Since we are trying to obtain a solution as closely related to the extracted SSH from OCCAM, we would expect Solution A to show less variation than Solution B. We can see from Figure 46 that solution A shows a more structured deviation from the OCCAM data, varying most at the maximum and minimum values. This is due to the smoothing caused by our choice of using a low order polynomial. We can see that we are also losing

the extremes of the signal in Solution B, but there is very little correlation of these changes with the structure of the OCCAM SSH.

Figure 48: 2-D image of the difference (in cm) between the surface solution from floats only and the OCCAM SSH with the mean signal removed. The axes are the scaled latitude and longitudes. This is solution A.

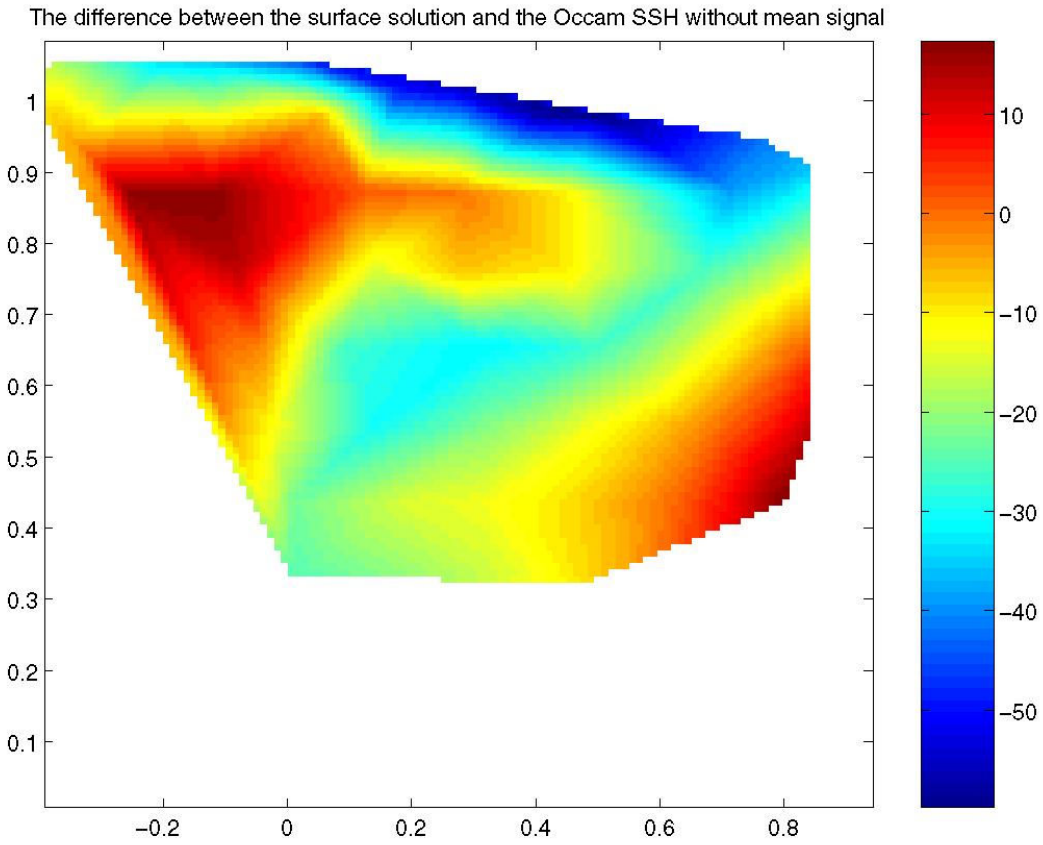

Figure 49: 2-D image of the difference (in cm) between the paired surface solution from floats only and the changes in the OCCAM SSH with the mean signal removed. The axes are the scaled latitude and longitudes. This is solution B.

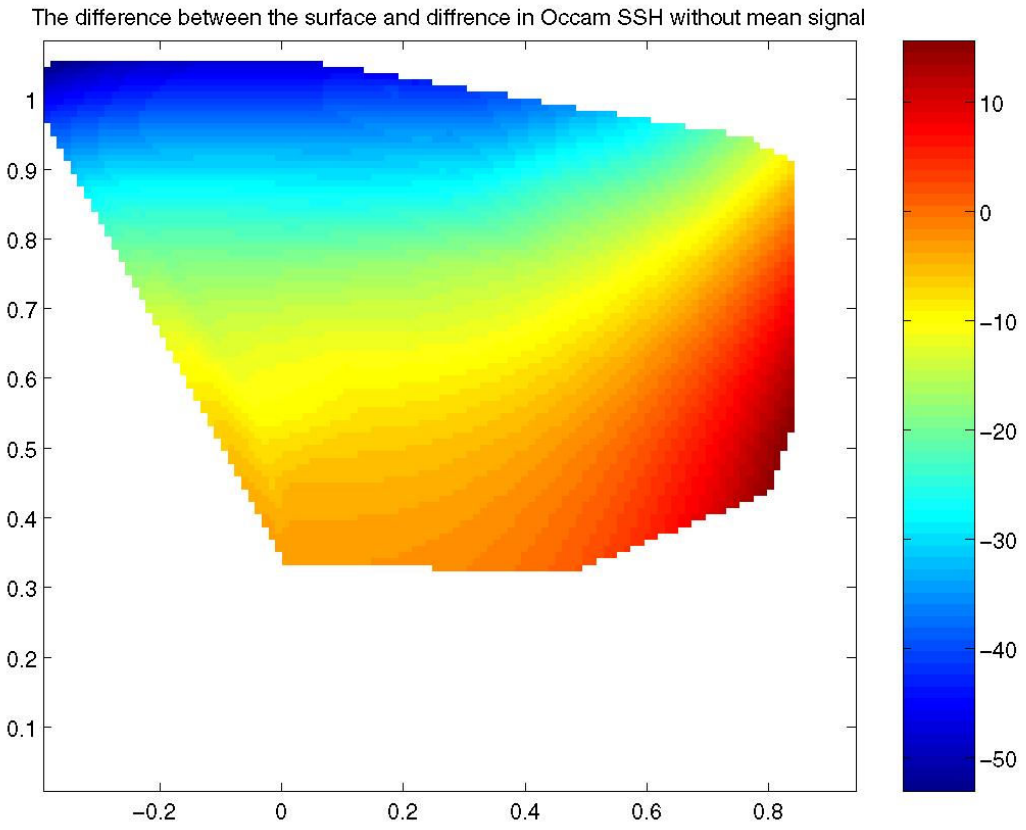

The Mean Square Error results for these calculations, which give a quantitative estimate of how well our solutions compare to the SSH, are discussed later in this chapter. We now present solutions where satellite altimetry has been added, and discuss the effects on the observed oceanographic features, the maximum and minimum of the signal and the MSE.

Results with the altimetry included in the solution:

We now show the effects of the addition of simulated satellite altimetry to the problem. We compare 'point' plots of the SSH solution obtained from the float and altimetry (Figure 50), and the SSH extracted at the float and satellite track positions from the OCCAM model (Figure 51). We also show a 2-D image of the surface solution (Figure 52) to allow a better examination of the oceanographic features reproduced by our method.

Figure 50: Dot plot surface solution obtained with both simulated floats and altimetry, showing values of the SSH (in cm) at the float stations and underneath the satellite tracks. The axes are the scaled latitudes and longitudes.

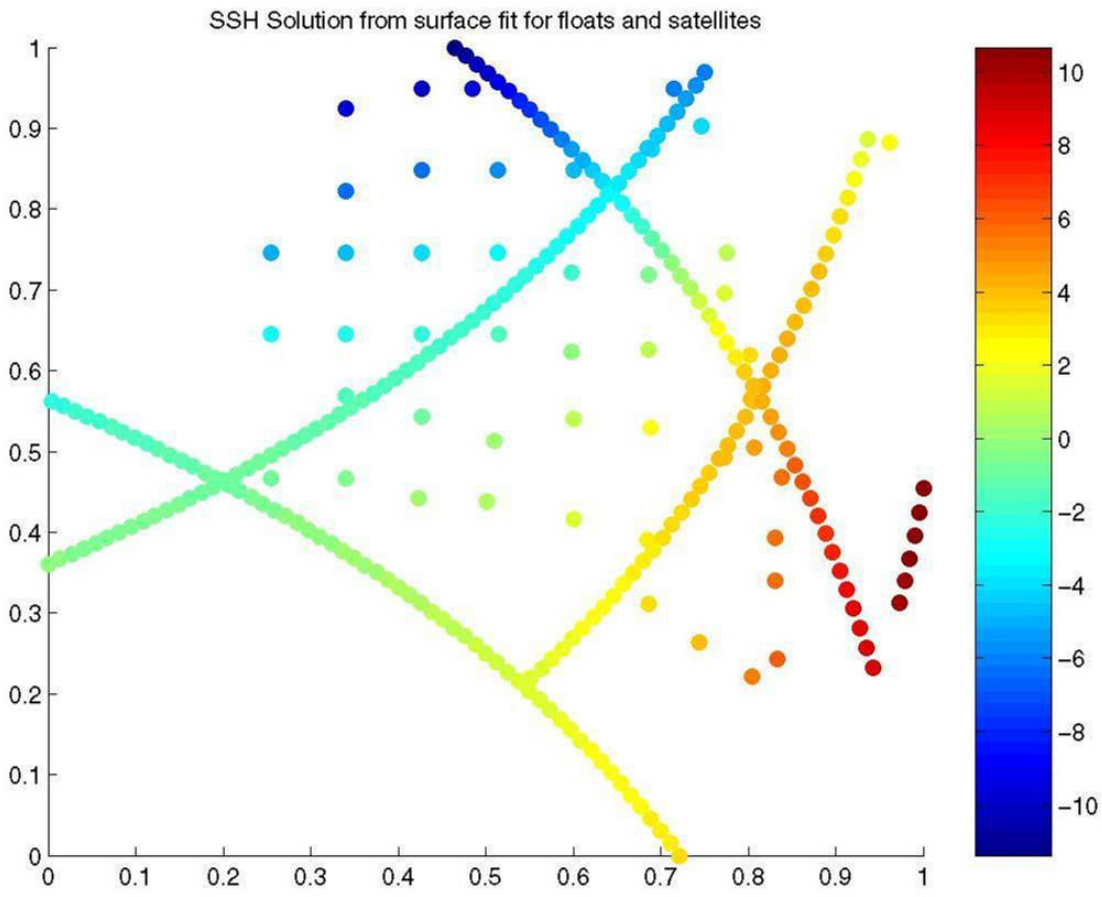

Figure 51: The OCCAM extracted SSH (in cm) at the same float and altimetry positions. The axes are the scaled latitudes and longitudes.

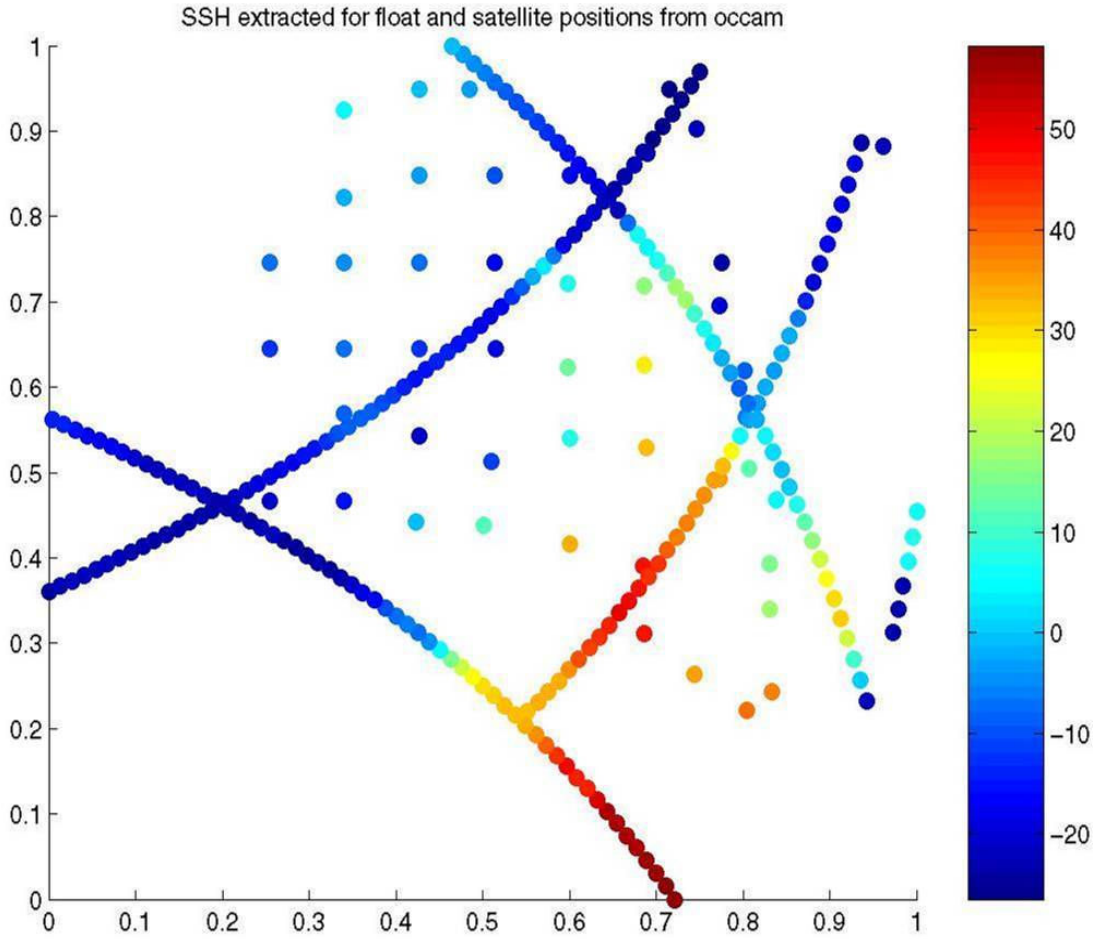

One feature of the two figures above that may appear odd is the slight divergence of the altimetry tracks. The tracks are in fact based on real TOPEX/Jason altimetry tracks, and diverge due to the effect of the rotational grid for the North Atlantic region used in the OCCAM model (see Chapter 3).

Figure 52: Surface solution for the same time steps using both simulated float and satellite altimetry.

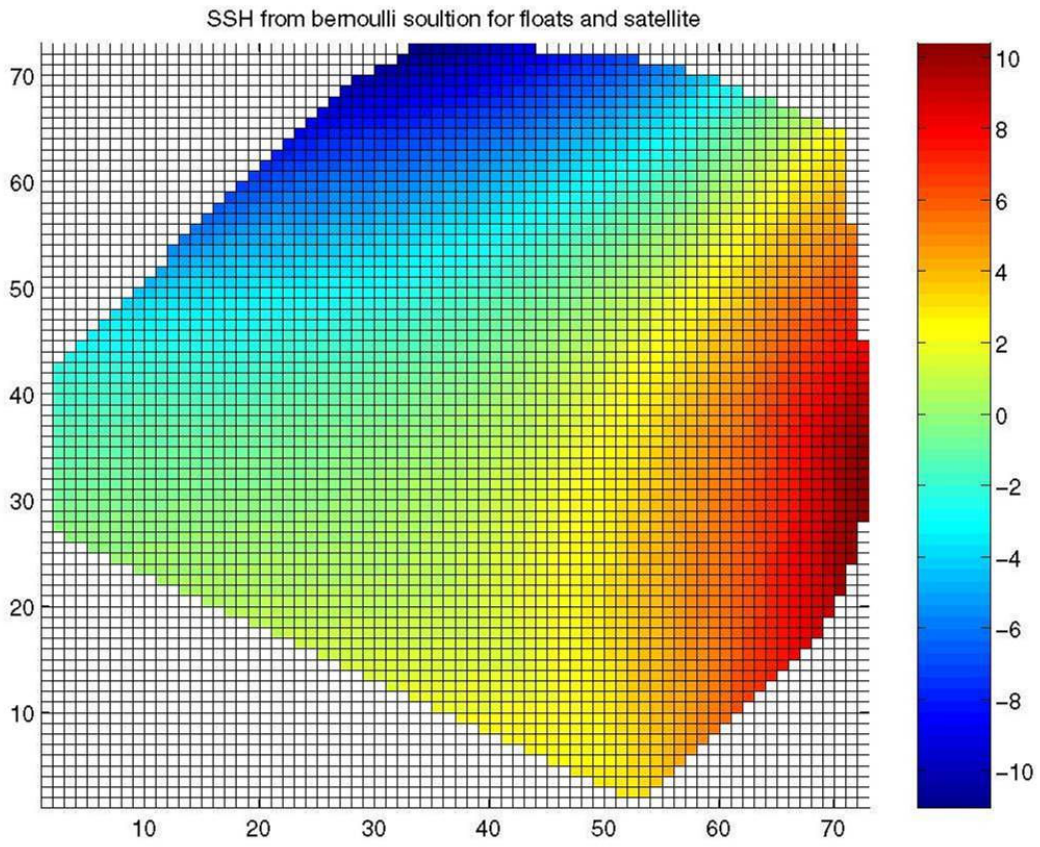

With the addition of the satellite altimetry to the method we notice that the magnitude of the signal in the SSH solution is reduced. Although we have seen some reduction to the maximum and minimum with the float only solution, this was only ±10 cm. When the satellites are added to the problem we see a much greater difference. The maximum/minimum range is reduced from ±50 cm for the expected signal to ±10cm. In the case of the earlier float only solution, we decided that the magnitude of the signal was reduced because the polynomial fit was of too low an order to reproduce the SSH signal accurately. There was too much smoothing of the signal taking place. The addition of the satellite altimetry seems to have increased this problem.

However, we will see later that the satellite altimetry reduces the MSE by half, suggesting a much more accurate fit to the data. It appears that though the altimetry data allows us to reproduce more of the structure of the original OCCAM signal, we may lose the extremes of the signal as a consequence, because the polynomial is too low in order and is still smoothing the signal too much.

Another effect on the solution when the altimetry is included is the domination of the altimetry over our float data. Our solutions typically involve data from around 50 floats and several thousand satellite altimetry points. Therefore in our solution information about changes in SSH dominates over the absolute SSH values from the Argo floats. The effects of this can be seen by making the same comparisons between our solutions and the OCCAM data as we made for the float only solutions. Plotting the difference between the surface solution and the OCCAM SSH with the mean signal removed (Solution A, Figure 53) shows a similar result to Figure 47, with the main differences associated with the maxima and the minima. However, plotting the difference between our paired surface solutions and the changes in the OCCAM SSH over the two time steps (Solution B, Figure 54), we see that there is much more correlation with the structure of the OCCAM SSH than we saw in Figure 49. Although the shapes are very similar the colour scales are very different. In figure 49 they go from -50 to +15 cm whereas in figure 54 they go from -14 to + 5cm. The RMSE is reduced from 47.4 cm to 28 cm.

Figure 53: Solution A, the differences (in cm) between the surface solution with altimetry and the OCCAM SSH without the mean signal. The axes are the scaled latitudes and longitudes.

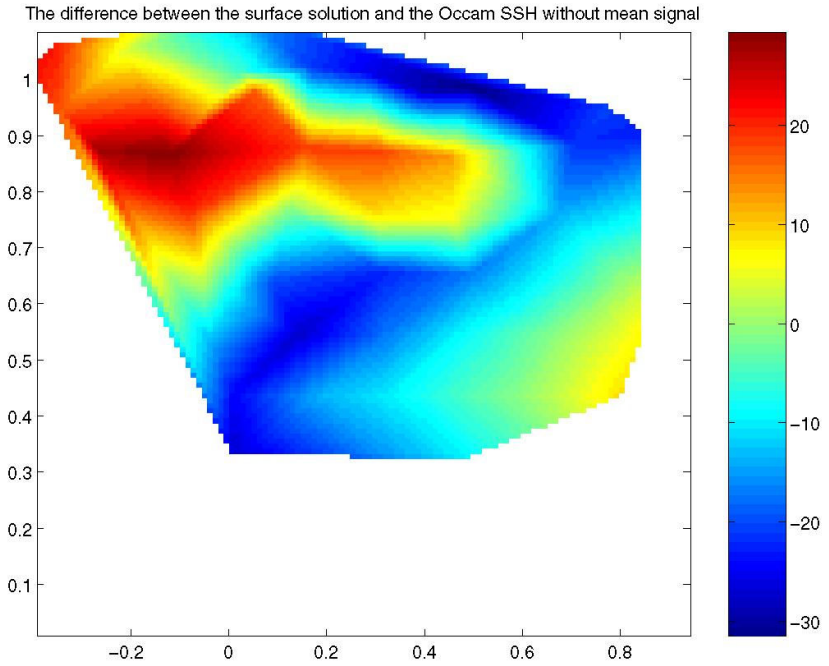

Figure 54: Solution B, the differences (in cm) between the surface solution with altimetry and the changes in SSH from OCCAM without the mean signal. The axes are the scaled latitudes and longitudes.

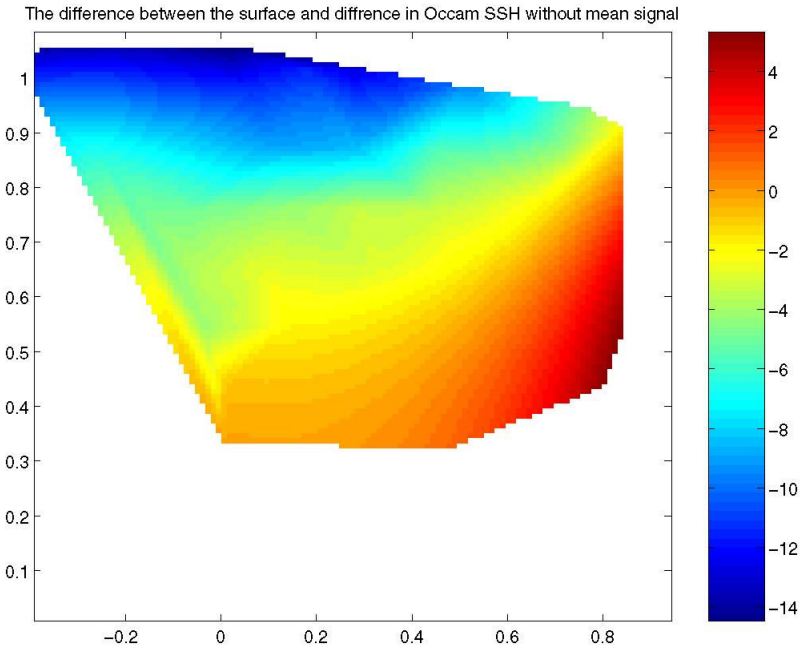

Figure 54 plots the difference in SSH seen between the two time steps (10 days) in the OCCAM model. It can be seen that the range of the minimum and maximum values for the differences in SSH from OCCAM are -5 to 15 cm whereas the extracted absolute SSH values are of the order of -50 to 50 cm. Therefore our solution with altimetry, where we see maximum and minimum signals in the range of -10 to 10 cm (Figure 50), is much closer in range to the change in the SSH between our two time steps, and not the absolute values. The altimetry has added more structure to our solution, but the large amount of satellite points by comparison to the number of float points in the solution causes it to be much closer to the changes in the OCCAM SSH than the absolute values.

This will clearly also be an issue in the "real" data solution as the amount of Jason altimetry is far greater than the number of ARGO floats used in the solution.

Figure 55: The difference in SSH (in cm) between two time steps of the OCCAM model.

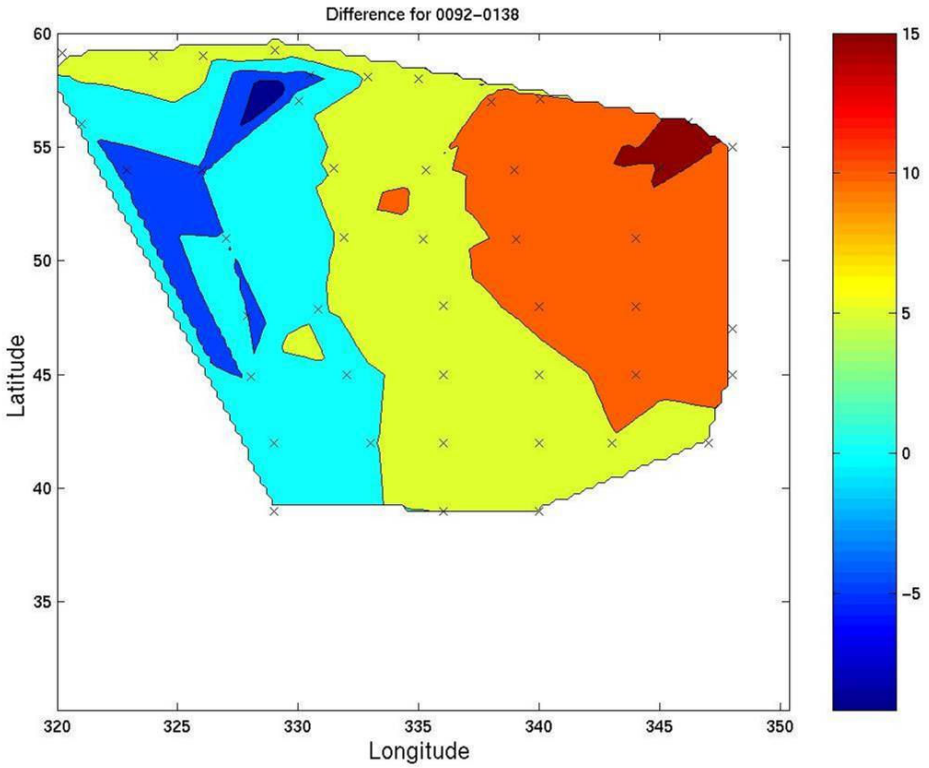

Test to see changes between time steps.

Before moving on to the real data solution, we ran paired solutions over three consecutive ten-day time steps to examine how much the region changes over these steps. These solutions (Figures 56-58) show only very small changes in the order of magnitude of the signals, with the main features (e.g. the low associated with the sub-polar gyre) remaining stable. As we would expect, we would have to run solutions over much longer time periods to show much significant change.

Figure 56: 2-D image solution for the simulated ARGO and Jason data, 1st 10-day time step. SSH for Figures 55-57 given in cm.

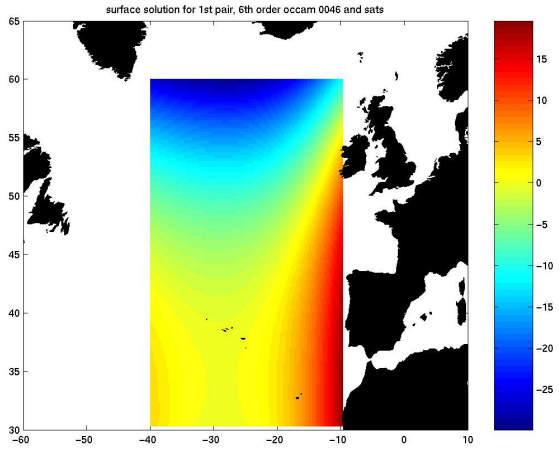

Figure 57: 2-D image solution for the simulated ARGO and Jason data, 2nd 10-day time step

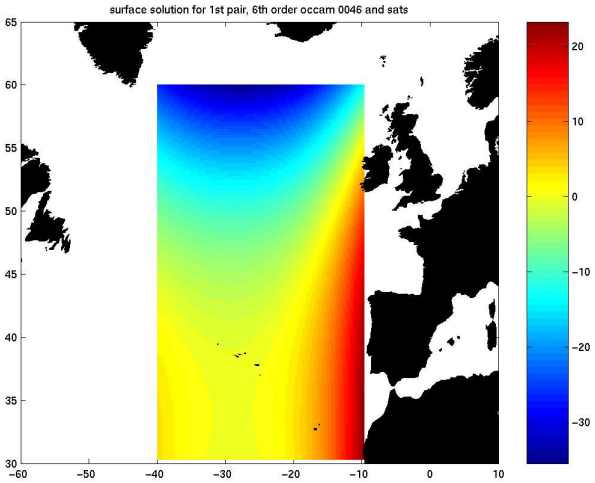

Figure 58: 2-D image solution for the simulated ARGO and Jason data, 3rd 10-day time step

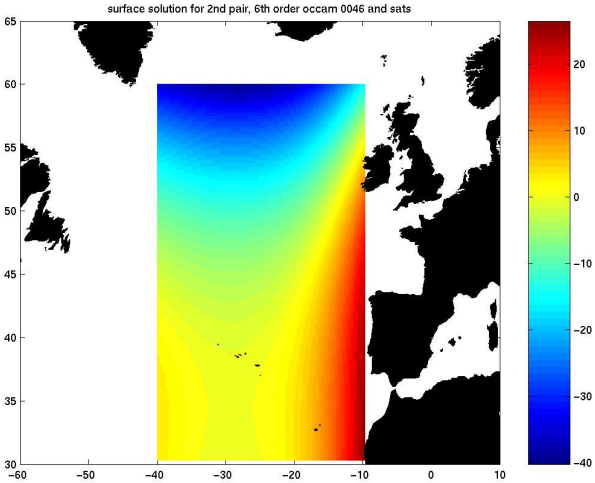

Applying a more complex polynomial surface fit:

In order to test if it was worthwhile fitting a higher order polynomial to the real data, we fitted 6^{th} and 7^{th} order polynomials to a float only solution of the same model data. These solutions are compared to the OCCAM data in the profiles in Figure 59. We see can that the 7^{th} order fit is reduced slightly in magnitude but the overall shape is very similar to the 6^{th} order fit. When we calculate the mean square errors at the end of this chapter, the value we obtain for the 7^{th} order fit (24 cm) is much closer to that of the solution including the altimetry (27 cm) than that of the float only solution (47 cm). As we would expect, the use of a higher-order polynomial reduces the smoothing of our surface solution. These differences are discussed in much greater detail at the end of this chapter and in the conclusions

Figure 59: Testing of 6th and 7th order polynomials (blue and red, respectively) against OCCAM SSH (green/black) and the OCCAM SSH minus mean signal (pink). The negative fits are due to changes in sign convention between the solutions. Vertical axis denotes the SSH in cm, horizontal axes shows float number.

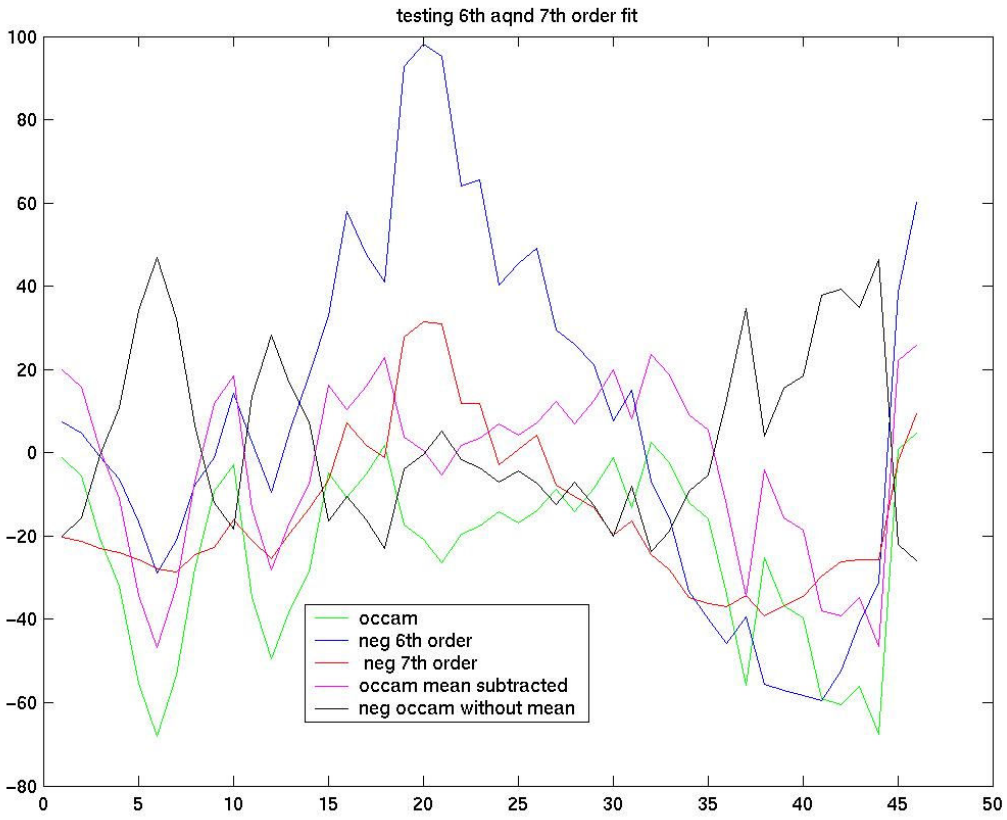

Changes made for the solution using "real" ARGO and Jason data:

Using the OCCAM model data gave us a great opportunity to properly test our method, as we knew what the solution should be. However, it was also much easier to work with model output than real data. For example, the model data had a standard grid arrangement, and unlike the real data sets were all in the same format. For these reasons we had to make some further changes to our method when we began to use real ARGO and Jason data.

Gridding of the satellite data/objective analysis

One of the key problems we encountered when using real rather than simulated satellite altimetry was that the different passes of the satellites were not necessarily on exactly the same positions each time, which led to missing data points or invalid data. Figure 60 illustrates this problem. The first pass of the satellite records data at the blue stars, while the second pass records at the red ones. This leads to complications when we wish to create a difference solution between the two time steps. We found that the simplest way to overcome this was to create a standard 6 X 6 km grid. We made this choice because the spacing between the satellite points is approximately 6 km. By using standard gridding routines in matlab, (meshgrid and griddata), we were able to create two uniform data sets to subtract from each other with very little error involved in doing so.

Figure 60: Schematic to show how different points may be obtained on different passes along the same satellite ground track.

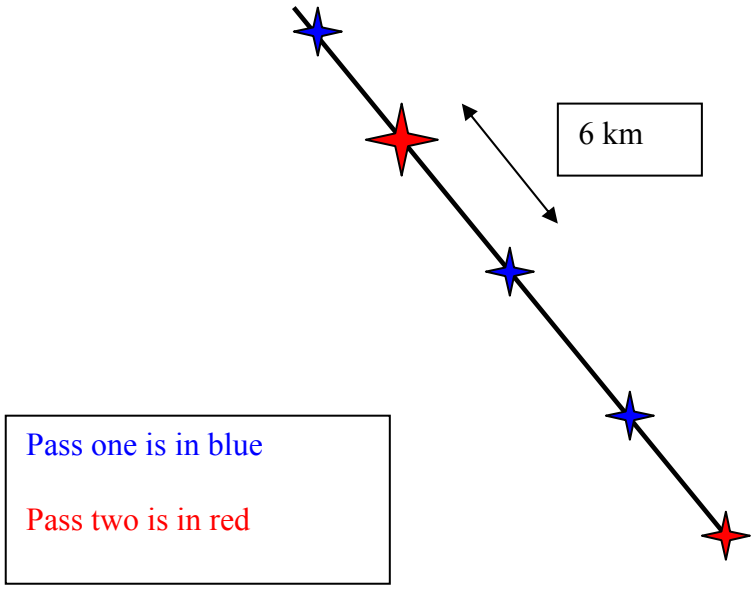

Changes made for the use of ARGO data in the method:

In our analysis we choose to use data from January 2003, in the second year of the ARGO program. We did this in the hope that some of the difficulties with the data set, e.g. technical problems with the floats, would have been ironed out by then, and that the data processing and correction routines would have improved. We found however that it was still not sufficient to just remove the absent data values from the data set. We needed to apply more stringent tests to remove bad data when extracting the profiles from the NETCDF files. We extracted the data every ten days, which guaranteed that

we did not have any overlap between the floats and prevented us from using the same float twice in different profiles. We only extracted profiles that had not been flagged as bad (a 99999 value), and that also had sensible data values for all of the properties, as follows:

Temperature range: [-3 40]

Salinity range: [20 40]

Pressure range: [0 7000]

By doing these extra tests we increased the accuracy of the solution by excluding obviously bad data.

We first compare a point solution, for the ARGO floats only, to the OCCAM model SSH, to check that our method produces reasonable results from real data. We then move on to producing paired surface solutions, first with float data only and then examining how this solution changes with the introduction of the satellite altimetry. In order to compare the different solutions with each other and the OCCAM SSH, they are all created on the same standard grid. We also test the different solutions by comparing the value of the mean square error for the different results.

Results from applying the Method to the "Real" data:

At this point in the study we have seen that our surface fitting methods are able to reproduce general oceanographic features of the OCCAM SSH with reasonably good success. However, we have also seen that the order of magnitude of the SSH signal has been reduced in our surface solutions, especially with the inclusion of the altimetry. Therefore, before moving on to applying the surface fit to the "real" data, we applied the "point" solution described in Chapter 4 to the ARGO floats. This quickly tests if our method can produce reasonable results from real data.

Figure 61: Point solution of real ARGO float data for comparison. SSH values are in cm.

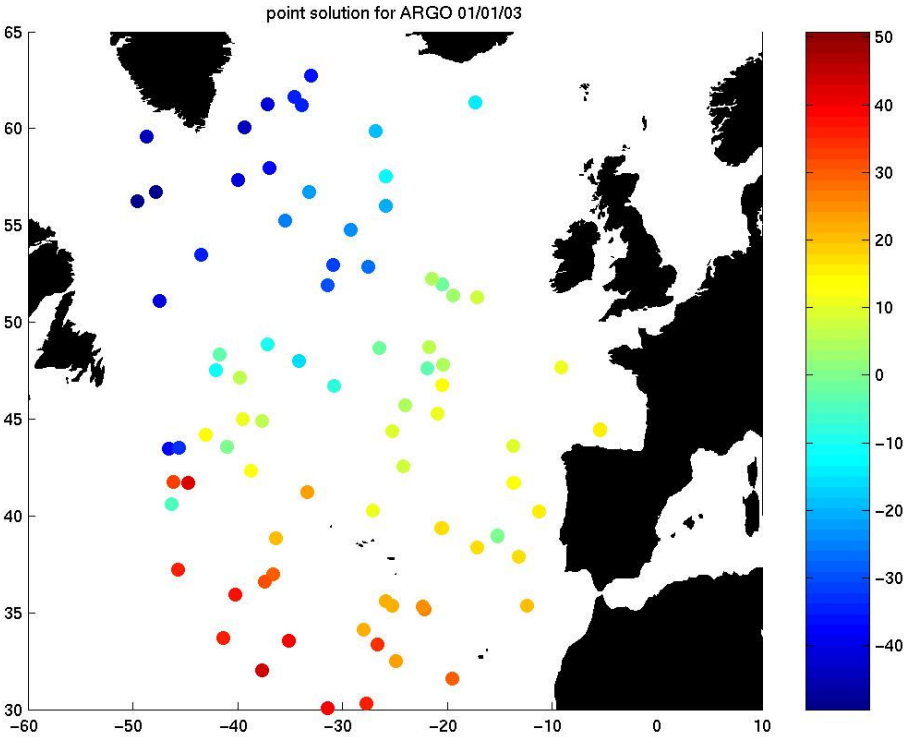

Figure 62: 2-D image of the same point solution. Note that SSH values are now in m.

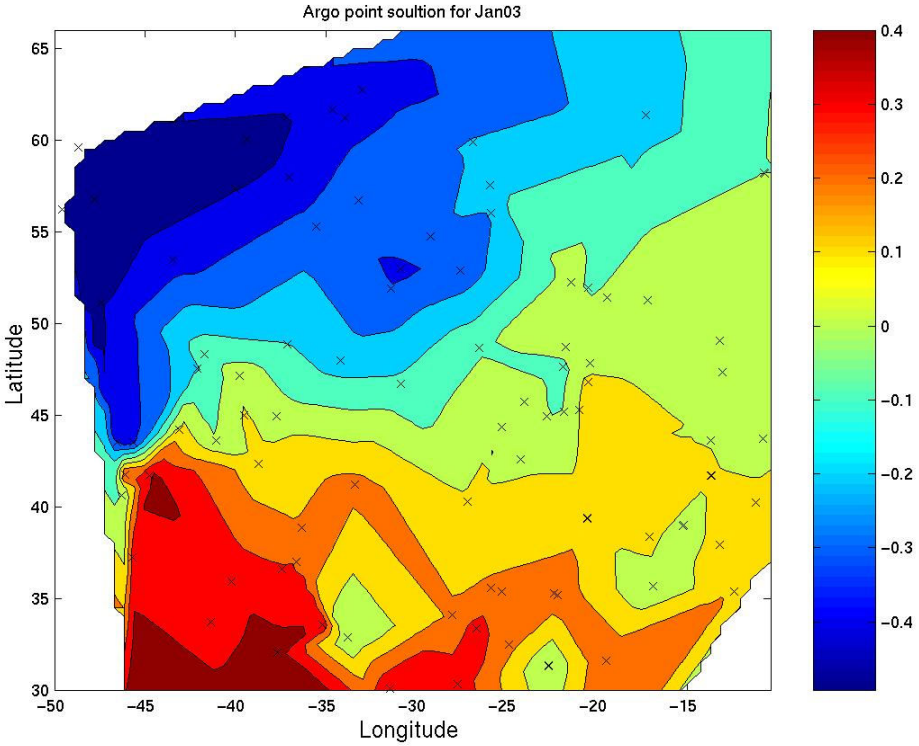

By comparing Figures 61 and 62 to plots of the OCCAM model SSH (e.g. Figures 30 and 32), we can see that the solution for the real ARGO data has a signal with similar features and magnitude. This suggests that the temperature and salinity data from ARGO are measured well enough to obtain a reasonable inverse solution and that we should be able to compare the "real" data and the OCCAM model sensibly.

Figure 63: Positions of the ARGO floats used for the two time steps of our paired solution.

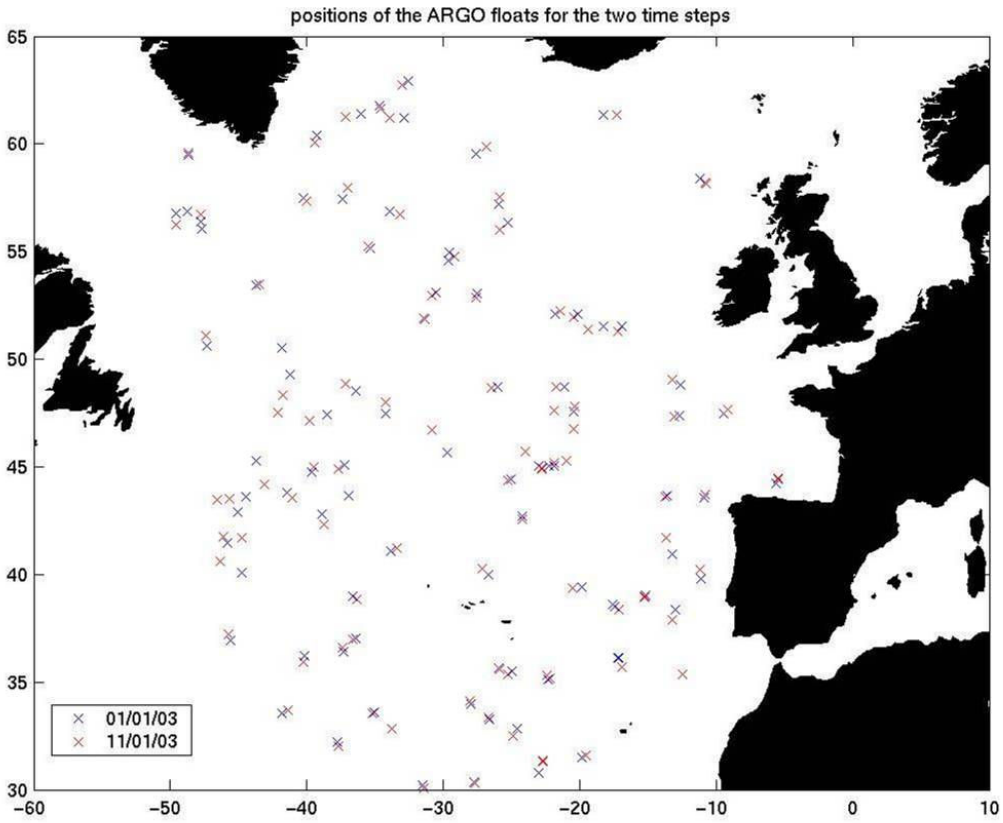

The ARGO and Jason data used in this experiment are from the first two weeks in January 2003. First we will look at the float only solutions, later incorporating the satellite altimetry to see how the results improve. We represent the data in two ways, firstly as a three dimensional surface and then as a 2-D image. Both are useful ways to look at the data. We have solved for the α parameters and then used the same standard grid as before to multiply out the 6th order polynomial equation and obtain a sea surface height solution. We then use a standard surface plotting and contouring routine in matlab. The surface fit (Figure 64) allows us to see clearly how we

have achieved the main aim of this program, namely obtaining a surface solution for the whole region of interest, but the 2-D image representation (Figure 64) is more useful when picking out the oceanographic features of the region.

Figure 64: Solution for the floats only using ARGO. The axes are the SSH in cm, and the scaled latitudes and longitudes.

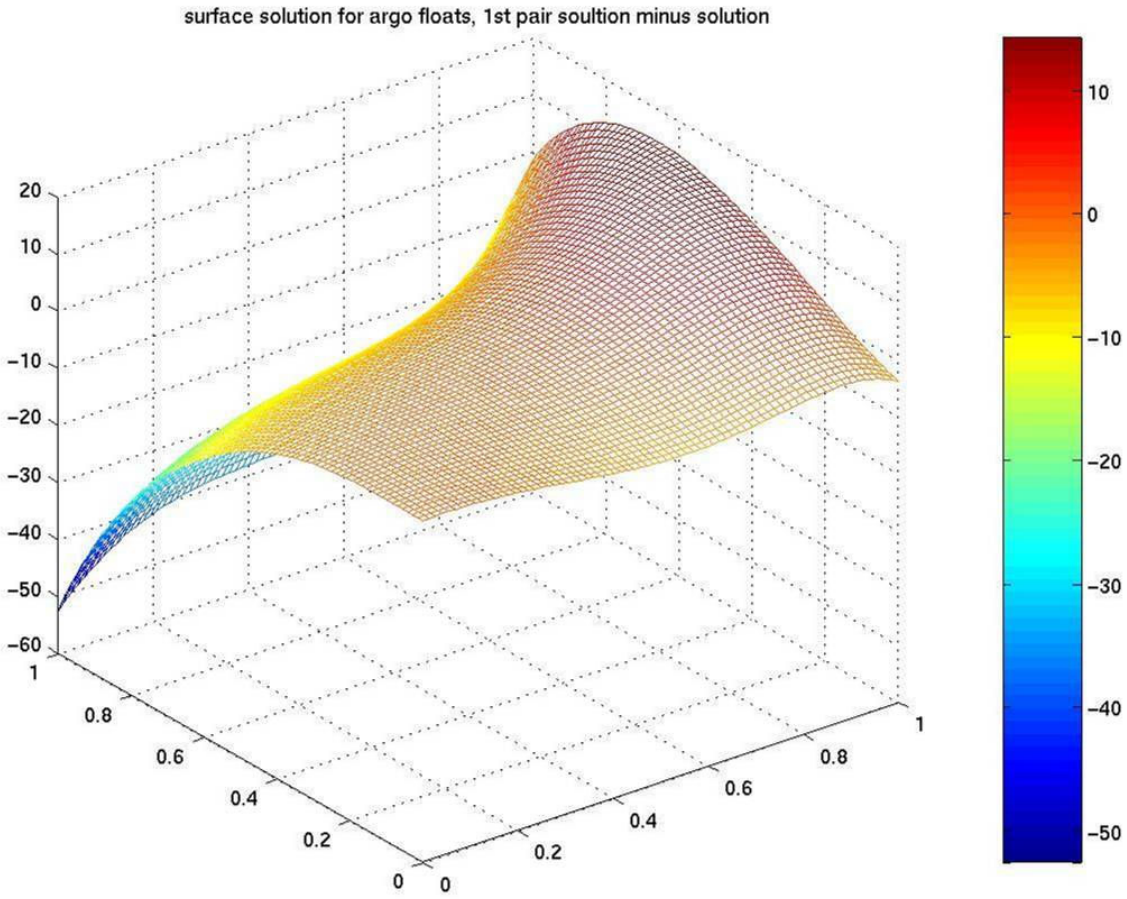

In the Figure 64 above we can clearly see the slope across the North Atlantic. It is positive (high) in the eastern region and negative (low) towards the North Western Greenland Front, which clearly shows the sub-polar gyre.

Figure 65: 2-D image surface solution for the 1st pair float only solution using ARGO. SSH values are in cm.

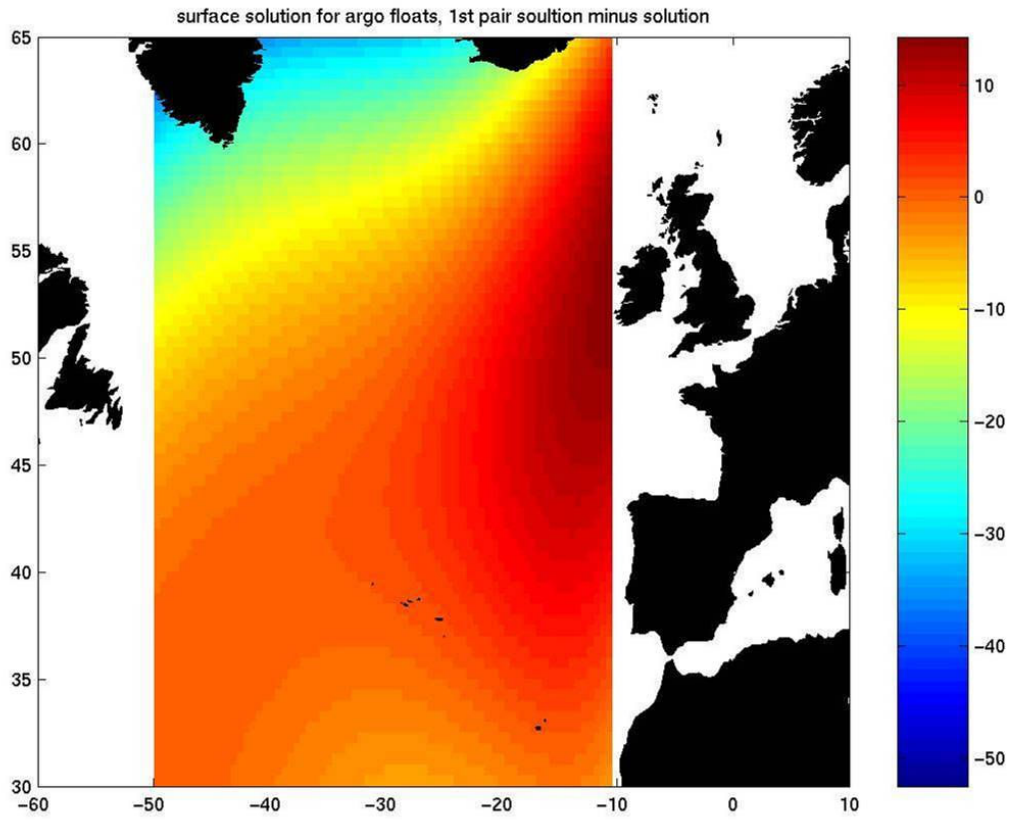

In the 2-D image representation (Figure 65) we can see that our surface solution can be correlated to the oceanographic features discussed in Chapter 2 (Figures 5 & 7). The dark red peak off the coast of Ireland at approximately 10° W, 50° N represents a topographic high caused by wind-driven movement of water with the North Atlantic Current, which is coming across from the south western corner of the figure. We can see a low associated with the sub-polar gyre around Greenland at 55° N, and possibly the northern boundary of the sub-tropical gyre at the bottom of the solution area. Though

the signal has been greatly smoothed by our choice of only using a 6th order polynomial, we see the general features which we would expect to find in a valid solution.

We then repeated the experiment, including satellite altimetry data in the problem (Figure 66), to see what difference this would make to our solution. We solved using two different areas of Jason data. Figure 67 is the solution using the area indicated in Figure 17(a). Figure 68 shows the solution using a larger area, as indicated in Figure 17(b) and Figure 66 below.

Figure 66: Example of ARGO and Jason positions solution in Figure 67. This is the larger Jason area used.

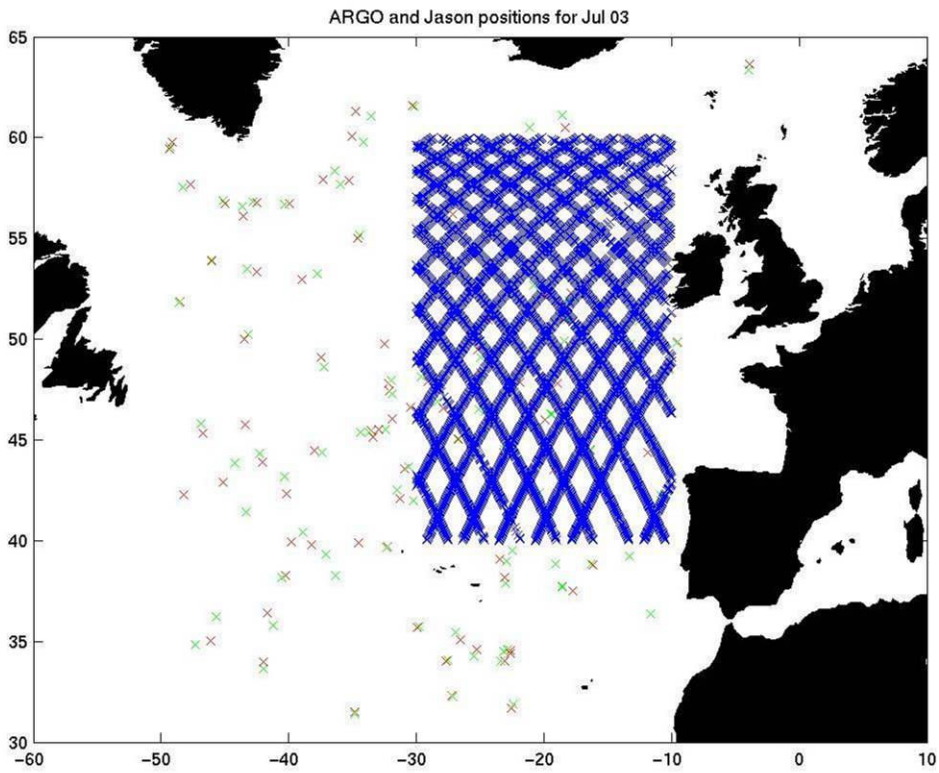

Figure 67: Smaller solution area using Jason data (see Figure 17(a) for data coverage). SSH is in cm.

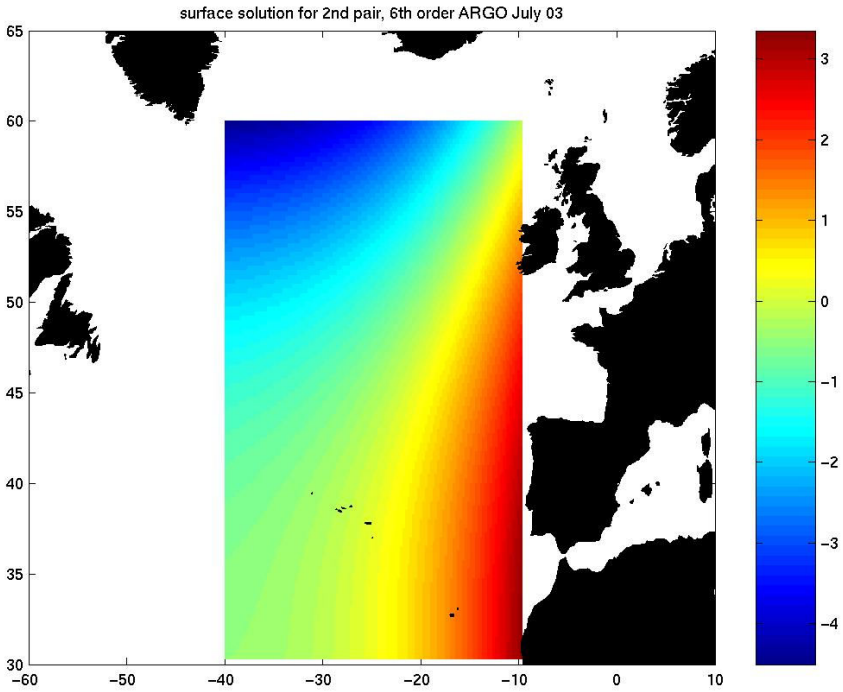

Figure 68: The solution for a larger area of Jason used. SSH also in cm.

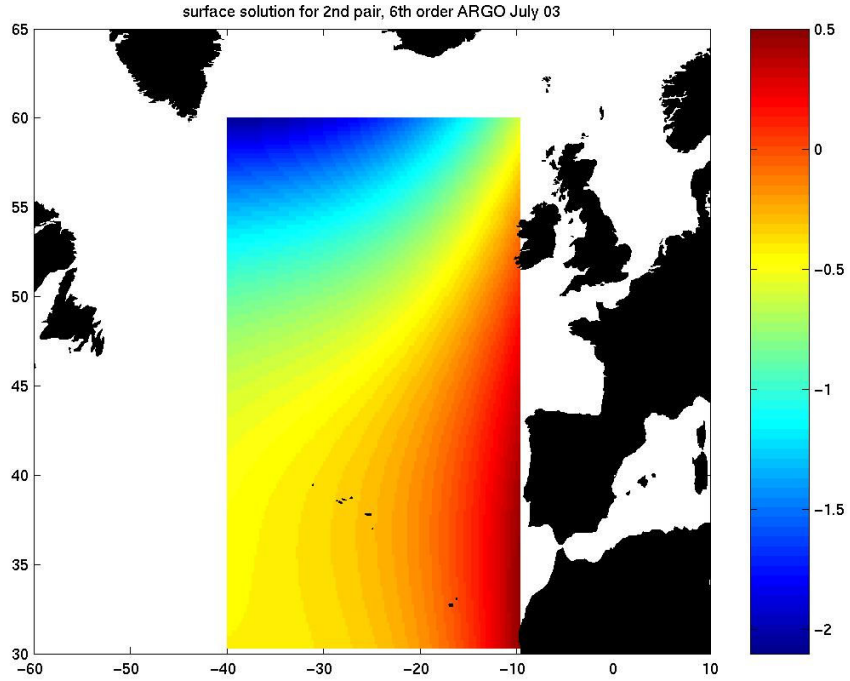

By comparison of Figures 67 and 68 with the float only solution in Figure 65 we can see two clear results. The first is that with the inclusion of more satellite data, we obtain more detail in our solution. The second is that there is a trade off in doing this as we also find that the magnitude of the signal is greatly reduced as the amount of altimetry data in the solution is increased. As we have already discussed, the inclusion of satellite data in our simulated solutions has a tendency to force the solution towards a difference solution rather than an absolute SSH. A plot of the difference in Jason altimetry between the two time steps of our "real" solution (Figure 69) shows most of the variation is of the order 10 cm or less. Therefore it seems that the small magnitude of the SSH signal in our "real" solutions is also due to this effect.

Figure 69: The difference in Jason altimetry for the 2 time steps plotted as a surface in meters

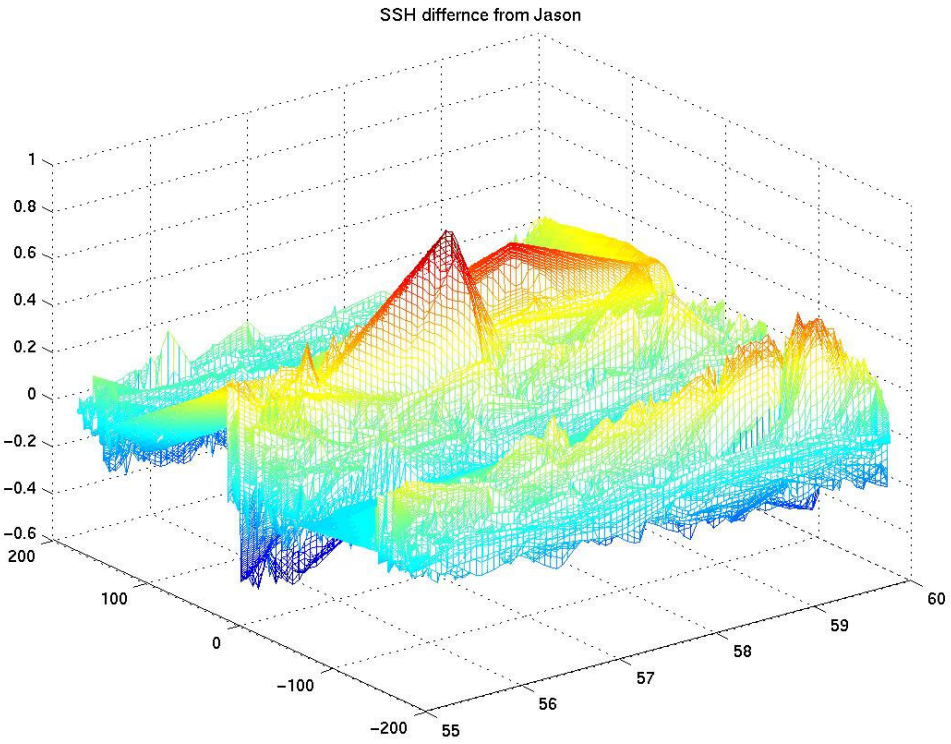

Up to this point all of the data, both real and simulated, that have been used in this project have been taken from January, the time of year when the SSH signal in the North Atlantic is expected to be higher and more variable due to greater storm activity. For comparison, we also ran a float only solution using data from July, which is plotted in Figure 70 below.

Figure 70: Float only solution using data from July rather than January. SSH in cm.

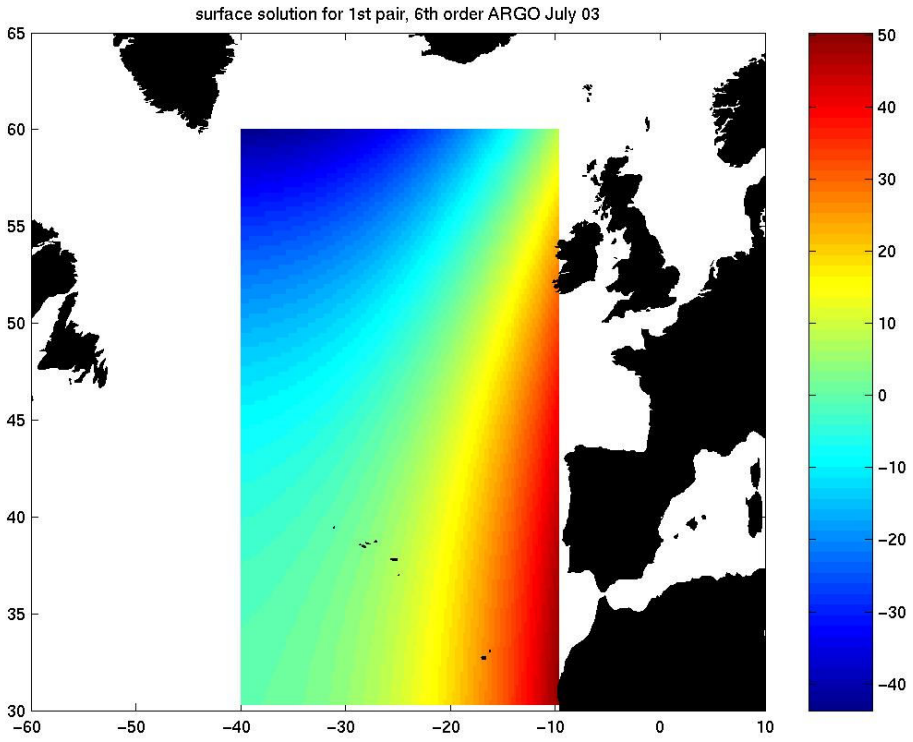

In comparison to Figure 65, the surface fit for this solution shows less small-scale variability. As we might expect, the reduced variability in actual SSH heights at this time of year mean that small scale features are even less likely to survive the smoothing effect of the polynomial.

Calculating the Mean Square Error:

Up to this point we have examined our solutions in a very qualitative way. We now apply Mean Square Error calculations to our solutions for a more quantitative assessment of their performance. We wish to see if the variance of the solution does in fact decrease with the addition of the altimetry, and if the altimetry solution is in fact closer to the changes in the SSH from the model rather than the absolute SSH values.

In a sense, any measure of the centre of a distribution should be related to some measure of the error in the data. If we have a number t, a good measure of the centre, then presumably we are saying that t represents the entire distribution better, in some way than other central measures.

The *mean square error* (MSE), is the measure of the quality of t, as a measure of the distribution. The error is the amount by which the estimator differs from the quantity to be estimated.

Equation 34 $$MSE(t) = \frac{1}{n}\sum_{i=1}^{k} f_i (x_i - t)^2 = \sum_{i=1}^{k} P_i (x_i - t)^2 = \frac{1}{n}[(X\text{-}t)^2]$$

Or we can think of the MSE as:

Equation 35 $MSE(t) = (\text{bias}(t))^2 + \text{variance}(t)$

MSE(t) is the average of the square of the distances between t and the data. The best measure of the centre, relative to this measure of error, is the value of t that gives us the lowest value of MSE.

To find the MSE for our solutions, we took the total number of OCCAM points (n) used in the solution, found the reciprocal of this value (1/n) and multiplied it by the sum of the squares of the difference between the OCCAM data and the surface solution $[(X-t)^2]$, when both of these data sets were mapped onto the same standard grid. This gives us an estimate of how well the model has predicted SSH at the points where we did not originally have OCCAM data. The mean square error calculations are in cm^2. We obtain the square root of this value to obtain the standard deviation in cm.

Mean Square Error Calculation results (MSE):

The table below shows the MSE results from three snap shots tested. We have used the same standard grid as before.

We place the OCCAM data, we used in the solution, on to the same standard grid as that of the surface solution. We did this in the same way as we have done previously.

We then compared the MSE calculations for each of our solutions with the both the changes in the OCCAM SSH and the absolute SSH extracted from the model.

From our earlier results in this chapter, we would expect that our solution should be closer to the changes in SSH than the absolute SSH. We would also expect to obtain a smaller MSE for the solution containing the satellite altimetry.

The upper half of the table below compares each of the solutions to the SSH from OCCAM. The lower part of the table is the comparison between the solution and the changes in SSH from OCCAM.

The units of the MSE are centimetres squared. We square root this result to give a measure in centimetres of the root mean square error (RMSE).

With the inclusion of the satellites the magnitude of the MSE is reduced in all cases. For the first time step we have 47cm reduced to 27cm for the solution containing altimetry.

More importantly the number is reduced in comparison to the OCCAM differences. The satellites have done a better job of reproducing the changes in the OCCAM SSH than the floats. This is the expected result.

Some solutions are better than others. The solutions for the 1st and 3rd time steps are better than those for the 2nd and 4th. There is no clear reason for this. It may be just due to the variability in those particular time steps or there may be a better coincidence between the float and satellite data sets.

Table 4: Table of MSE results. Top section of table Solution A (page 128) and bottom section Solution B (page 128)

Data	**MSE using OCCAM SSH/cm^2**	**square root of MSE /cm**
Point solution floats only 1st time step	681	29.1
Surface solution floats only 1st time step	2190	46.8
Surface solution floats & satellite 1st time step	747	27.3
7th order surface solution floats only 1st time step	584	24.2
Surface solution floats only 2nd time step	7410	86.1
Surface solution floats & satellite 2nd time step	2540	50.4
Surface solution floats only 3rd time step	11700	108
Surface solution floats & satellite 3rd time step	568	23.8
Surface solution floats only 4th time step	14900	122
Surface solution floats & satellite 4th time step	10600	103

Data	**MSE using changes in OCCAM SSH/cm^2**	**square root of MSE /cm**
Surface solution floats only 1st time step	2250	47.4
Surface solution floats & satellite 1st time step	783	28
7th order surface solution floats only 1st time step	621	24.9
Surface solution floats only 2nd time step	6810	82.5
Surface solution floats & satellite 2nd time step	2450	49.5
Surface solution floats only 3rd time step	9380	96.8
Surface solution floats & satellite 3rd time step	567	23.8
Surface solution floats only 4th time step	12000	109
Surface solution floats & satellite 4th time step	9230	96

Chapter 6

Generalized Additive Models, (GAM's):

Following on from chapter 5, where we have explained how we have fitted a simple polynomial function to the data to create a "surface" solution for the inverse, we now explore the other ways to solve this problem. How would we make the basis function more complex and what would happen if we were to do this? We could fit a piecewise polynomial, a spline to the data but instead we have chosen to fit a GAM, a generalized additive model. GAMS are explained in full in (Hastie, 2001). We took further details from Advanced Regression notes from the Statistics for Environmental Evaluation, Dept. of Statistics, University of Glasgow, written by A. Bowman and S. Wood, 2004.

We have chosen to fit a GAM as they are far more versatile than a standard line model. Normal linear models require us to know a great deal about the form of the relationship between the response variable, y, our sea surface heights in this case, and the predictor variables, latitude and longitude in our data. We would need to be able to write down exactly how y depended on our x's additive models attempt to give us a lot more freedom. The "kinks" in the model fit are decided by "smoothing terms" rather like the "knots" in a spline function. The greater the number of smoothing terms the smoother the

fit, the less smoothing terms and we would be fitting directly to the data points.

The linear model is replaced by an equation such as:

Equation 36 $$y_i = \beta_0 + \beta_1 x_{i1} + \beta_2 x_{i2} + m_1(x_{i3}) + m_2(x_{i4}) + m_3(x_{i5}, x_{i6}) + \varepsilon_i$$

Where the m_j are the smoothing functions and the ε_i's are independent random variable. Therefore y is given by some regular linear model terms plus the sum of some smooth functions of the predictors plus a random error term.

We now need some way of deciding these new smoothing terms, m_j. The smoothness is controlled during the model fit by penalized least squares. The model unknowns are fitted by minimizing a weighted sum of the residual sum of the squares and some measure of the wiggliness of the m_j's. For example the simple model:

Equation 37 $$y_i = m_1(x_{i1}) + m_2(x_{i2}) + \varepsilon_i$$

This would be estimated by finding the functions m_1 and m_2 minimizing

Equation 38 $$\sum_{i=1}^{n}(y_i - m_1(x_{i1}) - m_2(x_{i2}))^2 + \lambda_1 \int m_1''(x_1)^2 dx_1 + \lambda_2 \int m_2''(x_2)^2 dx_2$$

Where the two integrated square second derivative terms measure the wiggliness of the two smooth functions, and the parameters λ_1 and λ_2 control the trade-off between the model fit and the smoothness of the two terms.

Now we need to discover how the λ_j's may be estimated. If we choose to minimize the penalized residual sum of the squares, this would lead to zero. This means the model fits the data as closely as it can, but this means fitting the "noise" as well. One solution is to fit the solution to the data so they are not match to as closely as possible to the curve, but rather we emphasize the data points that are not being fitted for by the solution. This is cross validation. For given smoothing parameters, each data point is omitted from the dataset in turn, the model is fitted to the remaining data and the square of the error is predicted for the omitted datum. The average of these predicted errors is the cross validation score which is used for estimating the λ_j's. This idea is shown in the figure below.

Figure 71: Illustration of the principle of cross validation.

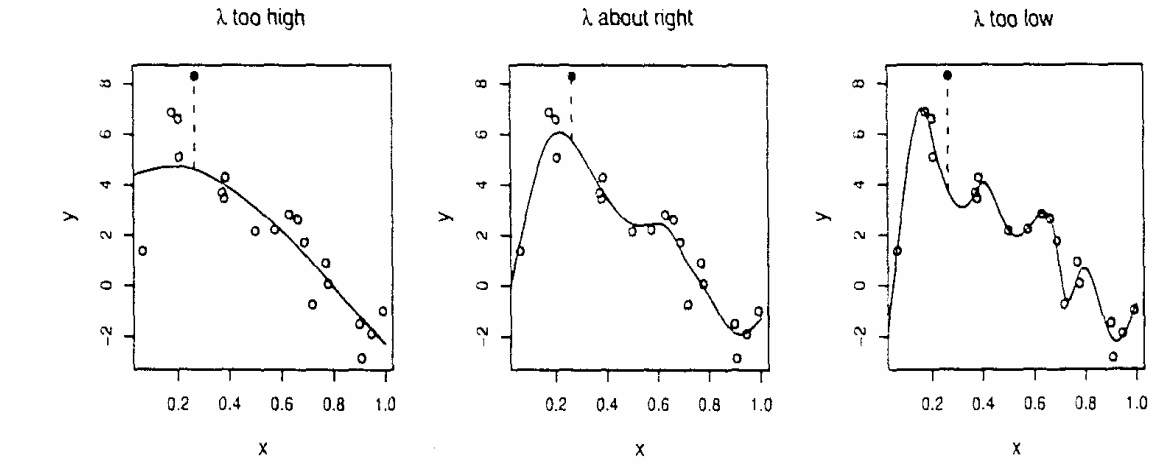

In figure 71, illustrates the principle of cross validation discussed above. In this case the fifth data point (solid black dot) has been omitted from the fitting and continuous line shows a penalized regression spline fitted to the remaining data (◦). When the smoothing parameter is too high the spline fits of the data poorly and does no better with the missing point. When λ is too low the spline fits the noise as well as the signal and the extra variability that this includes causes it to predict the missing datum poorly again. For the intermediate λ the spline is fitted the underlying signal quite well, but smoothing the noise, as a result the missing datum is reasonably well predicted. Cross validation leaves out each datum from the data in turn and considers the average ability of models fitted to the remaining data to predict the left out datum.

This example and figure have been taken from Advanced Regression notes from the Statistics for Environmental Evaluation, Dept. of Statistics, University of Glasgow, written by A. Bowman and S. Wood, 2004.

Results obtained for GAM fit:

In this section as we have explained we have taken our earlier "point" solution data for a few time steps and fitted the GAM to the data. This is meant as a test to see how well our polynomial surface has done in comparison to a more complex surface function.

We can see the results are very similar. We have obtained the same expected positive slope of the North Atlantic towards the eastern side of the basin. The results of the GAM are in metres, unlike some of our earlier results which are represented in centimetres. The "point" solution we have used here is the float only solution as a test. We chose this because our results so far have suggested that the float only solution is closer in magnitude to the original OCCAM data. Though the shape of the signal has not been altered by the inclusion of the altimetry there is a tendency for the magnitude in the signal to be reduced as we have seen in the previous chapter.

The next few three figures are the GAM fit obtained using the R programming package. These coincide with the first three time steps for all our solutions. If we go back to our point solution result obtained in chapter 4 figure 36, we will see the first time step has a solution range of [-20 40] cm. The extracted range of SSH from OCCAM is ± 50 cm, figure 32. our first time step solution from the GAM is in a range of [-10 30] cm. This is slightly lower than our

Bernoulli "point" solution we obtained and quite significantly lower than our expected SSH from OCCAM. But if we look at our 6^{th} order float only surface solution, which was ± 40 cm we are doing slightly better. But it is probably better to compare our GAM fit with that of the 7^{th} order more complex fit surface fit. This fit obtained a result of [-25 30] cm, which is a lot nearer to the value obtained by our GAM. Our other two time steps for our GAM solution are similar at , [-20 40] cm and ±20 cm.

From these results we can deduce as we have done with both the 7^{th} order polynomial fit for the floats only surface solution and the 6^{th} order solution containing the satellite altimetry that there is a trade off between obtaining a more complex higher resolved surface fit and the reduction in the magnitude of the signal obtained. We should note that any "smoothing" function must reduce the range of the signal. The extremes in the signal will be omitted.

Another key point to consider here is what difference it makes fitting the surface function after the inverse solution has been obtained, rather than solving for a surface as we have previously done. Our surface solution with floats only has done a better job than our "point" solution surface fit. This would suggest that we are better off solving for a surface. We have seen that we are able to increase the detail of the surface fit with both the addition of satellite altimetry and the use of a more complex polynomial surface. Though there has been some difficulties with a reduction in the magnitude of the signal.

Figure 72: GAM fit for float only data simulated in OCCAM, the 1st time step

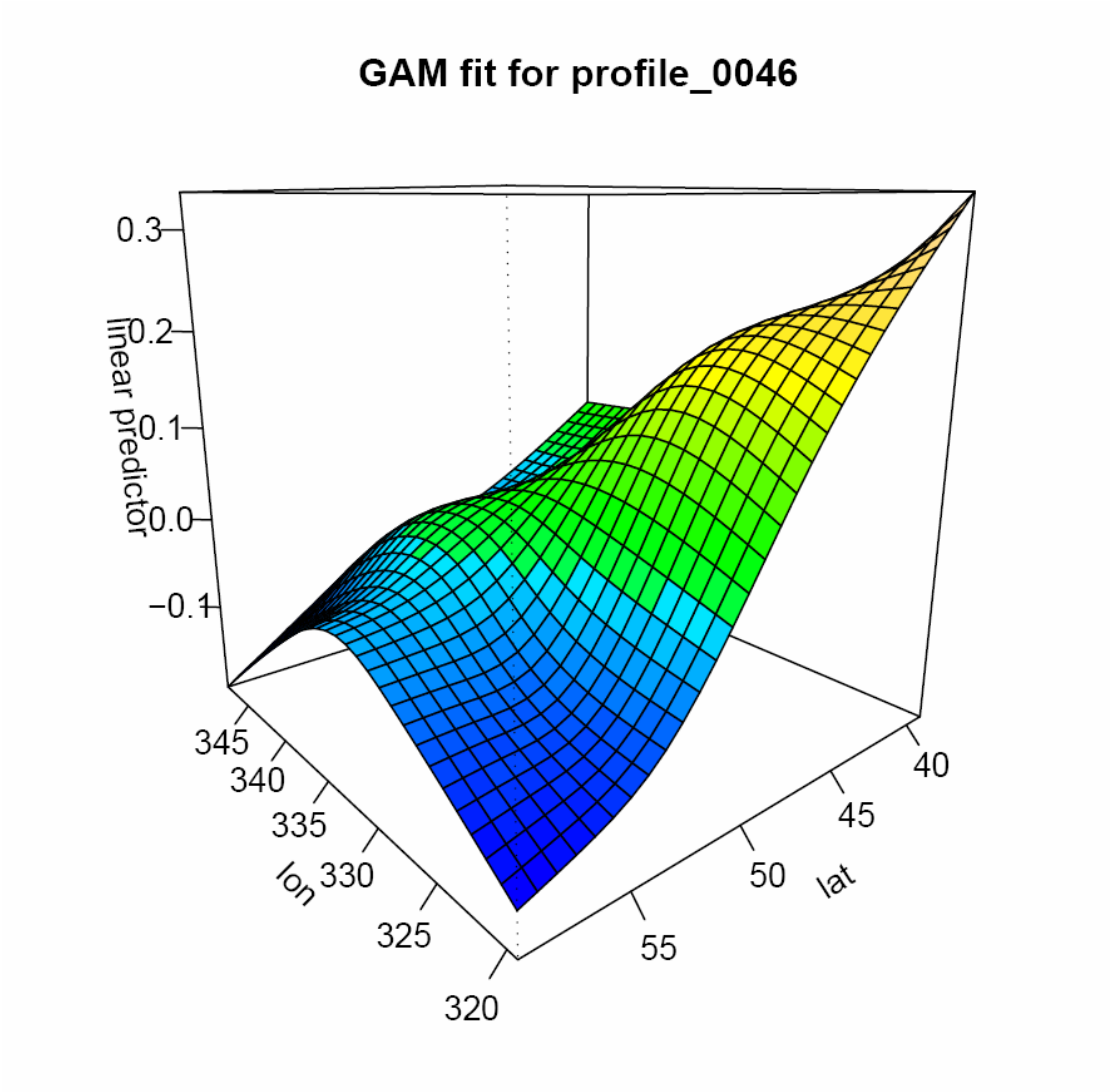

Figure 73: GAM fit for float only data simulated in OCCAM, the 3rd time step

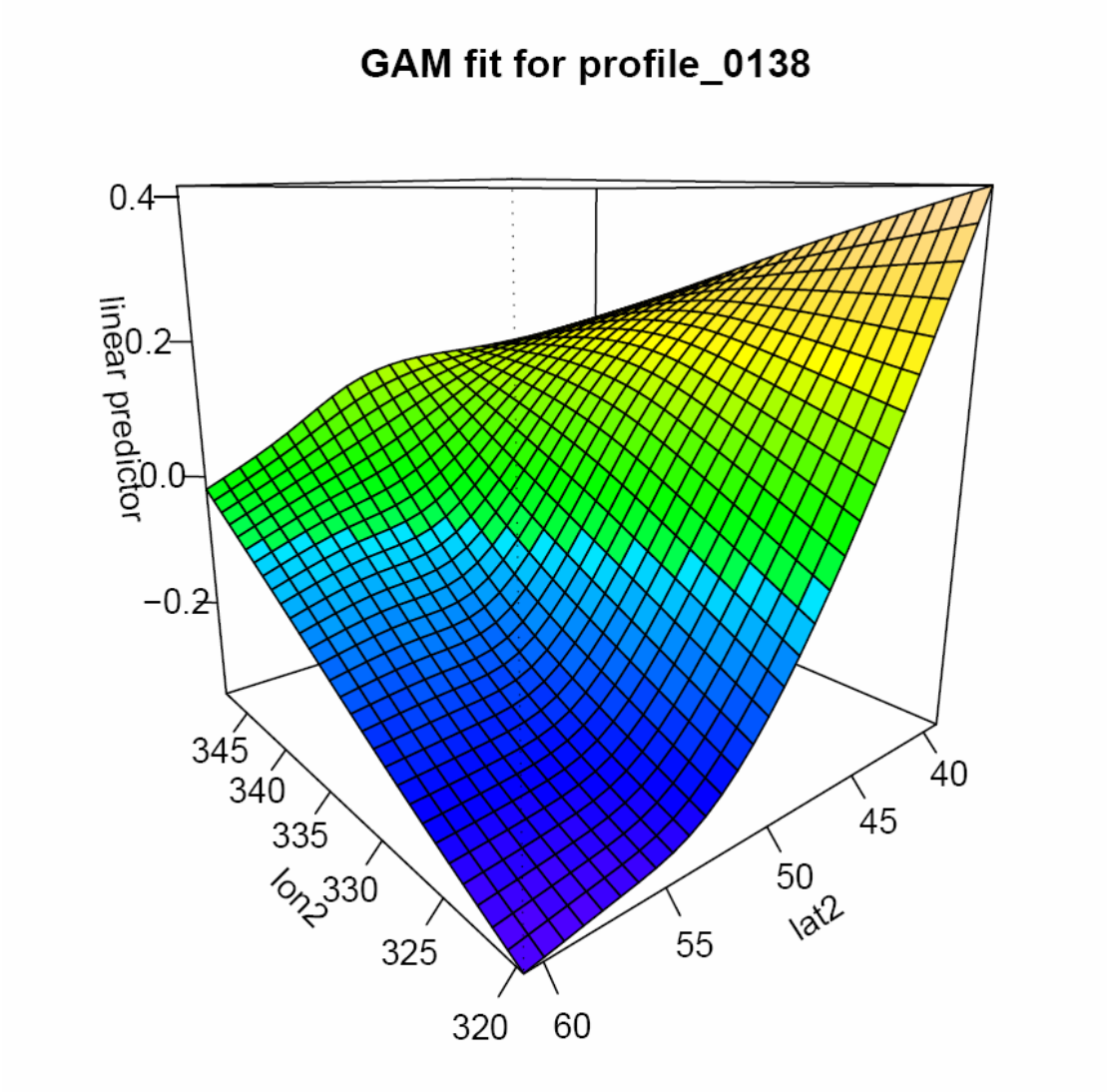

Figure 74: GAM fit for float only data simulated in OCCAM, the 4th time step

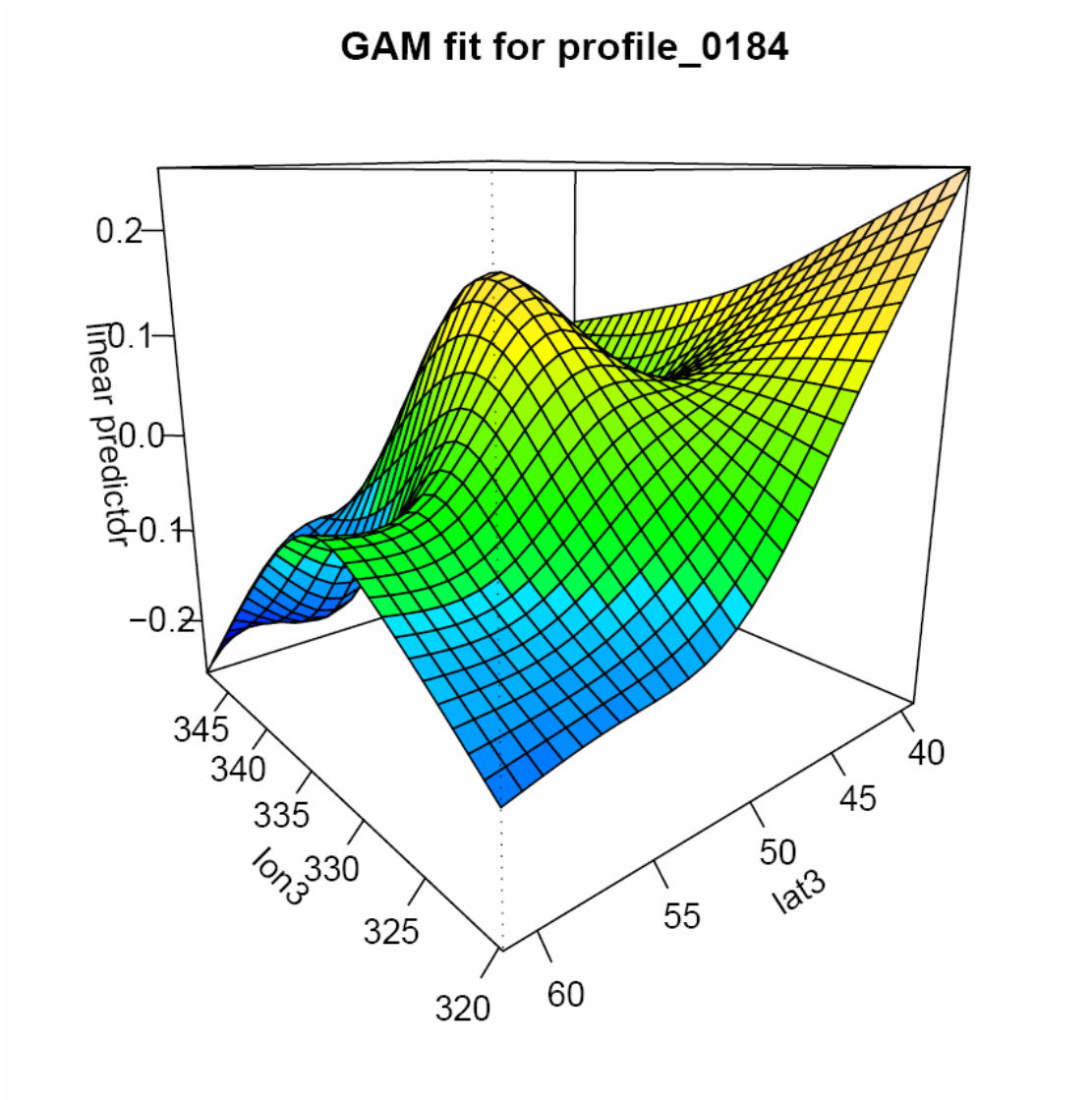

Chapter 7

Conclusions and Future work:

Introduction

In this thesis I have for the first time combined ARGO and satellite Altimetry in an inverse solution. ARGO is designed to work with altimetry but so far people have only tried to achieve this by combining these data with ocean models in complex assimilation schemes. As we move to operational oceanography there is a need for data products that are independent of the models and can be used for validation. My aim was to produce a non-model dependant method for combining these two data sets. If successful this would produce an additional way of validating ocean model predictions.

One difficulty with ARGO is that as a Lagrangian system the data are not on a regular grid. This means a lot of traditional data analysis methods cannot be used. I chose to use the Bernoulli inverse method to study this problem, in part this is because this method developed at the NOC and in principle it seemed suitable. Unfortunately the results did not live up to their expectations. Possible reasons for this will be given below.

Summary

After describing the problem and the datasets involved in chapters one to three, I outline my method in chapter four. After considering the various inverse methods that have been suggested I decided to use a variation on the Bernoulli method, (Killworth, 1986; Cunningham, 2000) for this problem. We have illustrated these methods in a region of the North Atlantic. The novel aspect of my version of this method is to fit a surface rather than obtaining sea surface height at individual points. This enabled me to solve for a sea surface height at points where I did not have a T/S profile which enables me to combine the solution with altimeter data. In chapter four I tested the established Killworth-Cunningham method using simulated floats in the OCCAM model. The use of the model enables me to test the method because I know the true value of the solution. However the use of the OCCAM model introduced its own problems. In particular I found that the velocity values at depth were very low, in fact the floats hardly moved at all. This was solved by raising the floats to a higher depth. Although with OCCAM we knew the solution operationally it was difficult to use due to the rotated grid and the format in which the data was stored. In chapter 4 I presented results from our "point" solution method , this was basically a rerun of the original method used by (Cunningham, 2000). I obtained a SSH of between ±40 cm with a bias of 5 cm and a RMSE value of 29.1cm calculated at the float positions. The OCCAM SSH extracted for the same points was between ±50 cm. These compare to the mean sea level anomaly created from TOPEX and ERS-2

altimetry for the same region by (Volkov, 2003) of between ±30 cm. In chapter five I introduced surface fitting and added satellite altimetry data to the problem. When I moved on to obtaining a float only surface solution, I obtained a SSH signal of ±40 cm, the same as our point solution. The RMSE difference was 46.8cm which appears a lot higher than the float point solution but this is because it calculated across the whole field rather than simply at the float positions. Though I could see the main oceanographic features of the region, the northern gyre and the North Atlantic Current, the smaller scale signals had been smoothed out by our low order polynomial fit. Introducing the altimeter data involves incorporating the unknown geoid. To solve this I proposed to use the difference between two altimeter passes since the geoid is constant this removes the problem. The addition of the satellite altimetry had three effects on our solution. First, I saw a much lower range of the signal between ±10 cm, second, I saw greater structure in our solution and third the RMSE falls to 27.3cm. The lower range of signal is not necessarily a problem though. As I have explained in chapter 5, I feel there are two reasons for this. The first is that the solution begins to coincide more with the changes in the SSH signal rather than the absolute values of SSH. I would expect this to be the case with the weighting due to the size of the altimetry component of the solution compare to that of the floats. We have ~100 floats by comparison to several thousand satellite altimetry points. The altimetry is measuring the change in the SSH over our two time steps in the paired solution, so it makes sense for our solution to reflect this. The OCCAM range of change in SSH is [-5 15] cm well comparable our solution of ±10 cm. The

RSME for this solution is 28cm. In this chapter I also extended the problem to using real ARGO and Jason altimeter data as opposed to OCCAM. I introduce another novel technique in chapter six, rather than using a polynomial to fit the surface as I did in the earlier chapters here I use a advanced non-parametric statistical method Generalised Additive Models (GAMs). With the GAM fit for technical reasons I was not able to do a MSE calculation. We saw the same reduction in the extremes of the signal, a range of [-10 30] cm.

Comparison with OCCAM

The results in general were poorer than expected. With OCCAM we could not recover the surface with any great confidence. To illustrate this we have included a schematic figure below, figure 75. In the figure the blue line represents the SSH we wish to obtain, the true signal. The green line is our "smoothed" surface fit obtained from the float only solution. We can see that the solution has been heavily smoothed due to fitting such a low order polynomial. We can see that we reproduce the maximum and minimum of the signal successfully but we lose the structure of the signal. The red line is our solution included the addition of the satellite altimetry. When we combine altimetry into the solution we can see that we solve for more of the structure in the signal but we lose the extremes of the signal. This is due to the constraints of using a low order polynomial function. If we were to use a higher order more complex function for the surface fit, the function would

possibly be able to respond to the higher structured solution in a way as to not lose the extremes of the signal.

Figure 75: Schematic to explain the difference between our surface solution with floats only and that including satellite altimetry. The blue line depites the SSH signal we wish to replicate. The green line is our "smoothed" 6th order polynomial surface fit with floats only. The red line is our 6th order surface fit with the altimetry included in the solution.

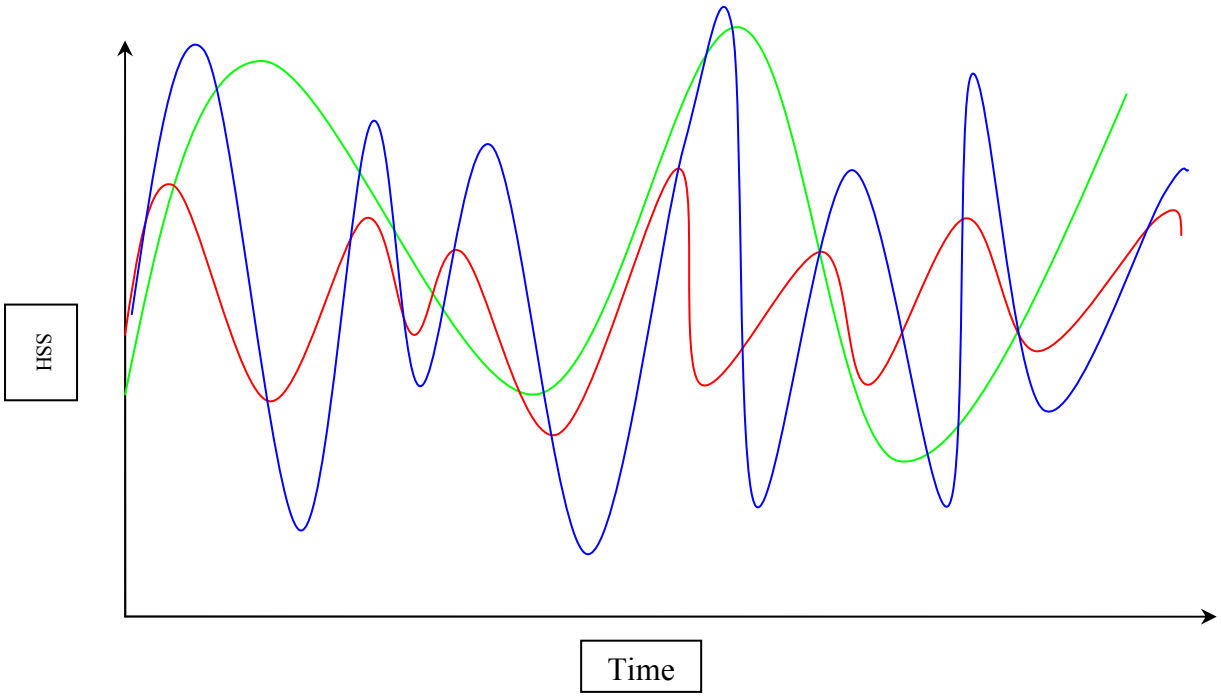

In order to examine the solutions in a more quantitative manner, we looked at the mean square errors of our results. We wished to see how well our

model did in predicting where we didn't have data. So we mapped the OCCAM SSH and OCCAM SSH differences on to the same standard grid as our solution. This meant that we could clearly compare our results with the solution we would expect to obtain. We calculated the mean square error first and then found the square root of these values to obtain the root mean square error (RMSE) in centimetres. The result was that with the addition of the satellite altimetry the RMSE was almost halved. In one case the value was reduced from 47 cm to 28 cm and in another time step by even more from 86 cm to 50 cm. This proves our conclusion that we are reproducing more of the structure of the signal with the inclusion of the satellite altimetry to the solution.

We then did a further test to see what would happen if we fitted a higher order polynomial to the solution. The result was very similar to that of the addition of the satellite altimetry. We obtained a higher resolution solution but of a lower order in magnitude, in a range of ±20 cm. The mean square error calculation reflected this result. The float only 6^{th} order polynomial gave a RMSE of 47 cm whereas the 7^{th} order fit gave a value of 24 cm. This was 3cm lower than the same time step solution with satellite altimetry included. We didn't try a 7^{th} order polynomial solution with the inclusion of altimetry, but if we had we would expect the solution to continue to improve.

Our result was promising. Our solution agreed well with the schematic of the expected circulation for the region created by Ellett (1993). This can be seen

by referring back to figures 5, 7 and 64. We can see a clear representation of the two gyred system we would expect in the North Atlantic. The range of the SSH signal was [-50 10] this is well within the bounds of reason when compared to both the OCCAM model, the SLA obtained by (Volkov, 2003) and the values obtained by the DUACS combined altimetry dataset, see figure 76 below. However our experience with OCCAM showed that although we could recover the general shape of the sea surface height field it was difficult to produce good estimates of the detailed height field. Thus our real world results should be treated with caution.

Figure 76: SSH obtained from DUACS for the 1st of Jan 2003 in meters.

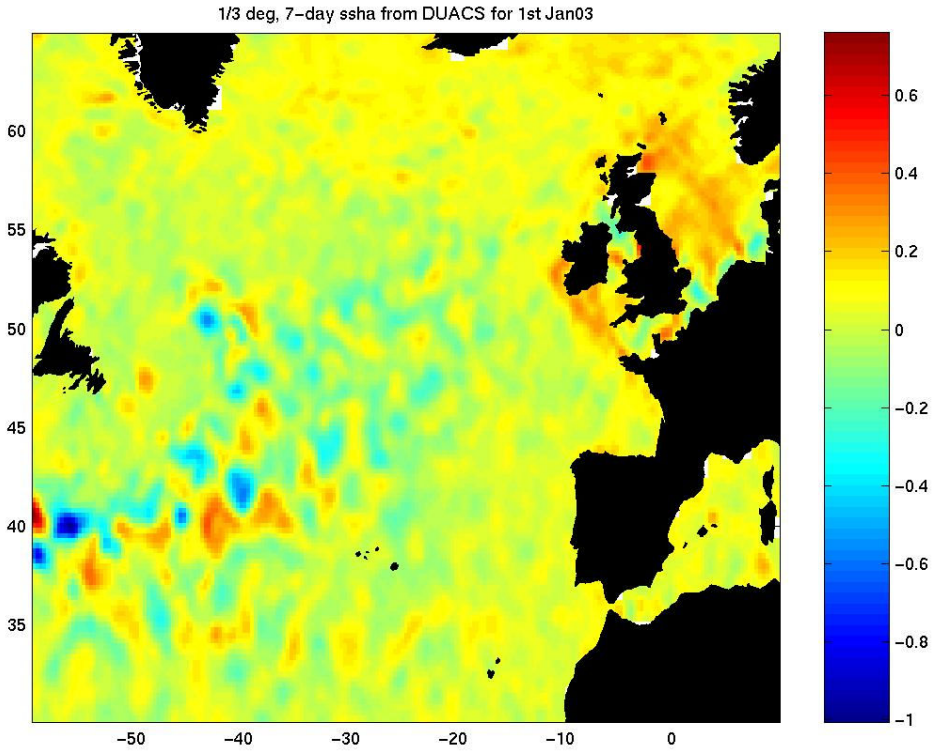

Why the Bernoulli method might not be working as well as expected

As stated above, with the OCCAM data the numerical comparison of my solution with the truth is poor, although the general oceanographic features are recovered. There are a number of possible reasons for why the Bernoulli method might give this poor fit.

(1) the Bernoulli method assumes steady state conditions whereas the data we use includes high frequency variations such as eddies. These high frequency variations will mean that our assumption that variables are conserved at crossings is not true.

(2) Another reason for a poor solution is the assumption of well defined water masses with a constant T/S relationship. In practise our method is spanning a large basin which contains a number of water masses. One method I used to try and overcome this was to search for the eight nearest neighbours for each float. This reduces the effect of differing water masses. However it is not possible to remove this difficulty completely.

(3) An additional problem is the rapid change in the sea surface height field. The altimeter data in particular is dominated by this high frequency variation. When I included the altimetry data in the solution this dominated the result as I had ~100 floats to several thousands altimeter points. This means that this

high frequency signals then over shadow the mean sea surface height field reflected in the ARGO data.

(4) The low order polynomial function I fit to the sea surface height field is very smooth. This could be an additional reason for the poor fit. In attempt to get around this problem I used a more adaptable function, GAM. The more complex I made the function the better the surface fits the true sea surface height from OCCAM out performing the point solution. For example when I went from the 6^{th} to the 7^{th} order solution the RMSE was reduced from 47 to 25cm. However because of the soothing involved we tend to loose the extreme values. Using a less smooth function we may be able to recover these extreme values. This would involve more polynomial terms or more smoothing terms in the GAM. Unfortunately I ran out of time before I could investigate this properly.

Models other than OCCAM

We used the OCCAM model because it was a high resolution model that was available at NOC and had the advantage of having a five day dumps which were easy to match to the ten day ARGO cycle. The model also has a free sea surface that makes analysis simpler. However it was not without its problems. The data was difficult to work with. In part this was due to the rotated grid and in part in the way the data was stored. Extracting the data was slow and on occasion the OCCAM team would move data without telling me. A more

serious problem was the non-existent flow below 1000m. This was worrying and may be due to lack of spin up in the model. However I did not have time to investigate why this was occurring and it does not seem to have been picked up by other analyses of OCCAM. For my purposes it was not a major problem as by moving my floats to a depth of 1000m good float simulations were obtained. It would be interesting to repeat my calculations with another model but time did not permit this. I do not think that this would change the quality of the results but would have allowed a larger numbers of experiments to be carried out and possibly to help in understanding why the results were disappointing. If I had a lower resolution model that did not resolve eddies I may possibly have obtained a better solution. It would be interesting to carry this out to investigate the effect eddies have on the solution.

Suggestions for future work

There are a number of improvements that could be made to the method. These include using a higher order polynomial or GAM to fit the sea surface, reducing the dominance of the altimeter data either by weighting or sub-sampling, matching the ARGO profiles to water masses.

(1) The surfaces we fit to the sea surface height are very smooth since the highest order polynomial we use was 7^{th} order. This clearly could not capture

sharp boundaries or high frequency variability such as eddies or the Gulf Stream. There are two ways we could tackle this problem. One is to use much higher polynomials. However is this computationally expensive and there is a danger of over fitting the data. The alternative is to use non-polynomial basis functions. In chapter six we experimented with GAMs and it would be interesting to develop these in the full methodology. There are alternative basis functions that could be used, for example wavelets.

(2) The altimeter data dominates because there are ten of thousands of altimeter points and only a hundred or so floats. As we discussed above the altimeter data is likely to be dominated by the eddy field which we know is poorly captured by the Bernoulli method. There are a number of possible solutions to this problem. One solution is to down weight the altimeter data, another is to sub-sample the data by taking every tenth or one hundredth point. Experiments would need to be carried out to optimise the amount of weighting or sub-sampling needed to balance the two data sets.

(3) In this work I use an eight nearest neighbours test to reduce the effect of different water masses. One can imagine a more complex scheme that would allocate each point on a profile to a distinct water mass. Crossing points from each water mass would be analysed separately and then recombined to form a complete solution.

Conclusion

We have successful developed the Bernoulli inverse method to combine altimetry and ARGO floats. We have shown that this does constrain our solution as hoped. Some suggested reasons for this have been given. Secondly we have developed this method to be used effectively on "real" time datasets. The matrix structure of the method makes it highly accessible to any dataset and of large sizes. The method is computationally efficient enough to run a large basin such as the North Atlantic region, mainly due to the fact that the majority of coding has been done using python. This is a very efficient computer language. As an aside to this we have shown it is possible to simulate ARGO floats in a model such as OCCAM to test our method. This was one of the most difficult parts of the project. The other difficulty being to incorporate the "real" data, as the data sets were in very different formats.

In conclusion, developing the method to include satellite data and solve for more than the SSH between a few data stations took so much time that we did not manage to apply the method in its most practical sense to real oceanographic issues. However we have developed a tool that can be made use of in analysing the ocean state. We have developed the means to obtain a sea surface elevation for the whole North Atlantic region rather than just at "points" every ten days from real time data. There are still some issues about the accuracy of the method that should be resolved before it could be used in practise.

References:

Alderson, S. G. and P. D. Killworth (2005). "A Preoperational Scheme for Calculating Sea Surface Height by Bernoulli Inverse of Argo Float Data in the North Atlantic." Journal of Atmospheric and Oceanic Technology **22**: 1416-1422.

Argo (1999). On the design and implementation of Argo
A global Array of profiling floats.

Bigg, G. R. (1986). "Sensitivity studies of a simple inverse method applied to the Cox and model." J. Geophys. Res **91**: 9639-9654.

Broecker, W. S. (1991). "The Great Ocean Conveyor." Oceanography **14**(2): 78-89.

Broecker, W. S. and T. H. Peng (1987). "The biggest chill." Natural History Magazine **97**: 74-82.

Chelton, D. B., Ries, J.C., Haines, B.J., Fu, L., Callahan , P. S. (2001). Geophysical effects on the Sea Surface Topography. Satellite Atlimetry and Earth Sciences, A handbook of techniques and applications. L. Fu, Cazenave, A., International Geophysical Series. **69:** 86 -89.

Cunningham, S. A. (2000). "Circulation and Volume Flux of the North Atlantic using Synoptic Hydrographc Data in a Bernoulli Inverse." journal of marine research **58**(1): 1-35.

Dickson, B., I. Yashayaev, et al. (2002). "Rapid freshening of the deep North Atlantic Ocean over the past four decades." Nature **41**: 832-836.

Dietrich, G., K. Kalle, et al. (1975). "General Oceanography." John Wiley, New York: 626 pp.

Fukumori, I. (2001). Data Assimilation by models. Satellite Altimetry and Earth Science, A Handbook of Techniques and Applications. L. Fu, Cazenave, A., International Geophysics Series. **69:** 237-266.

Gershenfeld, N. (1999). The Nature of Mathematical Modeling, Cambridge University Press.

Grose, T. J., G. R. Bigg, et al. (1994). "The Bernoulli inverse method: theory and practice." Deep-sea Res. **41**(5/6): 767-785.

Guinehut, S., Larnicol, G., Le Traon, P.Y. (2002). "Design of an array of profiling floats in the North Atlantic from model simulations." J. Marine Systems **35**(1-2): 1-9.

Hastie, T., Tibshirani, R., Friedman, J. (2001). The Elements of Statistical Learning, Springer**:** 257-299.

Heywood, K., J., E. McDonagh, L., et al. (1994). "Eddy kinetic energy of the North Atlantic subpolar gyre from satellite altimetry." J. Geophys. Res **99**(C11): 22,525-22539.

Hurrell, J. W. (1995). "Decadal trends in the North Atlantic Oscillation:Regional Temperatures and Precipitation." Science **269**.

Hurrell, J. W., Y. Kushnir, et al. (2001). "The North Atlantic Oscillation." Science **291**(5504): 603,605.

Institution, W. H. O. (1999). Observing the oceans in real time : Argo, Woods Hole Oceanographic Instituation**:** 12.

Killworth, P. D. (1986). "A Bernoulli Inverse Method for Determining the Ocean Circulation." J. Phys. Oceanogr. **16**(12): 2031-2051.

Killworth, P. D. and G. R. Bigg (1988). "An intercomparison of inverse methods using an eddy-resolving general circulation model." J. Phys. Oceanogr. **18**: 987-1008.

Krauss, W. (1986). "The North Atlantic Current." J. Geophys. Res **91**(C4): 5061-5074.

Krauss, W. (1993). "The North Atlantic Current and its associated eddy field: observations and model results, The North Atlantic Current System." A Scientific Report, Woods Hole Oceanographic Institute.

Lawson, C. L. and R. J. Hanson (1974). Solving Least Squares Problems, Prentice-Hall.

Macdonald, T. J. (2003). "Potential Enthalpy: A Conservative Oceanic Variable for the Evaluating Heat Content and Heat Flux." J. Phys. Oceanogr. **33**: 945-963.

Marsh, R. and A. P. Megann (2002). "Tracing water masses with particle trajectories in an isopycnic-coordinate model of the global ocean." Ocean Modelling **4**(1): 27-53.

McCartney, M. (1996). "North Atlantic Oscillation." OCEANUS **39**(2): 13.

McCartney, M. and L. D. Talley (1984). "Warm-to-cold water conversion in the northern North Atlantic Ocean." J. Phys. Oceanogr. **14**(5): 922-935.

McCartney, M. S. and R. G. Curry (2001). "Ocean gyre circualtion changes associated with the North Atlantic Oscillation." submitted J. Phys. Oceanogr.

McDougall, T. J. and D. R. Jackett (2000). "Potentail enthalpy and modified potential temperature: conserved oceanic varibles." in prep.

McPhaden, M. J. (1993). " TOGA-TAO and the 1991-93 El Niño-Southern Oscillation Event." Oceanography **6**: 36-44.

Naeije, M. C., E. J. O. Schrama, et al. (2005). The Radar Altimeter Database System RADS. Proc. International Geoscience and Remote Sensing Symposium (IGARSS), Honolulu, Hawai., T. I. Stein (ed.). IEEE Transactions ISBN 7803-6357-0.

Panofsky, H. A. (1949). "Objective Weather-Map Analysis." Journal of Meterology **6**: 386-392.

Saunders, P. M. (1995). "The Bernoulli function and flux of energy in the Ocean." J. Geophys. Res **100**(C11): 22647-22648.

Scott, F. and H. Stommel (1978). "Beta Spirals and absolute velocities in different oceans." Deep-sea Res. **25**: 961-1010.

Srokosz, M. (2004). "New experiment deploys observing array in N. Atlantic to investigate rapid climate change." EOS **85**(8): 78-83.

Stammer, D. (2004). Ocean Inverse Problem. 2nd Enivsat Summer School, Frascatti, Italy.

Tokmakian, R. (1994). "The Iceland-Faroe front: a synergistic study of hydrogaphy and altimetry." J. Phys. Oceanogr. **24**: 2245-2262.

Uppenbrink, J. (1999). "The North Atlantic Oscillation." Science **283**(5404): 948-949.

Volkov, D. L., van Aken,H.M. (2003). "Annual and Interannual Variability of Sea Level in the North Atlantic Ocean." J. Geophys. Res **108**(c6): 1-13.

Webb, D. J., A. C. Coward, et al. (1997). "A Multiprocessor Ocean General Circulation Model Using Message Posting." Journal of Atmospheric and Oceanic Technology **14**: 175-183.

Webb, D. J., B. A. d. Cuevas, et al. (1998). "The first main run of the OCCAM global model." Internal Document SOC. **34**.

Worthington, L. V. (1976). "On the North Atlantic circulation." Oceanogr. Stud. **6**: 1-110.

Wunsch, C. (1978). "The general circulation of the North Atlantic west of 50 W determined from inverse methods." Rev. Geophys. **16**: 583-620.

Wunsch, C. (1996). The ocean circulation inverse problem, Cambridge University Press.

Wunsch, C. and E. M. Gaposchkin (1980). "On using satellite altimetry to determine the general circulation of the oceans with application to geoid improvement." Rev. Geophys and Space Phys. **18**(4): 725-745.